MOLECULAR BIORECOGNITION OF COILED-COIL MOTIFS IN THE CONSTRUCTION OF HYBRID HYDROGELS AND DRUG-FREE MACROMOLECULAR THERAPEUTICS

by

Kuangshi Geoffrey Wu

A dissertation submitted to the faculty of
The University of Utah
in partial fulfillment of the requirements for the degree of

Doctor of Philosophy

Department of Pharmaceutics and Pharmaceutical Chemistry

The University of Utah

December 2010

The University of Utah Graduate School

STATEMENT OF DISSERTATION APPROVAL

The dissertation of **Kuangshi Geoffrey Wu**

has been approved by the following supervisory committee members:

Jindrich Kopecek	, Chair	**Sept. 21st, 2010** Date Approved
David W. Grainger	, Member	**Sept. 25th, 2010** Date Approved
James Herron	, Member	**Sept. 23rd, 2010** Date Approved
Hamid Ghandehari	, Member	**Oct. 1st, 2010** Date Approved
Patrick F. Kiser	, Member	**Sept. 24th, 2010** Date Approved

and by **David W. Grainger**, Chair of the Department of **Pharmaceutics and Pharmaceutical Chemistry**

and by Charles A. Wight, Dean of The Graduate School.

This dissertation is dedicated to my grandparents, who taught me to be a right person to do right things in the right way.

It is also dedicated to Larisa Cristina and Lorena Ailan Wu,

my guardian angels.

ABSTRACT

Molecular biorecognition is at the heart of all biological processes and has come to the center stage in designing new biologics. Coiled-coils result from molecular biorecognition of multiple protein α-helices. We have designed a series of coiled-coil motifs that self-assemble into supercoils, which in turn function as physical cross-linkers in the construction of hybrid biomaterials.

This dissertation describes our endeavors following the hypothesis below: the self-assembly of coiled-coil forming peptides into coiled-coils can be used as a cross-linking mechanism in the construction of hybrid hydrogels and the development of a drug-free macromolecular therapeutic.

In the first part, a macromonomer free radical copolymerization strategy was developed and HPMA graft copolymers containing coiled-coil motifs of different chain lengths were synthesized. Results indicated that the primary structure of these motifs greatly influenced gel formation. At least four heptads were needed to mediate effective gelation. The gelation process was highly dependent on the environmental temperature and copolymer concentration.

In the second part, a drug-free macromolecular therapeutic was designed to take full advantage of the facts that CD20 is one of the most reliable biomarkers for B-cell non-Hodgkin's lymphoma (NHL), and cross-linking of CD20 antigens induces apoptosis of B cells. The drug-free therapeutic was composed of two components: Fab' fragment of 1F5

anti-CD20 antibody conjugated with one coiled-coil motif (CCE) and polyHPMA copolymer grafted with multiple copies of the complementary coiled-coil motif (CCK). *In vitro* studies showed the conjugates could colocalize on Raji cell surfaces and a clinically relevant magnitude of apoptosis was achieved. A systemic NHL murine model was used to evaluate *in vivo* efficacy. Significant delay of hind-limb paralysis onset was observed after treatment. In groups receiving multiple-dose treatment, the surviving mice were disease-free and no presence of Raji B cell in bone marrow could be detected after 100 days.

In summary, the possibility of integrating molecular biorecognition of short non-natural coiled-coil motifs into new smart biomaterials is presented. This specific biorecognition can be used with or without adjuvant pharmacology to mediate a biofunctional process in combating diseases.

TABLE OF CONTENTS

LISTS OF TABLES

Table

LISTS OF FIGURES

Figure

ACKNOWLEDGEMENTS

First of all, I would like to thank my advisor Dr. Jindřich Kopeček for guiding me through this Ph.D. study. His dedication to science, hard-working spirit, and pursuit of excellence set up a great role model for me to follow for the rest of my life. To Pavla, thank you for being a mother standing by me all these years. I am grateful to my committee members, Dr. David Grainger, Dr. James Herron, Dr. Hamid Ghandehari and Dr. Patrick Kiser, for their great mentorship and advice during my study. I would also like to thank Dr. William Higuchi, Dr. Carol Lim, and Dr. Zheng-Rong Lu for their unconditional support to my fellowship applications. I am indebted to my friends and colleagues to their indispensable help whenever needed. This research was supported in part by the National Institutes of Health (NIH) under grant EB005288 and American Foundation for Pharmaceutical Education (AFPE) Pre-doctoral Fellowship.

I owe the deepest gratitude to my grandparents for raising me up as a right person doing the right things. To my parents, thank you for bringing me to this great nation for further development. To my lovely wife and daughter, you are the angels lighting up my life; together we are in pursuit of happiness.

This is such an amazing journey filled with excitement. I found myself, my love, a cause to pursue, and the meaning of life. Thanks again to all the wonderful people around me for making these possible.

CHAPTER 1

INTRODUCTION

1.1. Molecular biorecognition

Molecular biorecognition is at the heart of all biological events *(1, 2)*, defined as noncovalent forces that produce specific interactions between a biomolecule and its ligand, such as protein-protein *(2)*, RNA-protein *(3)*, and enzyme-substrate pairs *(4)*. Such recognition yields the specific interactions responsible for the essential processes of life, including genetic information trafficking, protein folding, cellular signal transduction, metabolism, and others. The growing knowledge base about molecular biorecognition has been a great inspiration to researchers for the design of new biomedical systems and devices.

The shape and energetic complementarity of interacting surfaces governs molecular biorecognition. This understanding has evolved from Emil Fischer's "key-and-lock" analogy in 1894 *(5)* to Paul Ehrlich's stereocomplementarity (side-chain theory of immunity) in 1900 *(6, 7)*, then to the modern "induced-fit" model *(3, 8, 9)*. Although the essential mechanism of biorecognition remains a mystery, the major molecular level factors contributing to complementarity have been well identified *(10)*. They include:

1. surface shapes of the interacting molecules
2. hydrogen bond(s) between molecules

3. ion-ion, dipole-dipole and ion-dipole interactions

4. van der Waals forces

5. hydrophobic interactions

The far-reaching consequence of molecular biorecognition is its role at the interface between medicine, biology and chemistry, with manifold implications and applications *(2, 11-13)*. Functioning as a key driving force, biorecognition has become a critical component for novel biomaterial designs, such as self-assembling materials *(14)* targeted drug delivery systems *(15-17)*, diagnostic devices with super sensitivity *(11)* and novel smart biomaterials *(18)*.

1.2. The coiled-coil motif

Coiled-coils are ubiquitous protein folding patterns in nature, composed of multiple α-helices self-assembled into left- or right-handed supercoils; with the self-assembling process tightly regulated by principles of molecular biorecognition. Since the first crystal structures of coiled-coils were solved in the 1950s *(19, 20)*, coiled-coil motifs have gained great attention and wide application *(21-30)*. These motifs have become the most intensively studied protein folding motifs due to their sequence periodicity, structural simplicity, designability, reversible self-assembly, and stimuli-sensitivity *(24)*.

1.2.1. Coiled-coil dissection

The α-helix is the building block for coiled-coils, to produce the multiple helices wrapping around each other following the “knobs-into-holes” packing rules *(31)*. Coiled-coil motifs can further assemble into fibrils or other shapes driven by mainly hydrophobic

interactions. The typical primary sequence of the α-helix has a unique feature of seven-amino-acid repeat – the heptad. The number of heptads in a single helix can range from 2 in a *de novo* designed motif *(32)* to 200 in natural proteins *(24)*. The seven amino acid positions of a heptad are conveniently designated as $(abcdefg)_n$. In general, *a* and *d* positions are occupied by hydrophobic residues (Leu, Ile and Val); *e* and *g* positions are oftentimes taken by charged residues (Glu and Lys); the remaining positions are mainly arranged with hydrophilic residues to adjust α-helical propensity, net charge and solubility *(33)*. The amino acid residue arrangement and major inter-chain interactions are often delineated by a helical-wheel diagram (Figure 1.1). The right-handed α-helices wind around the helical axis into left-handed supercoils, giving 3.5 residues per turn or one complete heptad after two turns *(21)*. The critical forces driving the amphipathic helices forming coiled-coils are interchain hydrophobic interactions between *a* and *d* positions in the core and ionic interactions (salt bridges) between *e* and *g* positions. Both types of interactions work together to determine the coiled-coil stability and specificity *(34, 35)*. Furthermore, the overall rotational and translational motions are another source of the driving forces unique to coiled-coils. Of course, other factors (e.g. hydrogen bonding) involved in molecular biorecognition apply to coiled-coil formation as well.

Coiled-coil specificity has three aspects: number of helices, relative orientation of helices and their helices oligomerization (homo- vs. hetero-) *(21, 24)*, as demonstrated in Figure 1.2. In engineered coiled-coils, there can be 2, 3, 4, 5 and 7 helical strands forming dimer, trimer, tetramer, pentamer and heptamer associations, respectively. Same (homo-) or different (hetero-) helices can associate into supercoils along the same (parallel) or opposite (anti-parallel) direction.

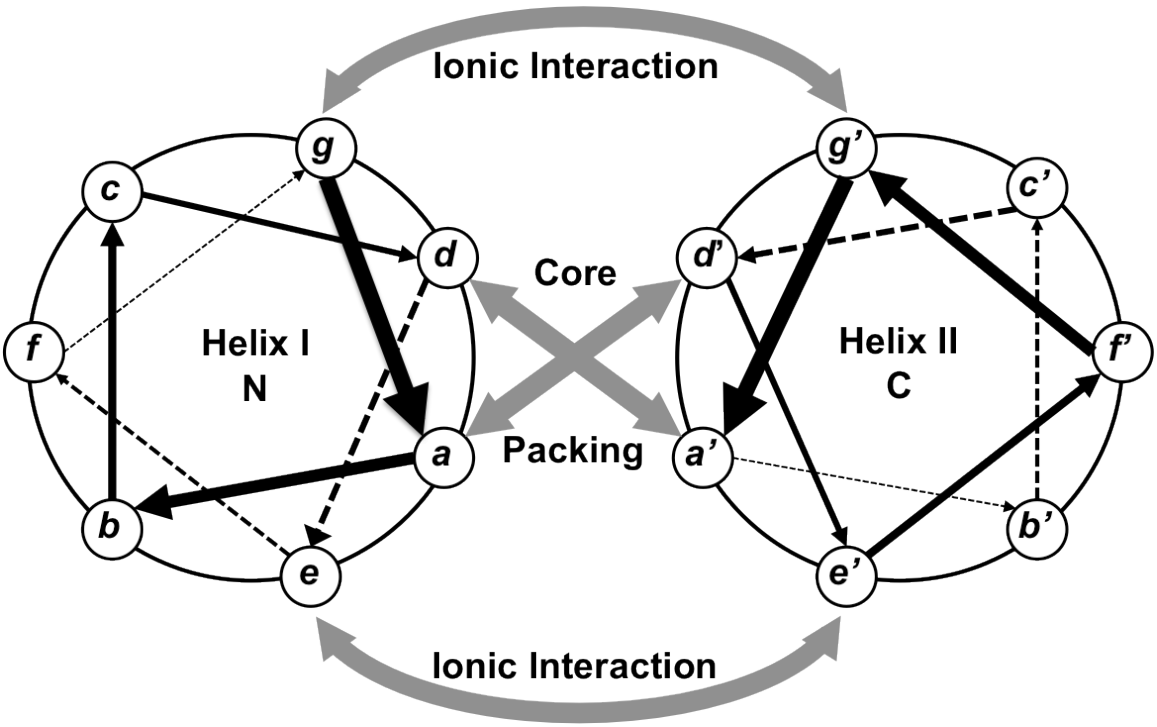

Figure 1.1. Helical wheel diagram of a coiled-coil composed of 2 α-helices aligned in anti-parallel orientation. Primary sequence of the α-helix has a characteristic 7 amino acid repeat, the heptad. *a* (*a'*) – *g* (*g'*) are 7 amino acid positions in one heptad. Appropriate arrangement of amino acids is required to allow for hydrophobic core packing and ionic interactions: *a* (*a'*) and *d* (*d'*) positions mainly for hydrophobic residues (e.g., leucine, isoleucine and alanine), e (e') and g (g') positions for charged residues (e.g., lysine and glutamic acid), and the remaining positions for residues to adjust α-helical propensity, net charge and solubility. α-Helices wind around the helical axis into supercoils with one complete heptad after 2 turns.

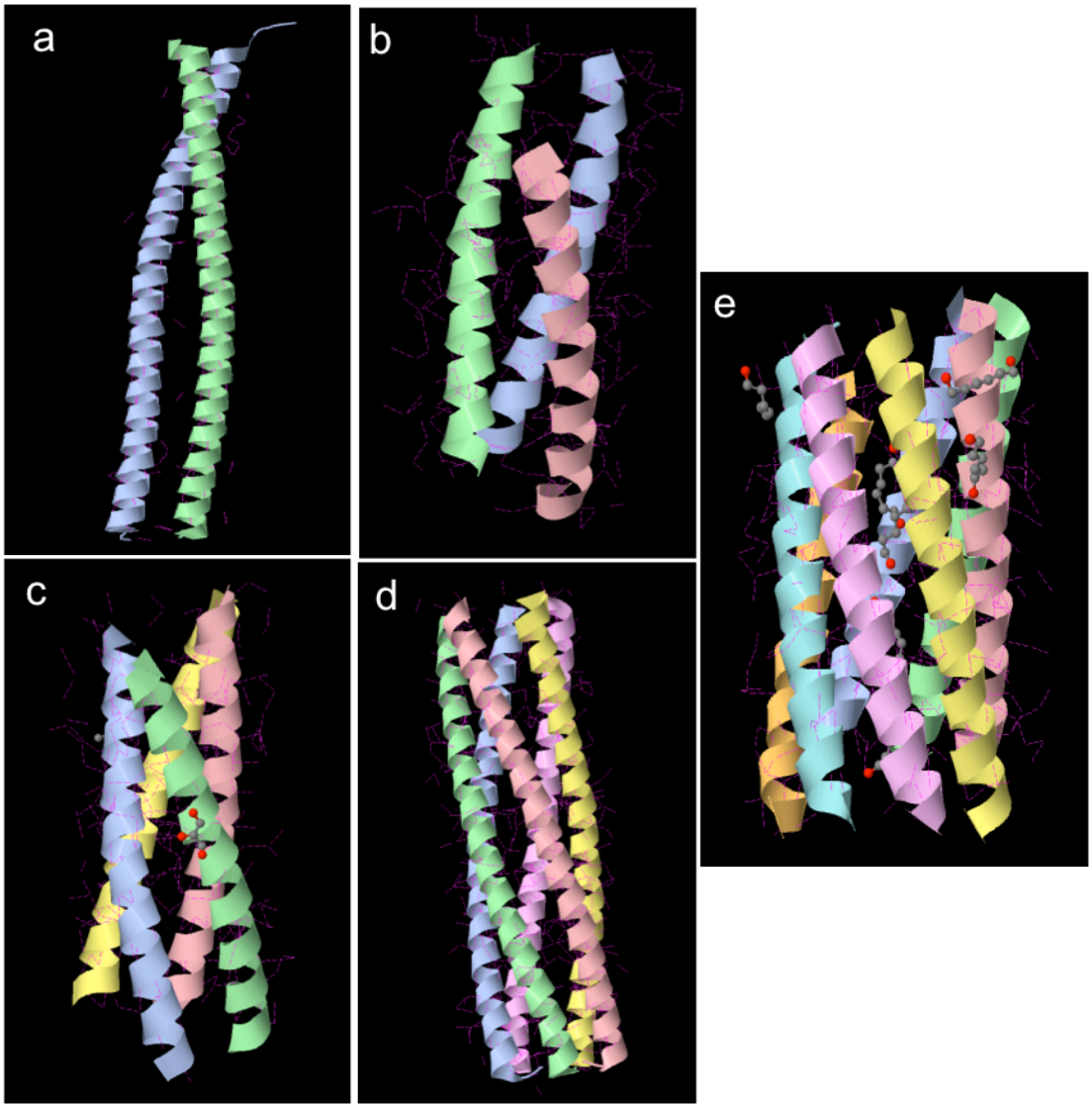

Figure 1.2. Examples of coiled-coils with different specificities: a) Parallel dimer (PDB entry 3MOV) *(36)*; b) Anti-parallel trimer (PDB entry 3K7Z) *(37)*; c) Parallel tetramer (PDB entry 2IPZ) *(38)*; d) Parallel pentamer (PDB entry 2GUV) *(39)*; e) 7-strand coiled-coil (PDB entry 2HY6) *(40)*.

Besides coiled-coils composed of heptad repeats, researchers have also confirmed the existence of right-handed coiled-coils consisting of 11/3 (11 residues in 3 turns), 15/4, 18/5, and 25/7 arrangements. Conformation exchange among random coil, coiled-coil and β-sheet was also observed upon changing their microenvironment, such as pH *(41, 42)* and addition of related biomolecules *(43)*. Since these phenomena are beyond the scope of this dissertation, no detailed discussion will be given.

1.2.2. *De novo* design of coiled-coil motifs

Due to its intriguing features, requirements for *de novo* design of coiled-coil motif must be elucidated to enable its further exploration for applications. Successful design of coiled-coil motifs lies in appropriate arrangement of residues to ensure all the key coiled-coil interactions. Specificity of the target coiled-coil motifs may be tailor-made toward different purposes with a possible sacrifice of stability.

Since the hydrophobic interactions between *a* and *d* positions are the major driving forces in coiled-coil formation, the proper selection of residues at these positions is of critical importance for resulting specificity and stability *(44, 45)*. Hodges' group *(46-48)* divided 20 natural amino acids into three groups regarding their ability to determine the number of helices in resulting coiled-coil. The first group of amino acids impart 100% specificity at both *a* and *d* positions: Arg, Lys, Asp (100% two helices) and Tyr (100% three helices). The second group imparts 100% specificity only at one of the two positions: Gln, His and Leu (100% three helices at *a*); Ile and Val (100% three helices at *d*); and Glu (100% two helices at *d*). The remaining residues have no specificity at either position.

High resolution crystal structures of coiled-coils also revealed the residue preference in the hydrophobic core *(31)*. For instance, in parallel dimeric coiled-coil *a* positions are enriched in β-branched residues Val and Ile, and *d* positions are abundant in γ-branched residue Leu. But in trimeric coiled-coil, both kinds of residues are equally represented and evenly distributed in *a* and *d* positions. Residue placements in other positions are also critical. Litowski and colleagues greatly improved the coiled-coil stability by replacing Ser with Ala in *b* positions based on the fact that Ala has a higher α-helical propensity *(33)*.

Additionally, there are two other ways to direct helix orientations: 1) introduction of hydrogen bonds via placing polar residues in the hydrophobic core; 2) manipulation of the ionic interactions by arranging charged residues at *e* and *g* positions. Kim's group had elaborated the successful control over parallel and anti-parallel orientation by incorporating asparagines (Asn) at *a* and/or *d* positions, although at the cost of stability *(49-52)*. Hodges and coworkers succeeded in aligning helices in preferred orientations by adjusting the attraction and repulsion between the charged residues (Glu and Lys) at *e*/*g*-*e'*/*g'* positions *(53-55)*. Moreover, they showed that the anti-parallel orientation imparted the highest overall stability and the minimum steric hindrance to the resulted coiled-coil *(54)*. Interestingly, Okaley and colleagues *(34)* directed the helical orientation (anti-parallel) by introducing Coulombic interactions between *d* (Arg) and *g'* (Glu) positions, and showed that this arrangement suffered less thermodynamic cost than burying two Asn's in the hydrophobic core *(56)*. The conformation interchange between coiled-coil and β-sheet could also be achieved by proper sequence design, as demonstrated by Koksch's group *(42)*. Eventually the overall side-chain property (polarity, charge and

shape) of amino acid residues determines the final conformation of a coiled-coil and the subsequent folding of the whole protein *(57)*.

Great effort has been expended to shorten the chain length of α-helices in order to minimize the synthesis workload. However, one needs to keep in mind that the helicity of peptides is closely related with the chain length in a cooperative manner, so are the coiled-coil stability and specificity *(58, 59)*. Kay's group reported that a minimum of three heptads (6 turns) was required for a stable two-stranded coiled-coil conformation and five or more appeared to be optimal *(60)*. This observation was in good agreement with later reports *(61, 62)*. Although one report claimed a successful design of helices containing only two heptads forming stable coiled-coils, the authors failed to identify the uniqueness of the design to allow for coiled-coil formation *(32)*.

Computational methods were developed to aid the rational *de novo* design of coiled-coil motifs. PairCoil and MultiCoil are multi-dimensional scoring algorithms to predict oligomerization state of coiled-coils *(63)*. Another modeling method employed energy minimization techniques to profile the aggregation of coiled-coils *(64)*. An open-source coiled-coil prediction algorithm is also available to estimate melting temperature (T_m) of dimeric coiled-coils as an indication for the strength of helix interactions *(65-67)*.

1.2.3. Self-assembly of coiled-coil motifs and their characterization

As crucial building blocks of organisms, α-helices do self-assemble into structures of higher orders to execute certain bio-functions. Due to the non-covalent nature of inter-chain interactions, helices can automatically associate into supercoils or dissociate upon appropriate stimuli. These molecular switches may include pH, temperature, ionic

strength, and presence/removal of biomolecules *(68)*. This phenomenon is called the stimuli-responsive self-assembly of coiled-coils. Self-assembly into coiled-coils is not only about helices winding into one another, but also allowing specific inter-chain interactions. Being "programmed" into the sequences *(69)*, these interactions essentially define the relative alignment and direction of the intertwined helices. In other words, supercoil conformation accommodates certain systematic side-chain interactions rather than the bending of the axis of the α-helix *(70)*.

Facilitated self-assembly of small coiled-coil motifs allows the building of supra-molecules with well-defined structures through only noncovalent interactions *(71, 72)*, as shown by our group in 1999 *(22)*. More importantly, the self-assembling process is programmable and controllable, which presents many potential applications. For instance, the resulting materials can possess various morphologies (e.g., rod, fibril, globule, etc.) by design for different purposes *(68, 73)*.

Different biophysical techniques were developed to "visualize" and quantify the self-assembly of coiled-coil motifs. The most commonly used ones are listed in Table 1.1. Several reagents frequently employed during the analyses are: trifluoroethanol (TFE), guanidine hydrochloride (GndHCl) and urea. TFE can only stabilize α-helices in the region with high helical propensity, but not induce α-helical structure from any given sequence; in other words, it is considered as a helical enhancing co-solvent rather than an inducing agent *(74)*. Due to their different solutropic interactions, GndHCl and urea promote different protein folding interactions during denaturation *(53)*: the charged GndHCl masks electrostatic interactions, hence it is mainly an indicative measurement of

Table 1.1. Frequently used biophysical techniques to characterize coiled-coils.

Techniques	**Description & Application**	**References**
Circular dichroism (CD) spectroscopy	Secondary structures, double minima at 208 and 222 nm indicating α-helices interaction	*(47)*
Analytical ultracentrifugation (AUC)	Molecular weight measurement and oligomerization state monitoring	*(48)*
High performance size-exclusion chromatography (HPSEC)	Oligomerization state monitoring	*(47, 48)*
GdnHCl and Urea denaturation	Coiled-coil stability and interaction analysis	*(54)*
X-ray crystallography	Crystal structure determination	*(75)*
Nuclear magnetic resonance (NMR)	Determination of structure and possibly protein folding kinetics	*(76, 77)*
Fluorescence resonance energy transfer (FRET)	Detection of coiled-coil formation, and orientation and degree of alignment	*(78)*

hydrophobic interactions; while the uncharged urea does not interfere with charged residues and it is an overall indication for both electrostatic and hydrophobic interactions.

1.2.4. Applications of coiled-coil motifs

Given the aforementioned attractive features of the coiled-coils, they are excellent models for protein engineering: the engineered coiled-coils have been translated into a wide variety of applications *(25, 79)*. In the modern biopharmaceutical field, coiled-coil motifs are employed to fabricate novel biomedical devices, such as drug delivery systems *(26)*, protein hydrogels *(23, 27)*, new therapeutics, affinity purification and biosensors *(80)*.

Two distinct research directions are a general focus and these are also the strategies adopted in this dissertation. First, coiled-coil motifs can be introduced as physical cross-linkers to mediate sol-gel transitions upon corresponding environmental stimuli. In 1999, our group pioneered not only the concept but also the possibility of super-imposing the properties of peptides and synthetic polymers *(22)*. Over 200 publications have been dedicated to this focus since then. Second, heterodimerization of coiled-coil motifs can be incorporated to develop pretargeted treatments for cancers *(24, 26)*, such as radioimmunotherapy for lymphomas *(81, 82)*. In this strategy, one strand of the coiled-coil is attached onto the homing device (i.e., anti-tumor antibody or Fab' fragment), and the other coil strand attached onto a therapeutic entity (e.g., drug or isotope). During the application, the first component is applied to pretarget/coat the target surface; then the second component is administered, "attracted" to the target surface due to the affinity biorecognition between the coiled-coil helices.

1.3. Physical Hydrogels

Hydrogels are polymeric materials that can absorb and retain substantial amount of water without breaking their three-dimensional scaffolds/networks *(83, 84)*. Pioneering work from Wichterle and Lím proved the feasibility of using "hydrophilic gels" for biomedical use because of their unprecedented properties, such as low reactivity in biological environments and porosity for metabolites exchange/transportation *(83)*. In 1968, hydrogels became the first biomaterials for human use in the form of soft contact lenses *(85)*.

Hydrogels can be categorized in several ways, such as synthetic (traditional), poly(amino acids)-based and hybrid hydrogels according to their composition; degradable and non-degradable hydrogels regarding their fate inside the body; covalent and physical hydrogels based on cross-linking mechanisms *(84)*.

Covalent hydrogel networks can be acquired by bulk radical copolymerization of chain-forming monomers and suitable cross-linkers *(86)*. For such purpose, typical monomers are mainly acrylate and methacrylate derivatives and so are the cross-linking agents, as listed in Table 1.2. Networks can be also built by cross-linking hydrophilic polymers (e.g., dextran, albumin and hyaluronic acid) derivatized with methacrylic acid *(87)*. Other chemical cross-linking methods are also available, including reaction between complementary groups, and radiations induced and enzyme catalyzed cross-linking, as summarized by Hennink and colleagues *(87)*. Interestingly, protein-based cross-linkers can be also used to build covalent hydrogels, such as engineered adenylate kinase *(88)*. By adjusting the feed ratio of monomers/polymers and cross-linking agents, one can achieve desired cross-linking density, degree of swelling, mechanical strength, porosity,

Table 1.2. Typical monomers and cross-linking agents for traditional hydrogel synthesis. Adapted from references *(84, 97)*.

Category	**Name**
Monomers	2-Hydroxyethyl methacrylate (HEMA)
	Acrylic acid
	Methacrylic acid
	N-Alkylmethacrylamides
	N-Alkylacrylamides
	N,N-Dialkylacrylamides
	N,N-Dialkylaminoethyl methacrylates
Cross-linking agents	Ethylene dimethacrylate (EDMA)
	N,N-Methylenediacrylamide
	Diethyleneglycol dimethacrylate

and subsequently water content in the resulting hydrogels *(83, 85)*. In comparison to free radical polymerization *(89, 90)*, controlled/living polymerization (e.g., RAFT *(91, 92)* and ATRP *(93, 94)*) enable researchers to prepare (co)polymers with better defined molecular architecture. In addition, facile click-chemistry *(95)* is gaining ground in building precisely controlled copolymers and hence "click-gels" *(96)*.

In contrast, physical hydrogel networks are interconnected via non-covalent interactions, which include molecular rcognition, ionic interactions, crystallization, hydrophilic and hydrophobic interactions, hydrogen bonds, and protein interactions *(87)*. Therefore, the chemical issues of cross-linking agents involved in covalent hydrogels are avoided *(87, 98)*. These hydrogels are oftentimes composed of different classes of building blocks with different mixed origins (natural vs. synthetic); if so, they can be also classified as hybrid hydrogels *(99, 100)*. As illustrated in the following sections, self-assembly of natural building blocks are commonly used as reversible cross-linking mechanism responding to various stimuli. Here physical hydrogels are reviewed in further details, with an emphasis on hybrid hydrogels containing protein/peptide components due to our research interest.

1.3.1. Coiled-coil mediated physical hydrogels

Kopeček's group pioneered research in physical hybrid hydrogels containing coiled-coil folding motifs *(22, 99)*. In 1999 *(22)*, this group first empirically proved that self-assembly of coiled-coil motifs into supercoils could be employed as physical cross-linkers in hydrogel formation: two genetically engineered His-tagged coiled-coil motifs composed of a natural protein sequence (CC1, 255 amino acids, a.a.) and a *de novo*

designed sequence (CC2, 72 a.a.), respectively, were chelated onto a hydrophilic *N*-(2-hydroxypropyl)methacrylamide (HPMA, Figure 1.3) copolymer backbone via Ni^{2+} ions; these motifs self-assembled into tetramers and cross-linked the linear copolymer, forming physical gel networks. Moreover, swelling dynamics of resulting hydrogels shared temperature-responsiveness at similar transition temperatures of corresponding peptides; in other words, properties of the peptide component could be superimposed and integrated into the final hybrid materials. Further studies *(101)* showed that tailor-made stimuli-responsiveness of such hydrogels could be achieved by manipulating primary structure of these coiled-coil forming peptides, such as sequence (coiled-coil vs. noncoil-coil domains), length (number of coiled-coil domains), etc. Physical hydrogels self-assembled from di- and tri-block polypeptides containing coiled-coil peptide blocks were also developed by the same group, and gel swelling kinetics were successfully adjusted by proper arrangement of peptide blocks *(59, 102)*. A common feature of these physical hydrogels is that peptides employed were generally long (>70 a.a.), and genetically engineered and biologically synthesized.

Enlightened by these successes, Kopeček's group continued with the "next generation" coiled-coil mediated physical hydrogels, with the peptide component of significantly shorter sequence by chemical synthesis. Coiled-coil sequences containing only three to five heptads were designed and synthesized using solid-phase peptide synthesis, then grafted onto polyHPMA backbone through a polymer-analogue strategy; gelation studies revealed that coiled-coil forming peptides could be as short as four heptads (28 a.a.) to mediate efficient cross-linking of HPMA copolymer backbones *(103)*.

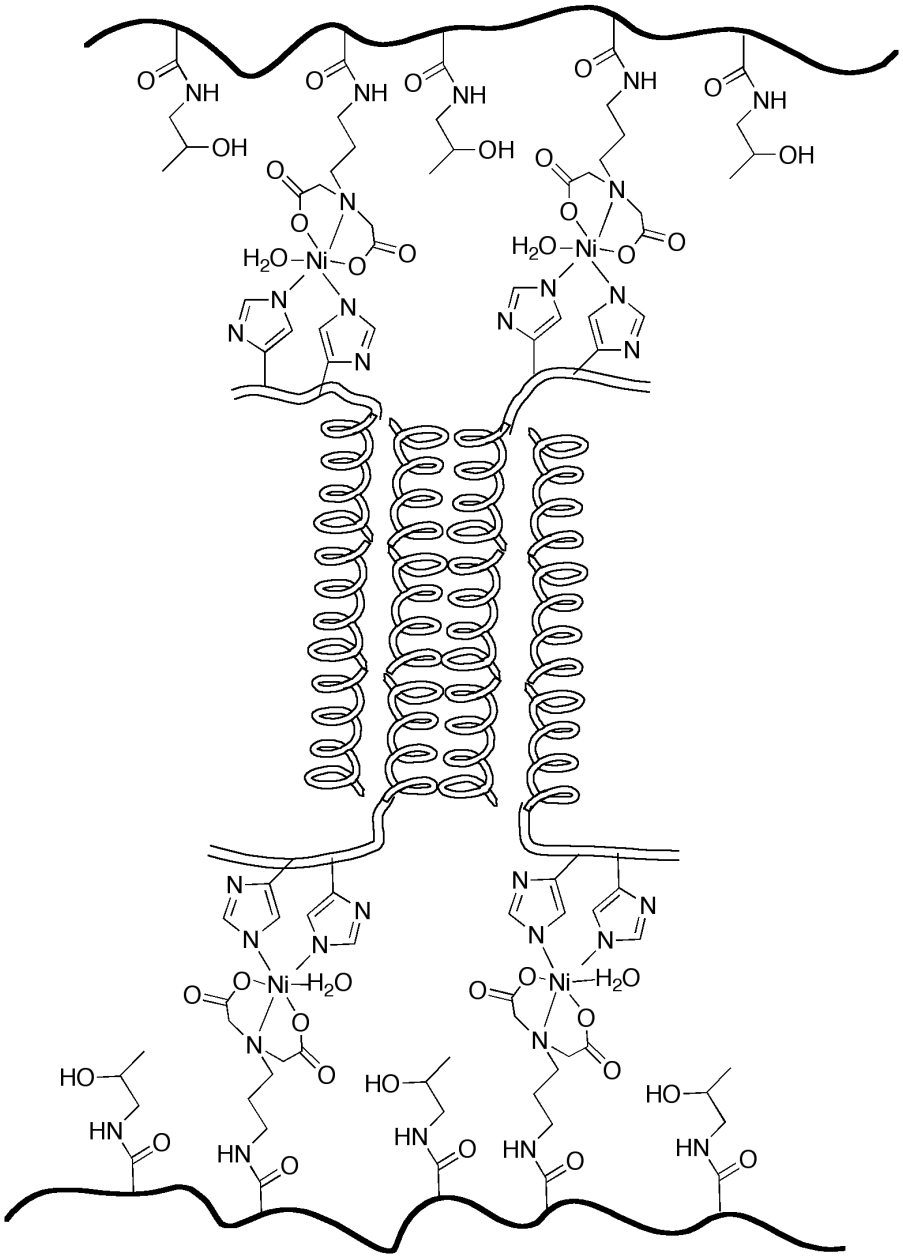

Figure 1.3. Hybrid hydrogel networks cross-linked by chelated coiled-coil motifs containing His-tags. Here the polymer backbone was poly(HPMA-co-DAMA) with pedant iminodiacetate groups for chelation with transition metal ions (e.g., Ni^{2+}). Coiled-coil forming peptides were attached with His-tags to chelate with the same metal ions. As shown, these motifs could form tetramers (one of the many possible confirmations) to physical cross-link the polymer backbones, resulting in hybrid hydrogel fromation. HPMA, *N*-(2-hydroxypropyl)methacrylamide; DAMA, *N*-(*N',N'*-dicarboxymethylamino propyl)methacrylamide. Adapted from reference *(22)*.

Similar to other coiled domains mentioned above, these short peptides self-associated into only homo-oligomers. To take one step further, a pair of complementary coiled-coil motifs (5 heptads in each), CCE and CCK, exclusively assembling into anti-parallel hetero-dimer, were designed and grafted onto polyHPMA backbone giving two complementary graft copolymers; upon mixing, two copolymers could reversibly self-assemble into hydrogels at concentrations as low as 0.1 wt%, which demonstrated excellent recognition between the two peptides; more interestingly, this design allowed the possibility of *in situ* hydrogel formation since individual components were water soluble *(104, 105)*. A general scheme of coiled-coil mediated physical hydrogels is shown in Figure 1.4a.

In this dissertation a continuous effort in building coiled-coil mediated physical hydrogels is described. Coiled-coil motifs of different lengths (3-5 heptads) were designed to form homooligomers as physical cross-linkers for gel formation. A new synthetic strategy, macromonomer copolymerization, was developed to prepare polyHPMA grafted with coiled-coil motifs; as possible influencing factors on gel formation, peptide sequences, copolymer concentration and environmental temperatures were scrutinized.

There are several intriguing features of coiled-coil mediate hybrid hydrogels in comparison to other monocomposition hydrogels. As pointed out above, the resulting hybrid constructs can possess unique properties by superimposing desired properties of both synthetic and peptide components *(22)*, which allows these hybrid hydrogels to synergize the advantages of both traditional and protein-based hydrogels while minimizing their shortcomings *(106)*: this synergism leads to stimuli-responsiveness not

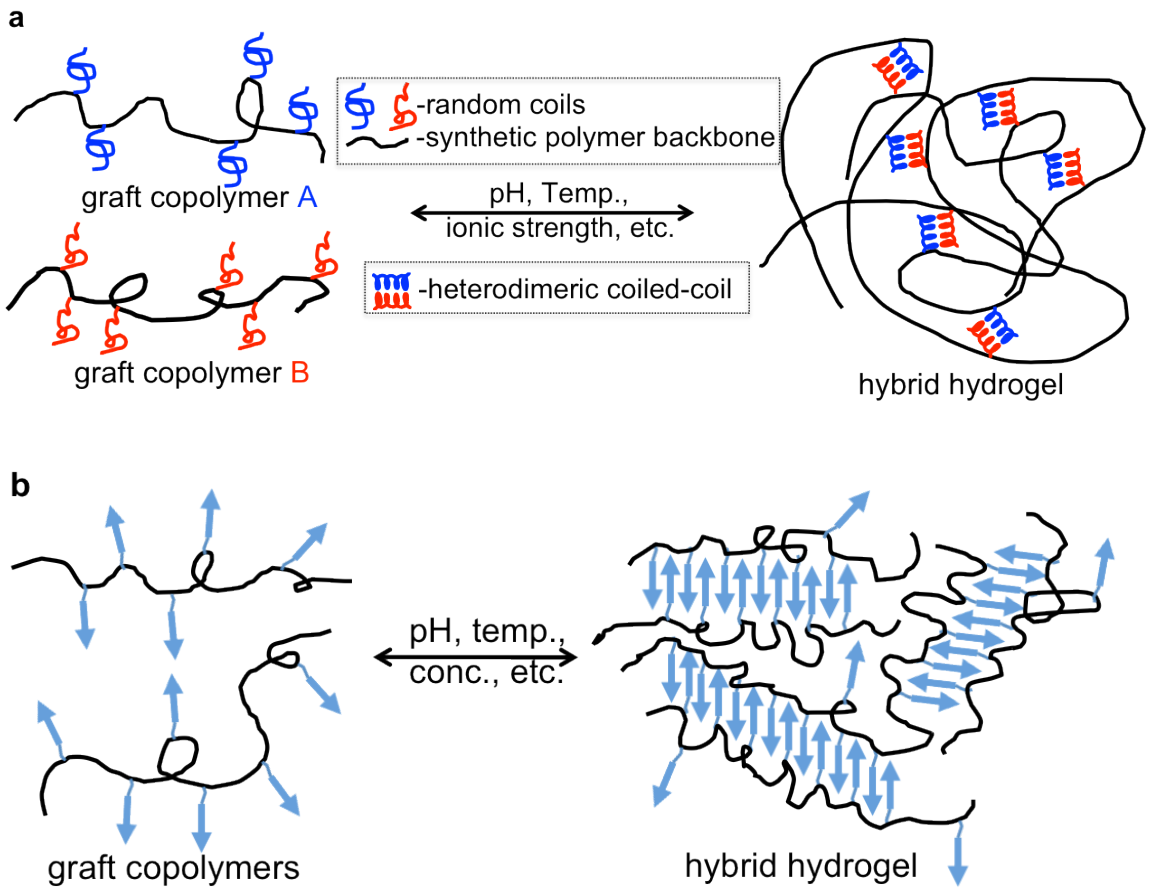

Figure 1.4. Typical hybrid hydrogels: a) coiled-coil mediated self-assembly of hybrid hydrogels; b) β-sheet mediated self-assembly of hybrid hydrogels.

only to conventional stimuli (e.g., temperature and pH) but also biomolecules, minimized immunogenicity, improved biocompatibility, and even novel biofunctions.

1.3.2. β-sheet mediated physical hydrogels

β-sheet is another commonly seen protein folding pattern and consequently a possible cross-linking mechanism for physical hydrogel construction *(23, 107)*. Indeed, β-sheet forming polypeptide-based hydrogels have been well studied *(108-110)* for various applications, such as drug delivery and tissue engineering *(107)*. As part of our research interest, hybrid hydrogels mediated by this folding pattern are briefly summarized here.

Stewart and colleagues *(111)* built a thermo-responsive hybrid hydrogel by using β-sheet forming domain, titin immunoglobulin (Ig) module (I28, 111 a.a.), to cross-link linear polyacrylamide copolymers with the help of metal complex formation between nickel ions and pendant nitrilotriacetic acids (NTA); hydrogels obtained could experience an unusual positive swelling with elevated temperature (from 35 to 85 ^{o}C). Kopeček's group *(112)* developed a diblock copolymer containing a β-sheet peptide (11 a.a.) segment and hydrophilic polyHPMA block that could self-assemble into fibrils; although the resulted architecture was not a hydrogel network, this study revealed the possibility of using short β-sheet peptides to construct self-assembling supermolecules and laid a foundation for further research in hybrid hydrogels. In addition, Tzokova et al. *(113)* found that a similar construct composed of poly(ethylene oxide) conjugated with β-sheet forming peptide (4 a.a.) could self-associate into soft hydrogels due to extra entanglements of the resulting β-sheet nanotubes. Indeed, a short while later Kopeček's

group reported *(114)* the success of preparing hybrid hydrogels mediated by self-association of β-sheet domains. In the design, a short peptide (Beta11, 11 a.a.) with strong propensity for β-sheet formation was designed and further randomly grafted onto polyHPMA backbone via polymer-analogue reactions; evaluation of resulting graft copolymers revealed that Beta 11's β-sheet tendency was preserved and could cross-link polymer backbones leading to hydrogel formation, a process dependent on several factors (e.g., temperature, copolymer concentration and graft density). Currently, a similar approach is being explored to construct a hydrogel scaffold to facilitate template-directed biomineralization, based on the fact that acidic proteins in β-sheet conformation are involved in bone formation *(115)*. An example of hybrid construct containing β-sheet peptides was depicted in Figure 1.4b.

Other protein domains or peptide motifs have also been exploited regarding their incorporation into physical hydrogels. For example, calmodulin and elastin-like peptides were employed to develop reversible hydrogels, drug delivery systems and biosensors, as reviewed by Banta and colleagues *(116)*.

1.3.3. Other physical hydrogels

As a typical example of ionic interaction mediated hydrogels, negatively charged alginate at physiological pH can be cross-linked by Ca^{2+} ions and the resulting gels have been used for protein drug delivery and living cell encapsulation *(98, 117)*. Stereocomplex formation can also mediate physical gelation as reported by Hennink's group: hydrogels was prepared by mixing dextran grafted with D- and L-lactic acid (low molecular weight) oligomers in aqueous solution *(118);* bioactivity of an enzyme

(lysozyme) could be preserved after being released from such hydrogels *(119)*. Physical hydrogels can also self-assemble from amphiphilic block and graft copolymers: for instance, poly(ethylene glycol)-block-poly(trimethylene carbonate) (PEG-b-PTMC) copolymer was developed as thermogelling material which could experience a sol-gel transition as temperature elevated, and transition temperatures could be manipulated by adjusting molecular weights of the blocks and polymer concentrations *(120)*.

Biomolecular complexes, products of specific biorecognition between biomolecules, can also serve as reversible physical cross-linkers in hydrogel construction *(121)*. Vinyl modified concanavalin A (Con A, a lectin binds glucose with a $K_d \approx 10^{-6}$ M) was copolymerized with glucosyloxyethyl methacrylate (GEMA) resulting in a slightly cross-linked interpenetrating network (IPN) with both chemical and physical (complex of Con A and glucose) cross-linkers, thus Con A was covalently immobilized in polymer network; in comparison to the physically entrapped Con A hydrogel network, the resulting hydrogels could experience reversible swelling in response to glucose and was a promising insulin delivery system in treatment of type I diabetes *(122)*. To explore the reversible binding of antibody and antigen, vinyl derivatives of rabbit IgG and goat anti-rabbit IgG were prepared and a semi-IPN composed of these two macromonomers was built using *N,N'*-methylenebisacrylamide (MBAA) as chemical cross-linker; results showed that the resultant hydrogels displayed swelling reversibility in concert with concentration change of free native rabbit IgG *(123)*. Following a similar strategy, Con A and antibody were molecularly "imprinted" into a hydrogel network, which could specifically respond to α-fetoprotein (AFP), a tumor-specific glycoprotein; reversible formation of lectin-AFP-antibody complex in response to free AFP was the cross-linking

mechanism rendering reversibility of the resulting hydrogels, which can be used as a biosensor for diagnosis of hepatoma and cirrhosis *(124)*.

1.4. Affinity ligand pairs in pharmaceutics: pretargeted anticancer therapeutics and prodrugs

Conceived by Reardan et al. in 1985 *(125)*, pretargeting strategy was developed to improve treatment efficiency of anticancer agents while minimizing their side effects *(126-129)*. Focusing on anticancer applications, general principle for pretargeting is to specifically deliver the originally nonspecific effectors to tumors with the help of tumor-specific moieties and even secondary helper molecules. Currently, there are two well-studied directions following this strategy: pretargeted therapeutics/diagnostics and (pre)targeted prodrugs. In both scenarios, biorecognition between components (e.g., antigen-antibody and enzyme-substrate) plays a critical role leading to the final therapeutic effects. As a critical strategy adopted in this dissertation, pretargeted therapeutics are comprehensively reviewed in section 1.4.1 below. Targeted prodrugs, as an important concept and reference for our research, are briefly summarized in section 1.4.2.

1.4.1. Pretargeted anticancer therapeutics

The working philosophy for pretargeted anticancer therapeutics is to consecutively administer tumor-specific targeting moiety containing a recognition component (pretargeting agent), followed by a modified active therapeutic agent (effector) that can

directly or indirectly bind to that aforementioned recognition component; thus, effector is preferably accumulated specifically at tumor site leading to desired therapeutic effects, with unbound effector rapidly cleared out of the body to minimize undesired side effects *(130)*. Therefore, pretargeting requires minimally two targeting components *(131)*: a pretargeting agent to find tumor-specific target and to specifically bind to effector, and an effector to specifically interact with the former by specific affinity designs and subsequently to exert therapeutic effects. This dissociation of therapeutics from tumor targeting distinguishes pretargeting from conventional targeting. Since the concept of pretargeting initiated and intensively exploited in the area of readioimmunotherapy (RIT) and imaging, the following discussion is conducted within the same context.

There are three major systems widely explored to build pretargeted therapeutics *(129)*: streptavidin-biotin (Figure 1.5), bispecific antibody-hapten (Figure 1.6) and oligomer-complementary oligomer (Figure 1.7). For each combination, distinct strategies have been developed according to its unique biological features. No matter which combination and strategy are employed, there are some general principles *(132)* to follow in the design so that unique advantages of pretargeting are ensured.

Successful effectors should possess the following chemical and physiologic properties *(132)*. These chemical properties are low molecular weight (generally < 10 kDa), hydrophilic to be compatible with biological environment, rapidly diffusible into extracellular fluid, negatively charged to avoid nonspecific binding, high-specificity toward the recognition component, and easy to be labeled with radionuclide. Physiologically, effectors should be cleared rapidly by kidney, with minimal organ uptake, high glomerular filtration rate (GFR, >100 mL/min), low immunogenicity and

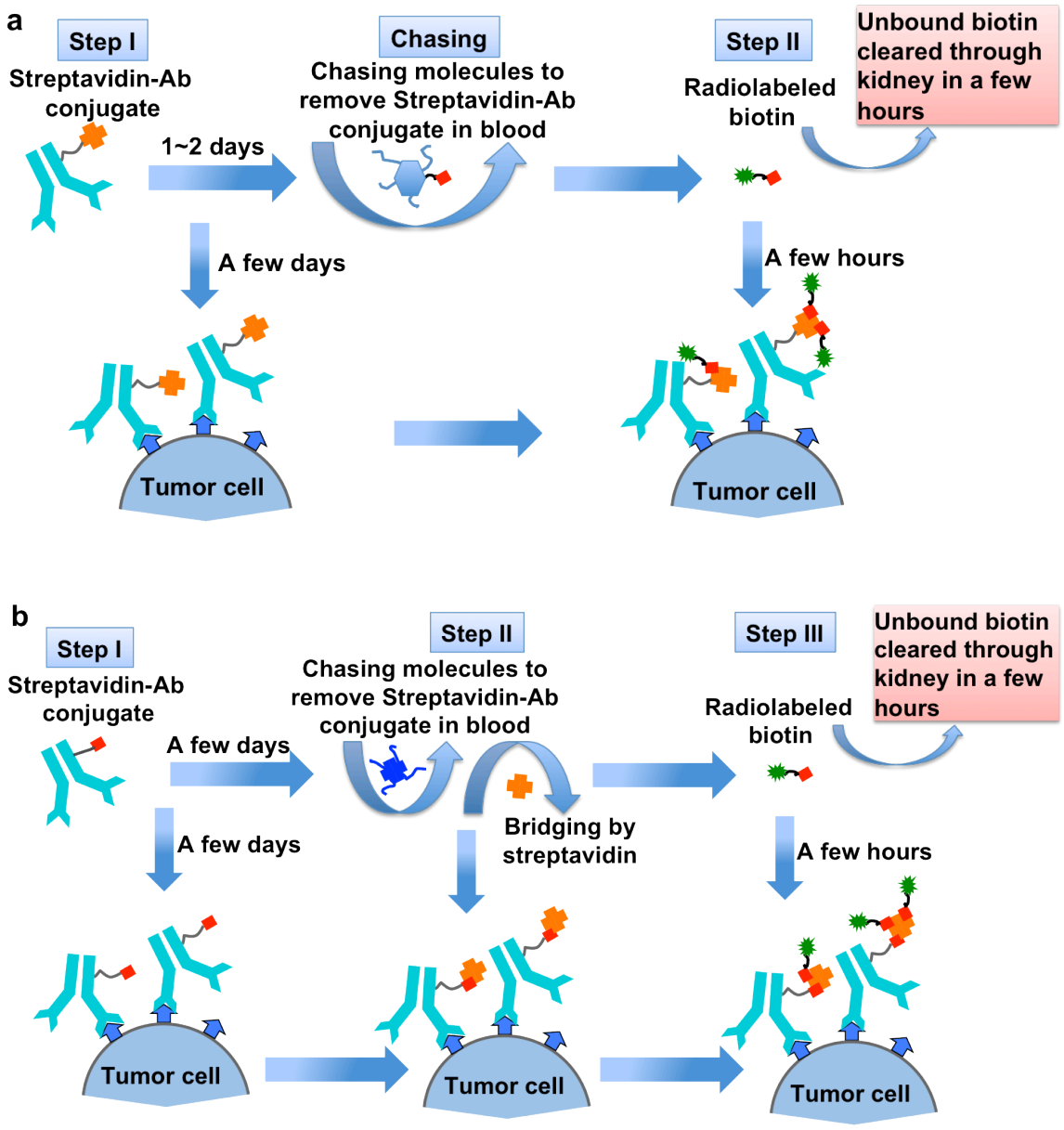

Figure 1.5. Streptavidin-biotin pretargeting strategies. a) Two-step strategy with streptavidin-Ab (StAv-Ab) as pretargeting agent and radiolabeled biotin as effector. In between a chasing step can be added to remove free (StAv-Ab) from blood so that maximum degree of effector binding to tumor cells can be achieved. Here galactosylated-biotin is shown as chasing agent. b) Three-step strategy with biotinylated-Ab as pretargeting agent, followed by chasing agent to remove free biotinylated-Ab from blood. Then streptavidin is injected to bind to localized biotins on cell surface, and finally radiolabeled biotin is administered. Here the chasing agent is avidin (a glycosylated protein). Adapted from references *(129,135)*.

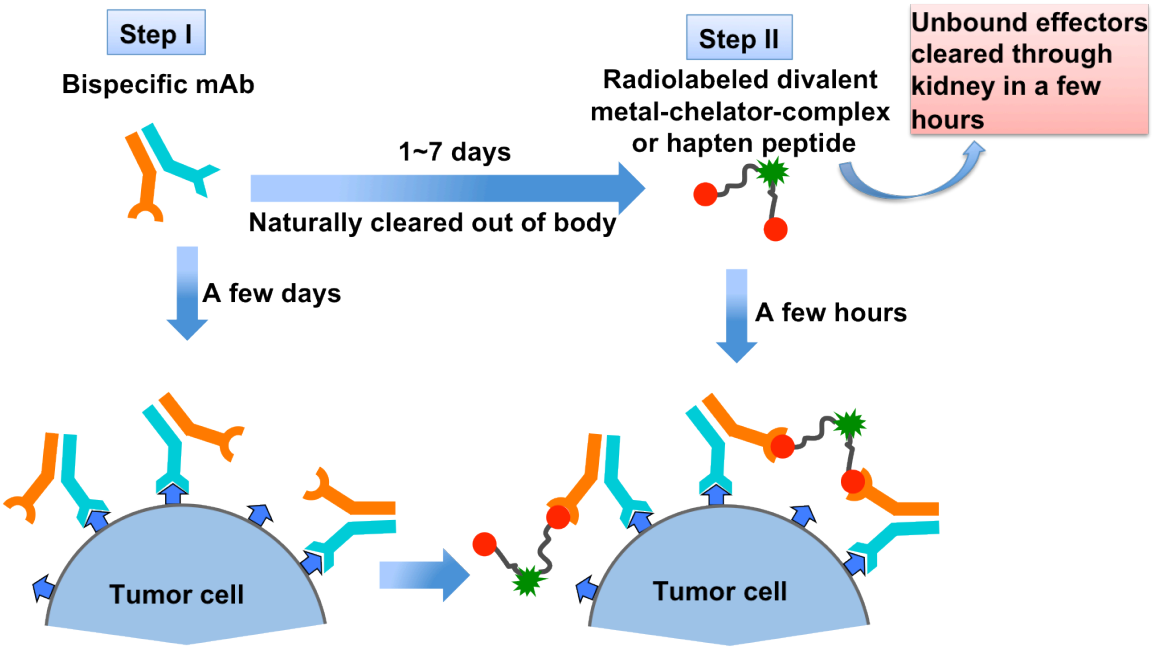

Figure 1.6. Bispecific mAb-effector pretargeting strategy. Here a typical two-step scheme is shown, using bispecific mAb and divalent effector. Bispecific mAb can both specifically recognize tumor-specific antigen and metal-chelator (e.g., DOTA) or hapten peptide (e.g., HSG). If a fusion protein is used as bispecific pretargeting agent, it may exhibit a rapid clearance from blood due to its smaller size in comparison to corresponding chemical Fab' X Fab' conjugate. mAb, monoclonal antibody. Adapted from references *(129, 135)*.

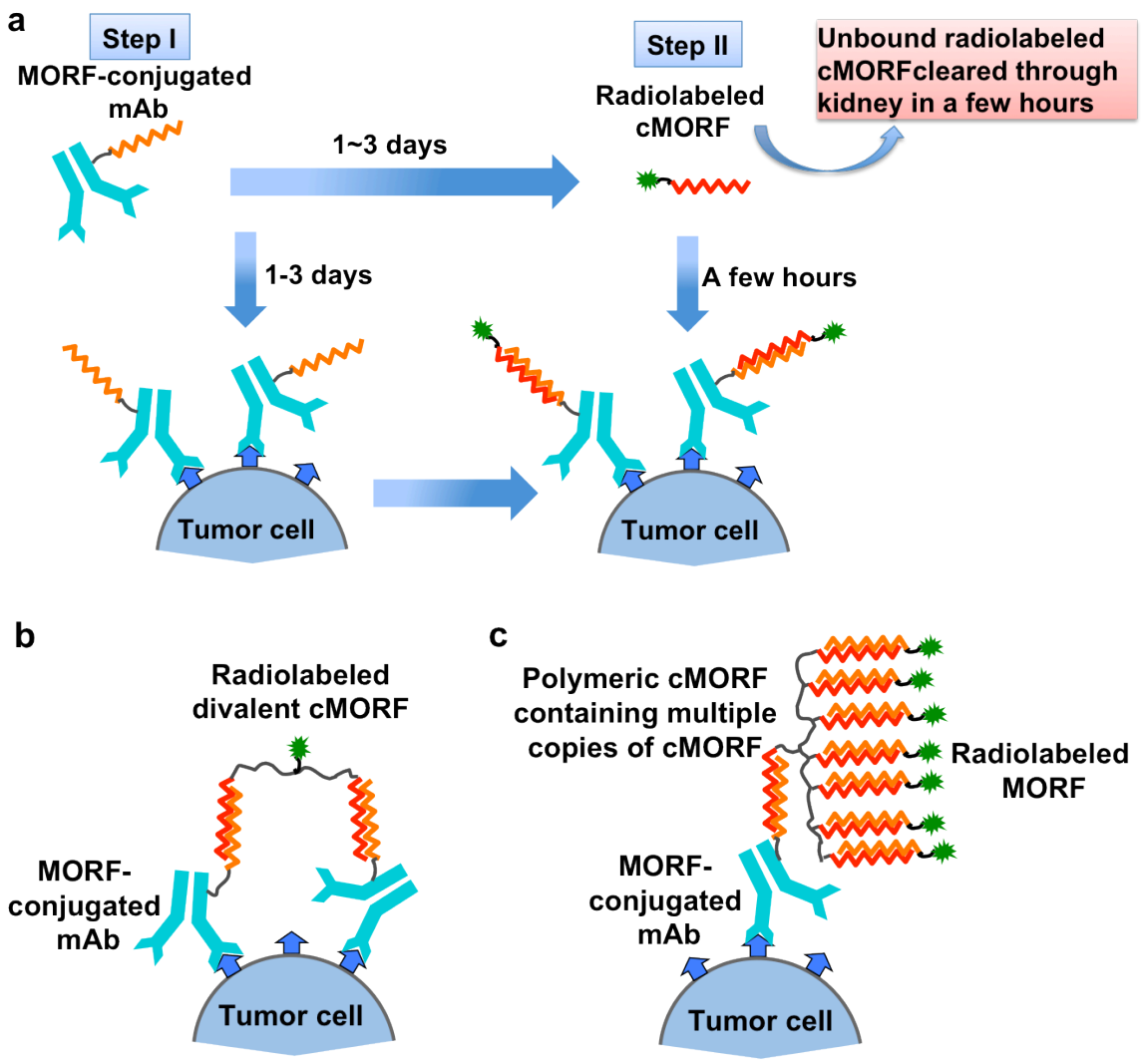

Figure 1.7. MORF-cMORF pretargeting strategies. a) a conventional pretargeting with two steps, containing MORF-conjugated mAb and monovalent radiolabeled cMORF; b) pretargeting with affinity enhancement effect due to divalent radiolabeled cMORF; c) pretargeting with multivalent amplification effect from a system containing MORF-conjugated mAb, polymeric cMORF, and monovalent radiolabeled MORF. MORF, phosphorodiamidate morpholino oligomer; cMORF, complementary MORF; mAb, monoclonal antibody. Adapted from reference *(129)*.

low protein-binding. Preferred properties of primary targeting moieties have no major difference from those for directly conjugated antibodies; however, modern pretargeting prefers genetically engineered antibodies over the randomly conjugated ones via cemical modification due to their high specificity, low immunogenicity, and uniform structure *(128, 133)*.

If these requirements are satisfied, pretargeted therapeutics can enjoy a superior advantage over their conventional counterparts (directly conjugated antibodies). Although directly radiolabeled monoclonal antibodies (mAbs) reach maximum tumor concentrations after 1-2 day, they circulate in the body for several more days, resulting in a low tumor/non-tumor (T/NT) ratio; consequently undesired damage to normal tissue results, especially to bone marrow. In pretargeting, "cold" pretargeting agents (modified mAbs) are not directly linked with radionuclides and their long-term presence does not induce toxicity; on the other hand, small radiolabeled effectors can find their pre-bound affinity targets within 1-3 h and nonlocalized ones are rapidly cleared from the body without accumulation. Therefore, pretargeting can achieve 2- to 3-fold enhancement of therapeutic agents over conventional targeting; if a chasing step is added to remove the free primary mAbs, the enhancement can be improved many fold *(130)*. In turn, accumulation to liver, spleen and bone marrow is greatly reduced, so is the toxicity *(132)*. Currently, pretargeted therapeutics are not perfect and limitations for different systems are discussed in corresponding sections.

1.4.1.1. Streptavidin-biotin system

Ultra-high affinity (K_d=10^{-13}~10^{-15} M) *(134)* between streptavidin (StAv, 60 kDa) and biotin (244.3 Da) makes them highly appropriate for pretargeting. Theoretically, both can be used as effectors; but the combination of radiolabeled StAv and biotinylated antibody (Ab) is not currently studied since the bulkiness of radiolabeled StAv leads to slow pharmacokinetics, violating the aforementioned design principles for effectors *(132)*. Therefore, the commonly seen effector is radiolabeled biotin; but the primary targeting agent can be StAv-Ab or biotinylated-Ab. Different strategies have been developed corresponding to different arrangements: two- and three-step strategies (Figure 1.5) *(135)*.

In two-step strategy (Figure 1.5a), StAv is conjugated to tumor-specific mAb via chemical conjugation or genetic engineering, and the resulting pretargeting agent (StAv-Ab) is first applied to bind tumor-specific antigen. Natural clearance of the unbound StAv-Ab can take up to several days due to their large sizes (~200 kDa) *(131)*, thus a chasing step (usually 1-3 days afterward) is often adopted to remove the residual from blood prior to the injection of effector; otherwise, the majority of the radiolabeled biotin will be retained in circulation without reaching the tumor site. For instance, galactose-coupled human serum albumin-biotin conjugate was designed for such a purpose: the albumin-biotin portion binds to StAv-Ab and blocks subsequent biotin binding; while the galatose portion serves for hepatocyte recognition so that the resulting complexes can be removed from blood and not compete for binding sites in the tumor *(136)*. Increasing the pretargeting interval achieves the same effect of clearing pretargeting antibody, but at a possible cost of reduced antibody expression because of internalization *(129)*. Finally,

"hot" biotin is administered, and localization of the effector to tumor and removal of the excess are obtained within a few hours, thanks to the rapid pharmacokinetics of effectors of small size *(137)*.

In a three-step strategy (Figure 1.5b), the pretargeting agent is biotinylated-Ab binding first onto tumor cells. Later an intermediary step is employed: injection of avidin (Av, the glycosylated analogue of StAv) to remove excess pretargeting agent (chasing), followed by the administration of StAv to bind to localized biotin (bridging). After a suitable interval (~1 day) for the body to remove Av and StAv, radiolabeled-biotin is applied and localized localized in tumor, bridging by the tetravalent StAv.

Pretargeting based on StAv-biotin is mainly used for RIT and imaging. Karacay et al. *(137)* developed a two-step StAv-biotin system and tested its therapeutic efficiency in colorectal cancer. In their design, a chemical conjugation method was adopted to prepare the pretargeting agent – StAv-MN14 (an anti-carcinoembryonic antigen (CEA) mAb), with biotin-D-peptide-DOTA -^{111}Indium (In) as effector and WI2 mAb (an anti-idiotype Ab) as chasing agent. *In vivo* results *(138)* demonstrated high tumor to blood ratio of the effector as 11:1 and 178:1 after 3 and 24 h, respectively; however, tumor accumulation of the effector via pretargeting was lower than the directly labeled Ab possibly due to the high concentration of endogenous biotin in mice and enhanced uptake of the effector by liver and kidney. ^{90}Yttrium *(139)* was also chelated to biotin as effector and genetic engineering allowed for the production of StAv-mAb fusion protein *(81, 140)* as a new generation pretargeting agent. Some of these newer pretargeting modalities are in clinical trials *(141)*. Three-step pretargeted therapeutics are also tested for cancer radiotherapy in patients *(135)*.

Overall, these pretargeting systems did display significant enhancement of T/NT ratio; however, this did not necessarily lead to high tumor retention of effectors (only ~20%) because rapid pharmacokinetics of effectors resulted in fast clearance and left insufficient time for desired target binding *(135, 138)*. This is actually a common issue for most pretargeting systems due to the unique design of effectors *(131)*. Specific to StAv-biotin systems, the immunogenicity of StAv is another major limit for their future application *(131)*.

1.4.1.2. Bispecific antibody-hapten system

First proposed by Reardan *(125)*, the other mode of pretargeting is to use bispecific Abs as pretargeting agents to localize radiolabeled effectors. A typical two-step scheme is illustrated in Figure 1.6: bispecific mAb is first administered and several days (1~7 days) are given to allow for binding and removal of excess mAb, where a chasing can be incorporated to facilitate the removal; then radiolabeled divalent effector is introduced, and tumor localization and residual removal are obtained within a few hours.

There are two ways to construct bispecific mAbs needed for pretargeting. A typical one *(135)* is chemical conjugation of Fab' fragments of mAbs (Fab' X Fab'), one against tumor-specific antigen and the other against effector, as first reported by Reardan et al. about 25 years ago *(125)*. This method results in an architecture equivalent to $F(ab')_2$ with a molecular weight around 100 kDa. Due to their bulkiness, removal of these bispecific mAbs from blood can take several days, before the injection of effectors *(135)*. Fortunately, genetic engineering enabled researchers to prepare bispecific mAbs in a form of fusion proteins with uniform chemical structures, ease of manufacture,

dramatically smaller sizes and subsequently preferred clearing kinetics. Rossi et al. *(142)* produced two bispecific diabodies (~50 kDa) and two bispecific trivalent binding proteins (~80 kDa) using *E. coli*., and these fusion proteins can specifically bind with CEA and HSG (histamine-succinyl-glycine, a hapten peptide). Indeed, majority of the diabodies could be cleared out of blood within 8 h while preserving similar binding affinities toward targets as corresponding chemical Fab' X Fab', and tumor-to-blood ratio was improved more than 20 times. Using such bispecific mAbs, a chasing step is not needed any more. Additionally, fully humanized bispecific mAbs will be able to avoid immunogenicity *(143)*, in comparison to the troublesome immunogenicity of StAv.

Besides tumor-specific antigen, bispecific mAbs need also to bind specifically to effectors. The exact effector target can be metal chelates (e.g., indium-ethylenediaminetrtraacetic acid, In-EDTA) or hapten peptides (e.g., HSG). Targeting at chelates may restrict these bispecific mAbs to only certain chelate complexes *(126)*, since the binding affinity between chealtor and corresponding antibody could be dramatically compromised by swapping radionuclides (e.g., from indium to gallium) *(125)*. An alternative is to use peptide haptens that allow for specific recognition for certain mAbs and chemical modification, but are not directly responsible for chelation. Thus, a flexible and universal effector platform compatible with various radionuclides (e.g., ^{90}Y, ^{111}In, ^{177}Lu and ^{99m}Tc) can be built *(143)*.

In contrast to the ultra-high affinity between StAv and biotin, binding between bispecific mAbs and haptens (or metal chelators) is weaker by 4-5 magnitudes ($K_d \approx 10^{-9}$ M). Therefore, effector valency is of great importance in determining tumor uptake and retention. Compared to monovalent effectors, divalent effectors can form more stable

complexes with bispecific mAbs, leading to higher tumor uptake *(144, 145)*, known as affinity enhancement effect *(129)*. Currently, the majority of the bispecific pretargeting systems employ divalent effectors, as show in Figure 1.6. In addition, multivalent bispecific mAbs *(146)* may further improve effector accumulation and T/NT ratio, as demonstrated by Rossi, et al. *(147)*: a trivalent fusion protein (hBS14, ~80 kDa) was produced to contain two binding sites for CEA and one for HSG; high tumor uptake of effector (^{111}In-bivalent HSG hapten, IMP-241), was observed and preferred T/NT ratio was achieved 3 h after injection.

1.4.1.3. Oligomer-complementary oligomer system

To dodge possible immunogenicity of the former two pretargeting systems, a new dimension of pretargeting was formulated using complementary oligonucleotides and different oligomers were designed and tested for such purpose *(148, 149)*. However, most of them were unsuccessful for different reasons, such as instability to nucleases, non-specific binding to serum and proteins, and even insolubility in aqueous solution *(150)*. In contrast, morpholino oligomers (MORFs) stood out with enhanced stability and acceptable water solubility *(151)*, and became widely used for pretargeting. Different pretargeting strategies based on MORFs are summarized in Figure 1.7: (a) conventional pretargeting with two steps, (b) pretargeting with affinity enhancement effect; (c) pretargeting with multivalent amplification effect.

In conventional two-step pretargeting (Figure 1.7a), MORF-conjugated mAb is prepared as pretargeting agent and applied first; after 2-3 days, radiolabeled cMORF is administered and localization can be measurably achieved around 3 h *(150, 152-156)*.

This is the most intensively studied modality due to its simplicity. Similar to the bispecific mAb pretargeting system, radiolabeled divalent cMORF is proposed to further enhance tumor uptake *(129)*, as depicted in Figure 1.7b. The third modality (Figure 1.7c), also called amplification targeting, is formulated based on a proof-of-concept studies from Hnatowich's group *(157, 158)*: after MORF-mAb, a polymeric cMORF construct containing multiple copies of cMORF is introduced as a intermediary bridging agent; then radiolabeled MORF is injected and subsequently radioactivity at tumor site should be amplified due to the multivalency effect. Research on the last two strategies is still on going.

In Chapter 3 and 4, we proposed a novel pretargeting system using specific biorecognition between a pair of complementary coiled-coil motifs to bridge Fab' fragment and effector. Similar to the concept of amplification targeting, our effector was a polymeric construct containing multiple copies of coiled-coil motif, and the pretargeting agent was Fab' fragment (anti-CD20 mAb) conjugated with one copy of the complementary motif. More importantly, our system contained neither radionuclide nor anticancer drug *(30)*.

1.4.1.4. Coordinating pretargeting agent and effector

In contrast to conventional targeting with direct linking of mAb and therapeutics, the biggest challenge for pretargeting is to coordinate the pretargeting agent and effector, mainly the interval between administrations and dosages. To do so, four variables need to be considered for typical two-step strategy: dosage of pretargeting agent, waiting duration prior to effector injection, dosage of effector, and waiting duration prior to

evaluation/detection. If chasing step is added or three-step strategy is employed, more factors will be involved for coordination. Currently, researchers are mainly relying on trial and error method to conduct optimization *(129)*. Focusing on relatively simpler two-step MORF system, Hnatowich's group *(129, 155, 156)* proposed a semiempirical model trying to quantify the following factors: maximum percent and absolute tumor accumulation (MPTA and MATA) of effector, antibody accessibility and tumor saturation dosage of effector. This model can be an excellent reference for the optimization of our system described in Chapter 3 and 4, because of the similarity of the two.

1.4.2. Targeted prodrugs

Targeted prodrugs are designed to selectively deliver therapeutics to tumor site, so as to minimize side effects; in comparison, classical prodrugs aim to improve poor physicochemical properties (e.g., solubility and stability) of the active form *(127)*. Both covalent and noncovalent linkage and active and passive targeting are employed in designing targeted prodrugs. Here, some typical examples are briefly discussed to demonstrate the current trends in targeted prodrug development; a comprehensive review can be found in reference *(127)*.

The first example is a prodrug containing two components (carrier and targeting agent) that are noncovalently interacting with each other, with the cargo physically entrapped inside the carrier. Similar to pretargeted anticancer therapeutics, active targeting is employed. Gaidamakova and colleagues *(128)* developed a "molecular vehicle for target-mediated delivery of therapeutics" using a binary system: vascular

endothelial growth factor (VEGF) fused with a peptide (15 a.a.) as recognition tag, and a polyethyleneimine (PEI, DNA carrier) conjugated with a protein fragment (adapter) recognizing the tag. During the application, these two components were mixed first to form a complex (PEI-VEGF) via specific recognition between the tag and adapter; and cargo DNA was physically loaded onto the carrier beforehand. DNA in turn was selectively delivered to cells expressing VEGF receptors (VEGFR-2) on the surface. *In vitro* evaluation showed 3-15 times of VEGFR-2-mediated enhancement of luciferase (reporter protein) activity in VEGFR-2^{+} cells than in VEGFR-2^{-} cells. In the design, authors successfully avoided chemical modification to targeting molecules so that such a platform (fused tag-conjugated adapter) could be universal for delivery of other cargos. Philosophically speaking, this system was equipped following pretargeting concept but delivered via conventional targeting fashion.

Another example falls in the category of antibody-directed enzyme prodrug therapy (ADEPT). Similar to typical pretargeting, ADEPT is a two-step strategy *(159, 160)*. First a construct of tumor-specific mAb and prodrug-activating enzyme (conjugate or fusion protein) is applied and actively located in tumor; after the enzyme is cleared from circulation, an inactive prodrug (substrate of the enzyme) is systemically given and selectively activated at tumor site to kill cancerous cells. The enzyme should be exogenous or expressed at a low concentration to limit the release of active drug at non-target; the prodrug should be a noncytotoxic substrate specific for that enzyme, and its active form should be small, diffusible and potent with bystander effect *(127)*. Francis et al. *(161)* conducted a phase I clinical trial to examine the efficiency of an ADEPT on CEA expressing tumors. In their studies, a conjugate (A5CP) was constructed by linking

$F(ab')_2$ fragment of A5B7 (a mouse anti-CEA mAb) and CPG2 (a bacterial enzyme carboxypeptidase); and the prodrug employed was ZD2767P (bis-iodo phenol mustard). Results showed that 26 out of 27 patients responded to the therapy, and ZD2767P was cleared rapidly from blood and no active drug was detected in circulation; however, the enzyme conjugate was not sufficiently localized in tumor, and human anti-mouse and anti-carboxypeptidase antibodies were produced in response to the enzyme conjugate. Therefore, a chasing step may be needed to reduce the immunogenicity or a more efficient targeting agent must be designed.

Prodrugs can also passively target tumor, taking advantage of the leaky vasculature and impaired lymphatic drainage in tumor tissue, both of which allow macromolecules and nanoparticles to penetrate and accumulate in tumor, known as enhanced permeability and retention (EPR) effect proposed by Maeda and colleagues *(162, 163)*. Kopeček and Duncan developed an HPMA copolymer conjugated with doxorubicin (DOX) via an enzyme-cleavable peptide linker (Gly-Phe-Leu-Gly, GFLG), and the final conjugate was designated as PK1 or FCE28068 *(164)*. PK1 has a molecular weight of 28 kDa (DOX, 8.5 wt%); GFLG is stable in plasma *(165)*, but subject to intracellular cleavage by lysosomal cysteine proteinase *(166)* that releases DOX. During application, the prodrug is passively targeted and retained in tumor due to EPR effect, and further uptaken by tumor cells via pioncytosis. Subsequently, the conjugated DOX is liberated in lysosomal compartment upon cleavage. In phase I clinical trial, PK1 demonstrated antitumor effect with attenuated dose-limiting toxicity in comparison to intact DOX *(163)*. This prodrug is now in phase II clinical trial *(167)*.

1.5. Cell death

Cell death plays a vital role in the development and homeostasis of organisms. There are two major types of mammalian cell death according to the widely used classification: apoptosis and necrosis *(168)*. However, recently discovered autophagy and cornification are considered as the third and fourth types of cell death. According to the definition of programmed cell death, apoptosis, autophagy and cornification are genetically controlled. Additionally, there are some atypical cell death modalities, including mitotic catastrophe, anoikis, excitotoxicity, Wallerian degeneration, pyroptosis, paraptosis, pyronecrosis, and entosis *(169)*. Cross-talk among different mechanisms are commonly seen. For instance, necrosis can be initiated or controlled by the programmed mechanisms under certain circumstances *(170)*. Accumulating knowledge about cell death has greatly facilitated the development of new therapeutic strategies for diseases.

1.5.1. Apoptosis

Apoptosis ("leaves falling from trees") was coined by Kerr et al. *(171)* to describe a specific series of morphological changes during cell death (Table 1.3). It is a form of programmed cell death, but not a synonym of programmed cell death.

Opposite to the effect of pleomorphoic adenoma gene producg (PLAG) *(172)*, activation of caspases sentences cells to one of the two distinct but convergent pathways: death-receptor (extrinsic) and mitochondrial (intrinsic) apoptotic pathways *(173)*. Death-receptor pathway involves the binding of death ligand (e.g., tumor necrosis factor (TNF)) to death receptor, subsequent formation of death-inducing signaling complex (DISC) and the activation of caspase 8, a central initiator of apoptosis. Activated caspase 8 can either

Table 1.3. Different cell death modalities. Adapted from Reference *(169)*.

Cell death modality	**Morphological features**
Apoptosis	Cell rounding-up Pseudopods retraction Cell and nucleus shrinkage (pyknosis) Nuclear fragmentation (karyorrhexis) Cytoplasmic organelles modification Plasma-membrane blebbing Engulfment by phagocytes
Autophagy	Absence of chromatin condensation Sequestration of cytoplasmic materials Formation and accumulation of double-membraned autophagosomes Little or no association with phagocytes
Necrosis	Cell and organelle swelling (oncosis) Rupture of surface membranes Spillage of cell contents Moderate chromatin condensation

directly activate caspase 3 (executor of apoptosis) or be detoured to mitochondrial pathway. In mitochondrial pathway, caspase 8 or intracellular stress induces the release of cytochrome *c*, which in turn activates caspase 9 (another initiator of apoptosis) through apoptosome. Activated caspase 8 and 9 share the same duty: activating caspase 3. Bcl-2 family proteins are the gatekeepers for apoptosis and they can be either death antagonists (e.g., Bcl-2 and Bcl-w) or agonists (e.g., Bax, Bak and Bad) *(174)*.

Apoptosis is the most thoroughly studied cell death mechanism and there is a collection of tools to qualify and quantify apoptosis. Microscopy is frequently used to visualize the morphological features of apoptotic cells and flow cytometry (e.g. fluorescence-activated cell sorting, FACS) is intensively used to quantify apoptosis *(169)*. Facilitated by flow cytometers, several standardized analysis methods were developed: caspase 3 activity assay *(175)*, terminal transferase dUTP nick end labeling (TUNEL) assay *(176, 177)*, and Annexin V/propidium iodide (PI) staining *(178, 179)*.

1.5.2. Autophagy

Autophagy ("to eat oneself") is a closely regulated lysosomal self-digestion process in which cells recycle and consume their own nonessential, redundant or damaged organelles and macromolecular components *(168, 180)*. Corresponding morphological features of autophagy are delineated in Table 1.3. Initially as a pro-survival pathway, autophagy can steer cells through nutrient deprivation or damages; but if the stress or damage is too severe to overcome, cells may die through apoptosis *(180)*. This a typical example of cross-talk between autophagy and apoptosis, which are acting in concert and counteracting each other at the same time *(181)*.

1.5.3. Necrosis

Necrosis (necroptosis) is manifested in cell and organelle swelling (oncosis), and rupture of plasma membrane and subsequent spilling of intracellular contents *(168, 169)*. Key features of necrosis are also listed in Table 1.3. Although considered as uncontrolled accidental form of cell death for a long time, growing evidence is suggesting that necrosis is also fine-tuned by some transduction pathways and catabolic mechanisms *(182)*. In contrast to apoptosis and autophagy, necrosis typically associated with inflammation caused by the spillage of cell contents.

1.5.4. Medical implications of apoptosis

The best-characterized apoptotic machinery has been revealed to play a critical role in many diseases, such as cancer, autoimmune disease, neurological disease, hepatitis, cardiovascular disease and sepsis *(168)*. In combating these diseases, two major strategies to modulate dysregulated apoptosis have been developed: induction and inhibition. For instance, Gleevec® was marketed to induce apoptosis by inhibiting tyrosine kinase to treat leukemia *(183)*, and Hycamtin® (topotecan) induces apoptosis by inhibiting topoisomerase I in ovarian cancer *(184, 185)*. Cyclosporine is being used to inhibit apoptosis in myocardial infarction by inhibiting mitochondrial permeability transition *(186)*.

1.6. Non-Hodgkin's lymphoma (NHL)

1.6.1. NHL overview

Non-Hodgkin's lymphoma (NHL) is a large group of lymphocyte (white blood cell) cancers, and it is one (6^{th}, projected in 2010 *(187)*) of the top ten cancers in the United States. NHL can occur to both sexes at any age and the age-adjusted incidence rate was 19.6 per 100,000 per year in 2007 *(188)*; and the projections for 2010 are 65,540 and 20,210 for new cases and deaths from NHL, respectively *(187)*. Common symptoms of NHL may include fever, unexplained weight loss, fatigue and larger than normal lymph nodes.

Classification of NHL is of great importance for reproducible diagnosis and subsequent treatments. Experiencing many classification systems and revisions, the current WHO classification (Table 1.4) has become a worldwide standard for clinicians and researchers *(189,190)*. This classification is mainly based on immunological features, genetic alterations and clinical characteristics of the disorders. In the United States, B-cell lymphoma, making up over 85% of NHL incidences, is much more common than its T-cell counterpart.

1.6.2. NHL treatments

NHL pathogenesis, phenotype and stage altogether determine the selection of therapeutic regimens. The treatments currently available and in clinical trials can be roughly categorized as: local surgery *(191)*, chemotherapy *(192)*, radiotherapy/RIT *(193)*, biotherapy (mainly referring to mAb-based therapy) *(194)* , and immunotherapy (e.g.,

Table 1.4. Different types of non-Hodgkin's lymphoma (NHL). Summarized from references *(189, 190)*.

Category	**Name**
Lymphoid tumors of B-cell lineage	Precursor B-cell lymphoblastic lymphoma
	Follicular lymphoma (FL)
	Mantel cell lymphoma (MCL)
	Small lymphocytic lymphoma (SLL)/ Chronic lymphocytic leukemia (CLL)
	Marginal zone B-cell lymphoma (MZL)
	Extranodal marginal zone lymphoma of mucosa-associate lymphoid tissue (Extranodal MZL of MALT)
	Splenic marginal zone lymphoma (SMZL)
	Nodal marginal zone lymphoma (NMZL)
	Lymphoplasmacytic lymphoma (LPL)
	Diffuse large B-cell lymphoma (DLBCL)
	Burkitt's lymphoma (BL)
Lymphoid tumors of T-/natural killer-cell lineage	Precursor T-lymphoblastic lymphoma/leukemia
	T-cell prolymphocytic leukemia (T-PLL)
	T-cell large granular lymphocytic leukemia (T-LGL)
	Aggressive natural killer-cell leukemia
	Adult T-cell leukemia/lymphoma
	Mycosis fungoides (MF)
	Others

vaccines) *(195)*. The combinations of these treatment modalities are frequently used to achieve better therapeutic outcomes.

Drug conjugates, especially polymeric drug conjugates, are promising in treating NHL. Polymeric modification can give a "facelift" for the anticancer agents with poorproperties. Such kind of improvement may include: 1) enhanced stability, 2) improved solubility, and 3) increased therapeutic effect with reduced side effects due to the EPR effect. Conjugation of L-asparaginase to PEG led to Oncaspar ®, which was approved by FDA in 1994 for NHL treatment; clinical trial results revealed that the enzyme's plasma half-life was extended from ~20 h (native) to ~360 h (conjugate) *(196)*, and pegylation indeed greatly decreased toxicity and hypersensitivity reactions *(197)*. Another well-studied anti-NHL drug conjugate is cyclodextrin-based polymer conjugate of camptothecin (IT-101): the native camptothecin (CPT) has poor solubility, and consequently high toxicity and low therapeutic efficacy; after conjugation to cyclodextrin, CPT's plasma half-life was prolonged from 1.3 to 17-20 h, preferential accumulation of the conjugate at tumor site was observed, and extended release of CPT from the conjugate was also achieved *(198, 199)*.

Recently, monoclonal antibody-drug conjugates (ADCs) have caused great attention and are considered as a new direction for fighting NHL *(200)*. A cohort of surface antigens for B-cell NHL has been identified: CD19, CD20, CD21, CD22, CD23, CD40, CD52 and CD80. Corresponding mAbs have been identified and explored for NHL treatment. Based on these antibodies, various ADCs have been developed and some are already in clinical trials. For example, calicheamicin was attached to inotuzumab targeting CD22, and the conjugate is now in phase I/II clinical trials; auristatin was

conjugated to brentuximab guiding the final ADC (SGN-35) to CD30 *(194)*. CD20-based ADCs will be discussed with further details in section 1.7.

1.6.3. Animal models for NHL study

Due to the prevalence of NHL, researchers have spent great effort finding an effective cure. Different animal models have been developed to simulate human NHL. Mice models are currently the best-established models to test different treatment modalities. This is mainly due to their low cost, ease of manipulation, and more importantly their surprisingly genetic similarity to human.

Currently two type of NHL mice models are in use: local solid tumor and systemic tumor models. Both models can be easily generated via s.c. and i.v. injection of lymphatic cells, respectively. The commonly used cell lines include Raji, Daudi, Ramos, Namalwa, Karpas 299 and L540 *(199, 201)*. In comparison, i.v. inoculation leads to a natural NHL model, a closer simulation of NHL in human body (non-localized and disseminated) *(202)*.

Two major strains of mice are commonly used in NHL study: athymic nude mice and severe combined immunodeficiency (SCID) mice. Athymic nude mice are mainly used to generate localized NHL tumor models after s.c. injection of tumor cells; the subsequent tumor size monitoring and tumor harvest are easy to be performed on these nude mice due to the absence of thick body hair *(199, 203)*. SCID mice, deficient in T- and B-cell functions, are generally considered permissive/tolerant for human tumor xenograft without rejection. Nonobese diabetic (NOD) *(204, 205)* and C.B-17 SCID *(206-208)* mice are two commonly seen strains used to construct systemic NHL models,

and they are developed to overcome the leakiness of the SCID mutation and the non-lymphoid specific mutation *(209)*. NOD SCID mice have all T, B and natural killer (NK) cell activities deficient; while C.B-17 SCID mice preserve the normal NK cell activity, which was reported to be helpful for the depletion of disease B cells upon treatment *(202)*. Therefore, C.B-17 SCID mice are a better choice at least for NHL studies and were employed in our *in vivo* experiments.

1.7. CD20 surface antigen

1.7.1. CD20 biology

CD20 is a nonglycosylated phosphoprotein of 33-37 kDa with four transmembrane domains, belonging to a membrane-spanning four-domains subfamily A (MS4A) *(210, 211)*. Its expression is restricted to the surface of nearly all (>95%) committed (normal and malignant) B-cells, and dramatically downregulated at the point of differentiation into plasma cells *(212, 213)*. However, it is not expressed on uncommitted hematopoietic progenitor stem cells *(213)* and plasma cells *(214)*, which implies that the normal B-cell homeostasis can be reestablished after treatment. In addition, CD20 is noninternalizing, nonshedding and noncirculating *(215)*. Thus it is considered as one of the most reliable phenotypic biomarkers for B-cell NHL and a very useful target for treating the same disease *(216-218)*.

CD20 can homo-oligomerize into dimer and tetramer *(219, 220)*. It is a substrate of and closely associated with tyrosine and serine kinases *(221, 222)*. It is also proved to be constitutively associated with lipid rafts in the cell membrane *(217, 223-225)*. Although there is no direct evidence of CD20 forming an ion channel, it has been strongly

suggested that CD20 is somehow intimately linked to store-operated calcium entry (SOCE) channels *(219, 226-228)*. These distinct structural features are believed to be related with the postulated functions of CD20 *(229)*: B-cell activation, proliferation and differentiation *(230, 231)*; membrane calcium conductance *(228)*; and induction and regulation of apoptosis *(217, 232)*.

1.7.2. Anti-CD20 antibodies

CD20 spans through B-cell membrane four times and hence presents a single extracellular loop of ~43 residues between the third and fourth transmembrane domains, providing epitopes for the binding of various antibodies *(215, 233*). However, there is a high degree of epitope variation among the antibodies, despite the small size of this loop. This may imply different potencies and consequences of the antibodies upon binding to CD20 *(234)*.

Due to the intriguing features of CD20 and proven value as a drug target, anti-CD20 mAbs of different origins (Table 1.5) have been identified, engineered and tested for the treatment of B-cell NHL. Based on the epitope and/or binding mode, these antibodies are divided into type I and II. Type I mAbs stabilize CD20 on lipid rafts, resulting in stronger C1q binding and complement-dependent cytotoxicity (CDC) induction. In contrast, type II mAbs do not stabilize CD20 but potently induce direct cell death (apoptosis) *(235)*. Type I is more commonly seen than type II. New mAbs are engineered for better therapeutic potency over the first generation rituximab: second generation is humanized or fully human antibodies without alteration to Fc region, and third generation is both humanized and Fc-region reengineered *(236)* . The rationale behind this evolution is to

Table 1.5. Various anti-CD20 monoclonal antibodies (mAbs)

Generation	Name	Isotype and description	References
1st	1F5 (type I)	mIgG2a; Up-regulates *c-myc* expression; Activates resting B-cells.	*(217, 238)*
	B1 (type II)	mIgG2a; Induces homotypic aggregation.	*(217, 234)*
	2H7	*mIgG2b.*	*(217, 234)*
	Rituximab (type I)	Chimeric: binding region of murine anti-human CD20 + hIgG1 heavy-chain + human κ constant region; Approved by FDA in 1997.	*(218)*
2nd	Y^{90}-ibritumomab tiuxetan (type I)	aka, Zevalin® from Biogen IDEC; Radioconjugate murine mAb; Approved in 2002.	*(239)*
	131I-tositumomab (type II)	aka, Bexxar® from GSK; radioconjugate with murine B1 mAb; Approved in 2003.	*(239)*
	Veltuzumab (type I)	Aka, IMMU-106, hA20; >90% humanized framework; Phase I/II trial.	*(240, 241)*
	Ocrelizumab (type I)	Fully humanized IgG1; Phase I/II trial.	*(242)*
	Ofatumumab (type I)	aka, HuMaxCD20; Fully human IgG1; Approved in 2009 for CLL.	*(243)*
3rd	GA101 (type II)	1st Fc-engineered type II humanized IgG1; 50-fold higher binding affinity; 10 to 100-fold increase in ADCC and direct cell apoptosis induction.	*(244)*
	AME-133v (type I)	Humanized IgG1; Fc-region engineered; Phase II trial.	*(245)*
	PRO131921(v114) (type I)	Humanized IgG1; Fc-region engineered; Phase I/II.	*(246)*

m, murine; h, human.

minimize infusion reactions and to diminish the development of human antibodies against the therapeutics *(237)*.

1.7.3. Anti-CD20 antibody-based treatments for NHL

At present, there are two major therapeutic modalities based on anti-CD20 antibodies available in clinical use: 1) bio-/immuno-therapy directly using unconjugated anti-CD20 mAbs, and 2) radio-immunotherapy using anti-CD20 antibody conjugates. In 1997, Rituximab (Biogen IDEC) became the first therapeutic mAb approved by US FDA *(247)*. Since the exact functions of CD20 are unclear, there are only some postulated mechanisms of action of rituximab, as illustrated in Figure 1.8: complement-dependent cytotoxicity (CDC), antibody-dependent cellular toxicity (ADCC) and direct induction of apoptosis *(215, 235)*. Now rituximab is the first-line monotherapy for follicular lymphoma, and is also used in combination with chemotherapy for indolent, intermediate and aggressive NHLs. However, rituximab is not perfect; it is accompanied by mild to serious side effects, such as fever, chill, hypotension, infusion reactions, tumor lysis syndrome (TLS), severe mucocutaneous reactions, progressive multifocal leukoencephalopathy (PML) (www.rituxan.com) *(215)*. PML is a rare and life-threatening brain disease caused by human polyomavirus John Cunningham virus (JCV), which causes myelin loss upon infection *(248)*. Recent studies indicated that the depletion of peripheral B cells after rituximab treatment motivates the release of heomatpoietic progenitor cells from bone marrow, which creates a favorable scenario for JCV migration and proliferation *(249)*. The mounting number of PML adverse event incidences is lighting up a regulatory red light for rituximab *(250)*. Also, resistance to

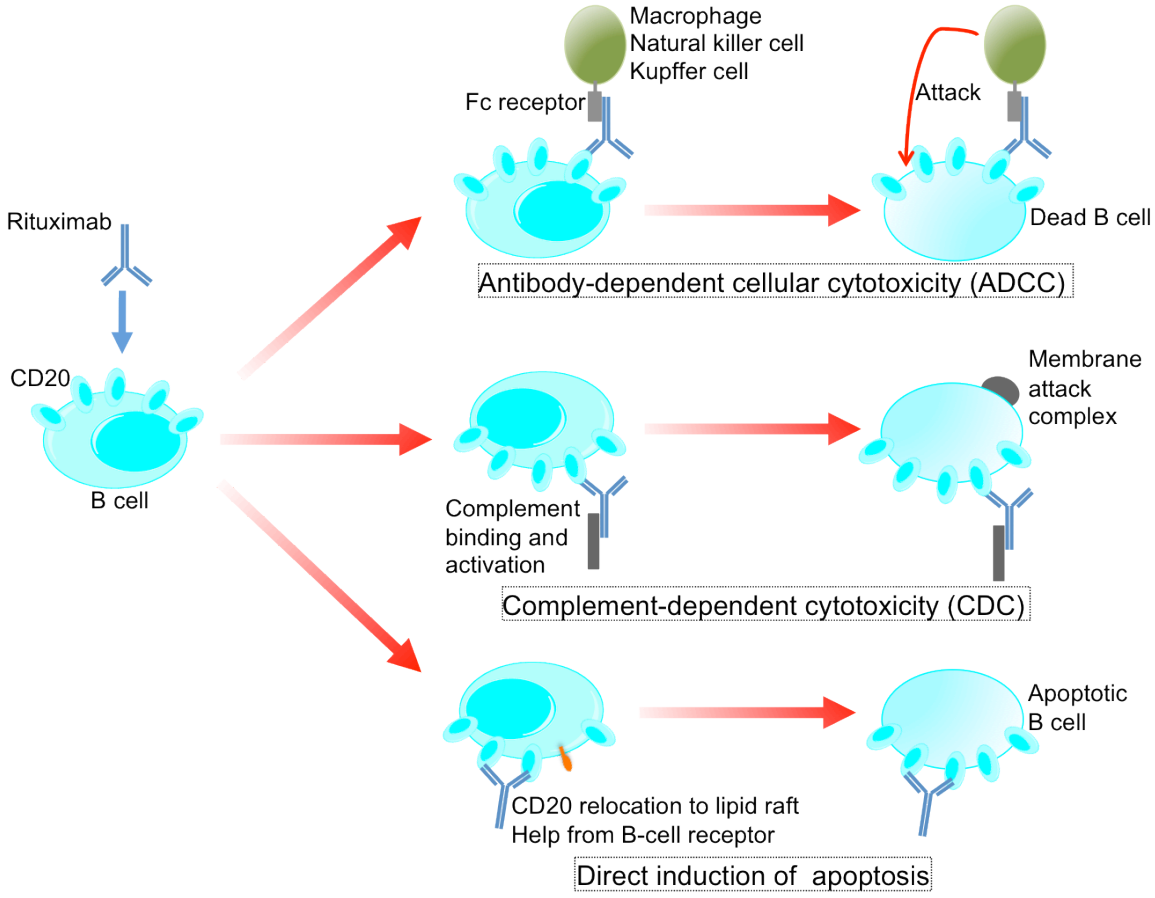

Figure 1.8. Putative mechanisms of action for rituximab. Adapted from references *(215, 235, 251)*.

rituximab has been observed *(218)*. Accumulating evidence is suggesting that polymorphism of Fcγ receptors in ADCC *(218, 251)* and the complement activation in CDC *(252)* contribute greatly to the resulting drug resistance and side effects.

The early success of rituximab heralded a new era in novel NHL treatment approaches. Radio-immunotherapy (RIT) for NHL treatment is an excellent example: conjugating radioisotopes with anti-CD20 antibodies to improve treatment efficacy while limiting toxic effects on normal cells. In February 2002, Yttrium-90 (^{90}Y)-ibritumomab tiuxetan (Zevalin® Biogen IDEC) was approved by FDA, the first FDA approved RIT conjugate. In June 2003, FDA approved another RIT conjugate, iodine-131 (^{131}I)-tositumomab (Bexxar®, GlaxoSmithKline), for the treatment of CD-20 positive follicular NHL. Both of them achieved satisfying therapeutic effect in patients, gauged by the response rate (RR) and complete remission (CR) rate *(216)*. Currently, the combination of RIT with other chemotherapeutic agents are in clinical trials *(237)*.

CD20-based antibody-drug conjugates (ADCs) have also been developed to improve therapeutic efficiency of the native anticancer agents. For instance, the aforementioned auristatin was "glued" onto rituximab and 1F5 antibodies via a lysosomally cleavable dipeptide (valine-citrulline) linker; results from *in vitro* and *in vivo* studies both indicated the ADCs could achieve better therapeutic effects than rituximab alone *(253)*.

Cross-linking of CD20 antigens is believed to trigger certain signaling pathway and further to result in direct apoptosis during the rituximab treatment *(217)*. Back in 2001, Ghetie and colleagues *(201)* already proposed that the homodimers but not monomers of rituximab induced the apoptosis in NHL. Supposedly, secondary antibodies should be a straightforward strategy to cross-link the primary anti-CD20 mAbs *(217)*. Following this

thread, Zhang et al. *(202)* generated a rituximab-dextrin polymer conjugate and their results proved that the hyper-cross-linking of CD20 antigens did lead to a clinically relevant level of apoptosis due to the multivalency effect of the conjugate; a goat anti-human secondary antibody was employed to cross-link rituximab as a positive control in this study.

To minimize the infusion reactions and other severe side effects of murine and chimeric antibody-based therapeutics, highly and fully humanized anti-CD20 antibodies have been developed and some are already in clinical trials *(241)*, as listed in Table 1.5. For example, a >90% humanized mAb, IMMU-106, was tested in a phase I/II dose-escalation study. Encouraging preliminary results in patients showed an overall RR of 53% and a CR rate of 40%, with a short infusion time and reduced infusion reactions compared to rituximab *(237)*.

1.8. Statement of objectives

The objective of this dissertation was to study the biorecognition of coiled-coil sequences in both hybrid biomaterials and macromolecular therapeutics, designed with affinity coiled-coil interactions: in particular, to determine the factors responsible for the coiled-coil mediated self-assembly of graft copolymers into hybrid hydrogels and to apply the biorecognition principles to a biological system. To this end, two major specific aims were formulated:

1) To synthesize HPMA copolymers grafted with coiled-coil forming peptides and to evaluate the relationship between peptide/graft copolymer structure and the self-assembly into hybrid hydrogels.

2) To design a system where coiled-coil biorecognition would mediate a biological process, apoptosis induction in CD20 positive B cells, to prove that coiled-coil formation at the cell surface could cross-link CD20 antigens and trigger apoptosis, and to further evaluate this system both *in vitro* and *in vivo*.

To accomplish these specific aims, self-assembly of coiled-coil motifs was employed as a core element in the design to mediate either gel formation or multivalent cross-linking events on B cell surface. In Specific Aim 1, we proposed a free radical macromonomer copolymerization strategy to synthesize polyHPMA copolymers grafted with coiled-coil motifs, whose self-assembly would in turn function as a cross-linking mechanism for novel hybrid hydrogel formation; moreover, we would like to examine the impact of sequence design and micro-environment on gel formation. These results are described in Chapter 2. In Specific Aim 2, the unique molecular biorecognition between two self-complementary coiled-coil motifs (CCE and CCK) was used to mediate the cross-linking of CD20 surface antigens, which could trigger respective signaling cascades and concomitantly induce apoptosis of the malignant B cells. These results are described in Chapters 3 and 4.

1.9. References

(1) Sarikaya, M., Tamerler, C., Jen, A. K., Schulten, K., and Baneyx, F. (2003) Molecular biomimetics: nanotechnology through biology. *Nat Mater 2*, 577-585.

(2) Wilchek, M., Bayer, E. A., and Livnah, O. (2006) Essentials of biorecognition: the (strept)avidin-biotin system as a model for protein-protein and protein-ligand interaction. *Immunol Lett 103*, 27-32.

(3) Williamson, J. R. (2000) Induced fit in RNA-protein recognition. *Nat Struct Biol 7*, 834-837.

(4) Bosshard, H. R. (1976) Theories of enzyme specificity and their application to proteases and aminoacyl-transfer RNA synthetases. *Experientia 32*, 949-963.

(5) Lichtenthaler, F. W. (1994) 100 years "Schlüssel-Schloss-Prinzip": what made Emil Fischer use this analogy? *Angew Chem Int Ed Engl 33*, 2364-2374.

(6) Ehrlich, P. (1900) On immunity with special reference to cell life. *Proc R Soc London 66*, 424-448.

(7) Roth, S. (1985) Are glycosyltransferases the evolutionary antecedents of the immunoglobulins? *Q Rev Biol 60*, 145-153.

(8) Koshland, D. E. (1958) Application of a theory of enzyme specificity to protein synthesis. *Proc Natl Acad Sci USA 44*, 98-104.

(9) Rini, J. M., Schulze-Gahmen, U., and Wilson, I. A. (1992) Structural evidence for induced fit as a mechanism for antibody-antigen recognition. *Science 255*, 959-965.

(10) Williams, D. H., Stephens, E., O'Brien, D. P., and Zhou, M. (2004) Understanding noncovalent interactions: ligand binding energy and catalytic efficiency from ligand-induced reductions in motion within receptors and enzymes. *Angew Chem Int Ed Engl 43*, 6596-6616.

(11) Sikes, H. D., Hansen, R. R., Johnson, L. M., Jenison, R., Birks, J. W., Rowlen, K. L., and Bowman, C. N. (2008) Using polymeric materials to generate an amplified response to molecular recognition events. *Nat Mater 7*, 52-56.

(12) Frederick, K. K., Marlow, M. S., Valentine, K. G., and Wand, A. J. (2007) Conformational entropy in molecular recognition by proteins. *Nature 448*, 325-329.

(13) Voskuhl, J., and Ravoo, B. J. (2009) Molecular recognition of bilayer vesicles. *Chem Soc Rev 38*, 495-505.

(14) Branco, M. C., and Schneider, J. P. (2009) Self-assembling materials for therapeutic delivery. *Acta Biomaterialia 5*, 817-831.

(15) Allen, T. M., and Cullis, P. R. (2004) Drug delivery systems: entering the mainstream. *Science 303*, 1818-1822.

(16) Lu, Z.-R., Kopečková, P., and Kopeček, J. (1999) Polymerizable Fab' antibody fragments for targeting of anticancer drugs. *Nat Biotechnol 17*, 1101-1104.

(17) Johnson, R. N., Kopečková, P., and Kopeček, J. (2009) Synthesis and evaluation of multivalent branched HPMA copolymer-Fab' conjugates targeted to the B-cell antigen CD20. *Bioconjug Chem 20*, 129-137.

(18) Kopeček, J. (2007) Hydrogel biomaterials: a smart future? *Biomaterials* 28, 5185-5192.

(19) Bailey, K. (1953) The structure of tropomyosin. *Proc R Soc Lond B Biol Sci 141*, 45-48.

(20) Huggins, M. L. (1957) The structure of alpha keratin. *Proc Natl Acad Sci USA 43*, 204-209.

(21) Lupas, A. (1996) Coiled coils: new structures and new functions. *Trends Biochem Sci 21*, 375-382.

(22) Wang, C., Stewart, R. J., and Kopeček, J. (1999) Hybrid hydrogels assembled from synthetic polymers and coiled-coil protein domains. *Nature 397*, 417-420.

(23) Nowak, A. P., Breedveld, V., Pakstis, L., Ozbas, B., Pine, D. J., Pochan, D., and Deming, T. J. (2002) Rapidly recovering hydrogel scaffolds from self-assembling diblock copolypeptide amphiphiles. *Nature 417*, 424-428.

(24) Yu, Y. B. (2002) Coiled-coils: stability, specificity, and drug delivery potential. *Adv Drug Deliv Rev 54*, 1113-1129.

(25) Mason, J. M., and Arndt, K. M. (2004) Coiled coil domains: stability, specificity, and biological implications. *Chembiochem 5*, 170-176.

(26) McFarlane, A. A., Orriss, G. L., and Stetefeld, J. (2009) The use of coiled-coil proteins in drug delivery systems. *Eur J Pharmacol 625*, 101-107.

(27) Banwell, E. F., Abelardo, E. S., Adams, D. J., Birchall, M. A., Corrigan, A., Donald, A. M., Kirkland, M., Serpell, L. C., Butler, M. F., and Woolfson, D. N. (2009) Rational design and application of responsive alpha-helical peptide hydrogels. *Nat Mater 8*, 596-600.

(28) Woolfson, D. N. (2010) Building fibrous biomaterials from alpha-helical and collagen-like coiled-coil peptides. *Biopolymers 94*, 118-127.

(29) Krishna, O. D., and Kiick, K. L. (2010) Protein- and peptide-modified synthetic polymeric biomaterials. *Biopolymers 94*, 32-48.

(30) Wu, K., Liu, J., Johnson, R. N., Yang, J., and Kopeček, J. (2010) Drug-free macromolecular therapeutics: induction of apoptosis by coiled-coil-mediated cross-linking of antigens on the cell surface. *Angew Chem Int Ed Engl 49*, 1451-1455.

(31) Harbury, P. B., Kim, P. S., and Alber, T. (1994) Crystal structure of an isoleucine-zipper trimer. *Nature 371*, 80-83.

(32) Dong, H., and Hartgerink, J. D. (2006) Short homodimeric and heterodimeric coiled coils. *Biomacromolecules 7*, 691-695.

(33) Litowski, J. R., and Hodges, R. S. (2002) Designing heterodimeric two-stranded alpha-helical coiled-coils. Effects of hydrophobicity and alpha-helical propensity on protein folding, stability, and specificity. *J Biol Chem 277*, 37272-37279.

(34) McClain, D. L., Gurnon, D. G., and Oakley, M. G. (2002) Importance of potential interhelical salt-bridges involving interior residues for coiled-coil stability and quaternary structure. *J Mol Biol 324*, 257-270.

(35) Kellis, J. T. Jr., Nyberg, K., Sali, D., and Fersht, A. R. (1988) Contribution of hydrophobic interactions to protein stability. *Nature 333*, 784-786.

(36) Lam, R., Xu, C., Bian, C. B., Mackenzie, F., Walker, J. R., Bountra, C., Weigelt, J., Arrowsmith, C. H., Edwards, A. M., Bochkarev, A., and Min, J. (2010) Crystal structure of human Lamin-B1 coil 2 segment. *Protein Data Bank*, doi: 10.2210/pdb3mov/pdb.

(37) Holton, J., and Alber, T. (2004) Automated protein crystal structure determination using ELVES. *Proc Natl Acad Sci USA 6*, 1537-1542.

(38) Liu, J., Deng, Y., Zheng, Q., Cheng, C. S., Kallenbach, N. R., and Lu, M. (2006) A parallel coiled-coil tetramer with offset helices. *Biochemistry 45*, 15224-15231.

(39) Liu, J., Zheng, Q., Deng, Y., Kallenbach, N. R. and Lu, M. (2006) Conformational transition between four and five-stranded phenylalanine zippers determined by a local packing interaction. *J Mol Biol 361*, 168-179.

(40) Liu, J., Zheng, Q., Deng, Y., Cheng, C. S., Kallenbach, N. R., and Lu, M. (2006) A seven-helix coiled coil. *Proc Natl Acad Sci USA 103*, 15457-15462.

(41) Bullough, P. A., Hughson, F. M., Skehel, J. J., and Wiley, D. C. (1994) Structure of influenza haemagglutinin at the pH of membrane fusion. *Nature 371*, 37-43.

(42) Pagel, K., Wagner, S. C., Samedov, K., von Berlepsch, H., Bottcher, C., and Koksch, B. (2006) Random coils, beta-sheet ribbons, and alpha-helical fibers: one peptide adopting three different secondary structures at will. *J Am Chem Soc 128*, 2196-2197.

(43) Krylov, D., Olive, M., and Vinson, C. (1995) Extending dimerization interfaces: the bZIP basic region can form a coiled coil. *EMBO J 14*, 5329-5337.

(44) Lyu, P. C., Liff, M. I., Marky, L. A., and Kallenbach, N. R. (1990) Side chain contributions to the stability of alpha-helical structure in peptides. *Science 250*, 669-673.

(45) Kwok, S. C., and Hodges, R. S. (2004) Stabilizing and destabilizing clusters in the hydrophobic core of long two-stranded alpha-helical coiled-coils. *J Biol Chem 279*, 21576-21588.

(46) Wagschal, K., Tripet, B., Lavigne, P., Mant, C. T., and Hodges, R. S. (1999) The role of position a in determining the stability and oligomerization state of alpha-helical coiled coils: 20 amino acid stability coefficients in the hydrophobic core of proteins. *Protein Sci 8*, 2312-2329.

(47) Wagschal, K., Tripet, B., and Hodges, R. S. (1999) De novo design of a model peptide sequence to examine the effects of single amino acid substitutions in the hydrophobic core on both stability and oligomerization state of coiled-coils. *J Mol Biol 285*, 785-803.

(48) Tripet, B., Wagschal, K., Lavigne, P., Mant, C. T., and Hodges, R. S. (2000) Effects of side-chain characteristics on stability and oligomerization state of a de novo-designed model coiled-coil: 20 amino acid substitutions in position "d". *J Mol Biol 300*, 377-402.

(49) Lumb, K. J., and Kim, P. S. (1995) A buried polar interaction imparts structural uniqueness in a designed heterodimeric coiled coil. *Biochemistry 34*, 8642-8648.

(50) Eckert, D. M., Malashkevich, V. N., and Kim, P. S. (1998) Crystal structure of GCN4-pIQI, a trimeric coiled coil with buried polar residues. *J Mol Biol 284*, 859-865.

(51) Lumb, K. J., and Kim, P. S. (1998) A buried polar interaction imparts structural uniqueness in a designed heterodimeric coiled coil. *Biochemistry 37*, 13042.

(52) Oakley, M. G., and Kim, P. S. (1998) A buried polar interaction can direct the relative orientation of helices in a coiled coil. *Biochemistry 37*, 12603-12610.

(53) Monera, O. D., Zhou, N. E., Kay, C. M., and Hodges, R. S. (1993) Comparison of antiparallel and parallel two-stranded alpha-helical coiled-coils. Design, synthesis, and characterization. *J Biol Chem 268*, 19218-19227.

(54) Monera, O. D., Kay, C. M., and Hodges, R. S. (1994) Electrostatic interactions control the parallel and antiparallel orientation of alpha-helical chains in two-stranded alpha-helical coiled-coils. *Biochemistry 33*, 3862-3871.

(55) Kohn, W. D., Kay, C. M., and Hodges, R. S. (1995) Protein destabilization by electrostatic repulsions in the two-stranded alpha-helical coiled-coil/leucine zipper. *Protein Sci 4*, 237-250.

(56) Lee, D. L., Ivaninskii, S., Burkhard, P., and Hodges, R. S. (2003) Unique stabilizing interactions identified in the two-stranded alpha-helical coiled-coil: crystal structure of a cortexillin I/GCN4 hybrid coiled-coil peptide. *Protein Sci 12*, 1395-1405.

(57) Kellis, J. T. Jr., Nyberg, K., and Fersht, A. R. (1989) Energetics of complementary side-chain packing in a protein hydrophobic core. *Biochemistry 28*, 4914-4922.

(58) De Crescenzo, G., Litowski, J. R., Hodges, R. S., and O'Connor-McCourt, M. D. (2003) Real-time monitoring of the interactions of two-stranded de novo designed coiled-coils: effect of chain length on the kinetic and thermodynamic constants of binding. *Biochemistry 42*, 1754-1763.

(59) Xu, C., and Kopeček, J. (2008) Genetically engineered block copolymers: influence of the length and structure of the coiled-coil blocks on hydrogel self-assembly. *Pharm Res 25*, 674-682.

(60) Su, J. Y., Hodges, R. S., and Kay, C. M. (1994) Effect of chain length on the formation and stability of synthetic alpha-helical coiled coils. *Biochemistry 33*, 15501-15510.

(61) Litowski, J. R., and Hodges, R. S. (2001) Designing heterodimeric two-stranded alpha-helical coiled-coils: the effect of chain length on protein folding, stability and specificity. *J Pept Res 58*, 477-492.

(62) Kwok, S. C., and Hodges, R. S. (2004) Effect of chain length on coiled-coil stability: decreasing stability with increasing chain length. *Biopolymers 76*, 378-390.

(63) Wolf, E., Kim, P. S., and Berger, B. (1997) MultiCoil: a program for predicting two- and three-stranded coiled coils. *Protein Sci 6*, 1179-1189.

(64) Smith, T. A., Hempstead, P. D., Palliser, C. C., and Parry, D. A. (2003) Modeling alpha-helical coiled-coil interactions: the axial and azimuthal alignment of 1B segments from vimentin intermediate filaments. *Proteins 50*, 207-212.

(65) Mason, J. M., Schmitz, M. A., Muller, K. M., and Arndt, K. M. (2006) Semirational design of Jun-Fos coiled coils with increased affinity: Universal implications for leucine zipper prediction and design. *Proc Natl Acad Sci USA 103*, 8989-8994.

(66) Hagemann, U. B., Manson, J. M., Muller, K. M., and Arndt, K. M. (2008) Selectional and mutational scope of peptides sequestering the Jun-Fos coiled-coil domain. *J Mol Biol 381*, 73-88.

(67) www.molbiotech.uni-freiburg.de/bCIPA.

(68) Lomander, A., Hwang, W., and Zhang, S. (2005) Hierarchical self-assembly of a coiled-coil peptide into fractal structure. *Nano Lett 5*, 1255-1260.

(69) Hashiyama, K., Takeuchi, A., and Makino, M. (2005) Effects of single amino acid substitutions at the predicted coiled-coil or hydrophobic region on the self-

assembly of phi29 replication protein, gp1. *Biochem Biophys Res Commun 331*, 1310-1316.

(70) Cohen, C., and Parry, D. A. (1990) Alpha-helical coiled coils and bundles: how to design an alpha-helical protein. *Proteins 7,* 1-15.

(71) Ryadnov, M. G., and Woolfson, D. N. (2005) MaP peptides: programming the self-assembly of peptide-based mesoscopic matrices. *J Am Chem Soc 127*, 12407-12415.

(72) Kokona, B., Kim, A. M., Roden, R. C., Daniels, J. P., Pepe-Mooney, B. J., Kovaric, B. C., de Paula, J. C., Johnson, K. A., and Fairman, R. (2009) Self assembly of coiled-coil peptide-porphyrin complexes. *Biomacromolecules 10*, 1454-1459.

(73) Dong, H., Paramonov, S. E., and Hartgerink, J. D. (2008) Self-assembly of alpha-helical coiled coil nanofibers. *J Am Chem Soc 130*, 13691-13695.

(74) Sonnichsen, F. D., Van Eyk, J. E., Hodges, R. S., and Sykes, B. D. (1992) Effect of trifluoroethanol on protein secondary structure: an NMR and CD study using a synthetic actin peptide. *Biochemistry 31*, 8790-8798.

(75) Gonzalez, L. Jr., Plecs, J. J., and Alber, T. (1996) An engineered allosteric switch in leucine-zipper oligomerization. *Nat Struct Biol 3*, 510-515.

(76) Walsh, S. T., Cheng, H., Bryson, J. W., Roder, H., and DeGrado, W. F. (1999) Solution structure and dynamics of a de novo designed three-helix bundle protein. *Proc Natl Acad Sci USA 96*, 5486-5491.

(77) d'Avignon, D. A., Bretthorst, G. L., Holtzer, M. E., and Holtzer, A. (1998) Site-specific thermodynamics and kinetics of a coiled-coil transition by spin inversion transfer NMR. *Biophys J 74*, 3190-3197.

(78) Pagel, K., Seeger, K., Seiwert, B., Villa, A., Mark, A. E., Berger, S., and Koksch, B. (2005) Advanced approaches for the characterization of a de novo designed antiparallel coiled coil peptide. *Org Biomol Chem 3*, 1189-1194.

(79) Ryadnov, M. G. (2007) Peptide alpha-helices for synthetic nanostructures. *Biochem Soc Trans 35*, 487-491.

(80) Chao, H., Bautista, D. L., Litowski, J., Irvin, R. T., and Hodges, R. S. (1998) Use of a heterodimeric coiled-coil system for biosensor application and affinity purification. *J Chromatogr B Biomed Sci Appl 715*, 307-329.

(81) Green, D. J., Pagel, J. M., Pantelias, A., Hedin, N., Lin, Y., Wilbur, D. S., Gopal, A., Hamlin, D. K., and Press, O. W. (2007) Pretargeted radioimmunotherapy for B-cell lymphomas. *Clin Cancer Res 13*, 5598s-5603s.

(82) Pagel, J. M., Hedin, N., Drouet, L., Wood, B. L., Pantelias, A., Lin, Y., Hamlin, D. K., Wilbur, D. S., Gopal, A. K., Green, D. J., Appelbaum, F. R., and Press, O. W. (2008) Eradication of disseminated leukemia in a syngeneic murine leukemia model using pretargeted anti-CD45 radioimmunotherapy. *Blood 111*, 2261-2268.

(83) Wichterle, O., and Lím, D. (1960) Hydrophilic gels for biological use. *Nature 185*, 117-118.

(84) Kopeček, J., and Yang, J. (2007) Hydrogels as smart biomaterials. *Polym Int 56*, 1078-1098.

(85) Wichterle, O. (1968) US patent 3361858.

(86) Xue, W., Champ, S., and Huglin, M. B. (2001) Network and swelling parameters of chemically crosslinked thermoreversible hydrogels. *Polymer 42*, 3665-3669.

(87) Hennink, W. E., and van Nostrum, C.F. (2002) Novel crosslinking methods to design hydrogels. *Adv Drug Deliv Rev 54*, 13-36.

(88) Yuan, W., Yang, J., Kopečková, P., and Kopeček, J. (2008) Smart hydrogels containing adenylate kinase: translating substrate recognition into macroscopic motion. *J Am Chem Soc 130*, 15760-15761.

(89) Galina, H., and Rupicz, K. (1980) Cyclization in chain-crosslinking copolymerization. *Polym Bull 3*, 473-480.

(90) Yeh, P.-Y., Kopečková, P., and Kopeček, J. (1994) Biodegradable and pH-sensitive hydrogels: synthesis by crosslinking of *N,N*-dimethylacrylamide copolymer precursors. *J Polym Sci A Polym Chem 32*, 1627-1637.

(91) Scales, C. W., Vasilieva, Y. A., Convertine, A. J., Lowe, A. B., and McCormick, C. L. (2005) Direct, controlled synthesis of the nonimmunogenic, hydrophilic polymer, poly(*N*-(2-hydroxypropyl)methacrylamide) via RAFT in aqueous media. *Biomacromolecules 6*, 1846-1850.

(92) Kirkland, S. E., Hensarling, R. M., McConaughy, S. D., Guo, Y., Jarrett, W. L., and McCormick, C. L. (2008) Thermoreversible hydrogels from RAFT-synthesized BAB triblock copolymers: steps toward biomimetic matrices for tissue regeneration. *Biomacromolecules 9*, 481-486.

(93) Matyjaszewski, K., and Xia, J. (2001) Atom transfer radical polymerization. *Chem Rev 101*, 2921-2990.

(94) Bencherif, S. A., Siegwart, D. J., Srinivasan, A., Horkay, F., Hollinger, J. O., Washburn, N. R., and Matyjaszewski, K. (2009) Nanostructured hybrid hydrogels prepared by a combination of atom transfer radical polymerization and free radical polymerization. *Biomaterials 30*, 5270-5278.

(95) Kolb, H. C., Finn, M. G., and Sharpless, K. B. (2001) Click chemistry: diverse chemical function from a few good reactions. *Angew Chem Int Ed Engl 40*, 2004-2021.

(96) Crescenzi, V., Cornelio, L., Di Meo, C., Nardecchia, S., and Lamanna, R. (2007) Novel hydrogels via click chemistry: synthesis and potential biomedical applications. *Biomacromolecules 8*, 1844-1850.

(97) Kopeček, J. (2009) Hydrogels: From soft contact lenses and implants to self-assembled nanomaterials. *J Polym Sci A Polym Chem 47*, 5929-5946.

(98) Kuo, C. K., and Ma, P.X. (2001) Ionically crosslinked alginate hydrogels as scaffolds for tissue engineering: part 1. Structure, gelation rate and mechanical properties. *Biomaterials 22*, 511-521.

(99) Kopeček, J., Tang, A., Wang, C., and Stewart, R. J. (2001) De novo design of biomedical polymers: hybrids from synthetic macromolecules and genetically engineered domains. *Macromol Symp 174*, 31-42.

(100) Tang, A., Wang, C., Stewart, R. J., and Kopeček, J. (2001) The coiled coils in the design of protein-based constructs: hybrid hydrogels and epitope displays. *J Control Release 72*, 57-70.

(101) Wang, C., Kopeček, J., and Stewart, R. J. (2001) Hybrid hydrogels cross-linked by genetically engineered coiled-coil block proteins. *Biomacromolecules 2*, 912-920.

(102) Xu, C., Breedveld, V., and Kopeček, J. (2005) Reversible hydrogels from self-assembling genetically engineered protein block copolymers. *Biomacromolecules 6*, 1739-1749.

(103) Yang, J., Xu, C., Kopečková, P., and Kopeček, J. (2006) Hybrid hydrogels self-assembled from HPMA copolymers containing peptide grafts. *Macromol Biosci 6*, 201-209.

(104) Yang, J., Xu, C., Wang, C., and Kopeček, J. (2006) Refolding hydrogels self-assembled from *N*-(2-hydroxypropyl)methacrylamide graft copolymers by antiparallel coiled-coil formation. *Biomacromolecules 7*, 1187-1195.

(105) Yang, J., Wu, K., Koňák, Č., and Kopeček, J. (2008) Dynamic light scattering study of self-assembly of HPMA hybrid graft copolymers. *Biomacromolecules 9*, 510-517.

(106) Jia, X., and Kiick, K. L. (2009) Hybrid multicomponent hydrogels for tissue engineering. *Macromol Biosci 9*, 140-156.

(107) Cavalli, S., Albericio, F., and Kros, A. (2010) Amphiphilic peptides and their cross-disciplinary role as building blocks for nanoscience. *Chem Soc Rev 39*, 241-263.

(108) Aggeli, A., Bell, M., Boden, N., Carrick, L. M., and Strong, A. E. (2003) Self-assembling peptide polyelectrolyte beta-sheet complexes form nematic hydrogels. *Angew Chem Int Ed Engl 42*, 5603-5606.

(109) Rapaport, H., Grisaru, H., and Silberstein, T. (2008) Hydrogel scaffolds of amphiphilic and acidic beta-sheet peptides. *Adv Funct Mater 18*, 2889-2896.

(110) Rughani, R. V., Salick, D. A., Lamm, M. S., Yucel, T., Pochan, D. J., and Schneider, J. P. (2009) Folding, self-assembly, and bulk material properties of a de novo designed three-stranded beta-sheet hydrogel. *Biomacromolecules 10*, 1295-1304.

(111) Chen, L., Kopeček, J., and Stewart, R. J. (2000) Responsive hybrid hydrogels with volume transitions modulated by a titin immunoglobulin module. *Bioconjug Chem 11*, 734-740.

(112) Radu, L. C., Yang, J., and Kopeček, J. (2009) Self-assembling diblock copolymers of poly[*N*-(2-hydroxypropyl)methacrylamide] and a beta-sheet peptide. *Macromol Biosci 9*, 36-44.

(113) Tzokova, N., Fernyhough, C. M., Topham, P. D., Sandon, N., Adams, D. J., Butler, M. F., Armes, S. P., and Ryan, A. (2009) Soft hydrogels from nanotubes of poly(ethylene oxide)-tetraphenylalanine conjugates prepared by click chemistry. *Langmuir 25*, 2479-2485.

(114) Radu-Wu, L. C., Yang, J., Wu, K. G., and Kopeček, J. (2009) Self-assembled hydrogels from poly[*N*-(2-hydroxypropyl)methacrylamide] grafted with beta-sheet peptides. *Biomacromolecules 10*, 2319-2327.

(115) Segman-Magidovich, S., Grisaru, H., Gitli, T., Levi-Kalisman, Y., and Rapaport, H. (2008) Matrices of acidic beta-sheet peptides as templates for calcium phosphate mineralization. *Adv Mater 20*, 2156-2161.

(116) Banta, S., Wheeldon, I. R., and Blenner, M. (2010) Protein engineering in the development of functional hydrogels. *Annu Rev Biomed Eng 12*, 167-186.

(117) Lin, H. R., and Yeh, Y. J. (2004) Porous alginate/hydroxyapatite composite scaffolds for bone tissue engineering: preparation, characterization, and in vitro studies. *J Biomed Mater Res B Appl Biomater 71*, 52-65.

(118) de Jong, S. J., De Smedt, S. C., Wahls, M. W. C., Demeester, J., Kettenes-van den Bosch, J. J., and Hennink, W. E. (2000) Novel self-assembled hydrogels by stereocomplex formation in aqueous solution of enantiomeric lactic acid oligomers grafted to dextran. *Macromolecules 33*, 3680-3686.

(119) de Jong, S. J., van Eerdenbrugh, B., van Nostrum, C. F., Kettenes-van den Bosch, J. J., and Hennink, W. E. (2001) Physically crosslinked dextran hydrogels by

stereocomplex formation of lactic acid oligomers: degradation and protein release behavior. *J Control Release 71*, 261-275.

(120) Kim, S. Y., Kim, H. J., Lee, K. E., Han, S. S., Sohn, Y. S., and Jeong, B. (2007) Reverse thermal gelling PEG-PTMC diblock copolymer aqueous solution. *Macromolecules 40*, 5519-5525.

(121) Miyata, T. (2010) Preparation of smart soft materials using molecular complexes. *Polymer J 42*, 277-289.

(122) Miyata, T., Jikihara, A., Nakamae, K., and Hoffman, A. S. (2004) Preparation of reversibly glucose-responsive hydrogels by covalent immobilization of lectin in polymer networks having pendant glucose. *J Biomater Sci Polym Ed 15*, 1085-1098.

(123) Miyata, T., Asami, N., and Uragami, T. (1999) A reversibly antigen-responsive hydrogel. *Nature 399*, 766-769.

(124) Miyata, T., Jige, M., Nakaminami, T., and Uragami, T. (2006) Tumor marker-responsive behavior of gels prepared by biomolecular imprinting. *Proc Natl Acad Sci USA 103*, 1190-1193.

(125) Reardan, D. T., Meares, C. F., Goodwin, D. A., McTigue, M., David, G. S., Stone, M. R., Leung, J. P., Bartholomew, R. M., and Frincke, J. M. (1985) Antibodies against metal chelates. *Nature 316*, 265-268.

(126) Reilly, R. M. (2006) Radioimmunotherapy of solid tumors: the promise of pretargeting strategies using bispecific antibodies and radiolabeled haptens. *J Nucl Med 47*, 196-199.

(127) Singh, Y., Palombo, M., and Sinko, P. J. (2008) Recent trends in targeted anticancer prodrug and conjugate design. *Curr Med Chem 15*, 1802-1826.

(128) Gaidamakova, E. K., Backer, M. V., and Backer, J. M. (2001) Molecular vehicle for target-mediated delivery of therapeutics and diagnostics. *J Control Release 74*, 341-347.

(129) Liu, G., and Hnatowich, D. J. (2008) A semiempirical model of tumor pretargeting. *Bioconjug Chem 19*, 2095-2104.

(130) Meredith, R. F., and Buchsbaum, D. J. (2006) Pretargeted radioimmunotherapy. *Int J Radiat Oncol Biol Phys 66*, S57-59.

(131) Sharkey, R. M., Karacay, H., Cardillo, T. M., Chang, C. H., McBride, W. J., Rossi, E. A., Horak, I. D., and Goldenberg, D. M. (2005) Improving the delivery of radionuclides for imaging and therapy of cancer using pretargeting methods. *Clin*

Cancer Res 11, 7109s-7121s.

(132) Goodwin, D. A., and Meares, C. F (1997) Pretargeting: general principles. *Cancer 80*, 2675-80.

(133) Backer, M. V., Aloise, R., Przekop, K., Stoletov, K., and Backer, J. M. (2002) Molecular vehicles for targeted drug delivery. *Bioconjug Chem 13*, 462-467.

(134) Weber, P. C., Ohlendorf, D. H., Wendoloski, J. J., and Salemme, F. R. (1989) Structural origins of high-affinity biotin binding to streptavidin. *Science 243*, 85-88.

(135) Goldenberg, D. M., Sharkey, R. M., Paganelli, G., Barbet, J., and Chatal, J. F. (2006) Antibody pretargeting advances cancer radioimmunodetection and radioimmunotherapy. *J Clin Oncol 24*, 823-834.

(136) Ong, G. L., Ettenson, D., Sharkey, R. M., Marks, A., Baumal, R., Goldenberg, D. M., and Mattes, M. J. (1991) Galactose-conjugated antibodies in cancer therapy: properties and principles of action. *Cancer Res 51*, 1619-1626.

(137) Karacay, H., Sharkey, R. M., Govindan, S. V., McBride, W. J., Goldenberg, D. M., Hansen, H. J., and Griffiths, G. L. (1997) Development of a streptavidin-anti-carcinoembryonic antigen antibody, radiolabeled biotin pretargeting method for radioimmunotherapy of colorectal cancer. Reagent development. *Bioconjug Chem 8*, 585-594.

(138) Sharkey, R. M., Karacay, H., Griffiths, G. L., Behr, T. M., Blumenthal, R. D., Mattes, M. J., Hansen, H. J., and Goldenberg, D. M. (1997) Development of a streptavidin-anti-carcinoembryonic antigen antibody, radiolabeled biotin pretargeting method for radioimmunotherapy of colorectal cancer. Studies in a human colon cancer xenograft model. *Bioconjug Chem 8*, 595-604.

(139) Axworthy, D. B., Reno, J. M., Hylarides, M. D., Mallett, R. W., Theodore, L. J., Gustavson, L. M., Su, F., Hobson, L. J., Beaumier, P. L., and Fritzberg, A. R. (2000) Cure of human carcinoma xenografts by a single dose of pretargeted yttrium-90 with negligible toxicity. *Proc Natl Acad Sci USA 97*, 1802-1807.

(140) Sato, N., Hassan, R., Axworthy, D. B., Wong, K. J., Yu, S., Theodore, L. J., Lin, Y., Park, L., Brechbiel, M. W., Pastan, I., Paik, C. H., and Carrasquillo, J. A. (2005) Pretargeted radioimmunotherapy of mesothelin-expressing cancer using a tetravalent single-chain Fv-streptavidin fusion protein. *J Nucl Med 46*, 1201-1209.

(141) Forero, A., Weiden, P. L., Vose, J. M., Knox, S. J., LoBuglio, A. F., Hankins, J., Goris, M. L., Picozzi, V. J., Axworthy, D. B., Breitz, H. B., Sims, R. B., Ghalie, R. G., Shen, S., and Meredith, R. F. (2004) Phase I trial of a novel anti-CD20 fusion protein in pretargeted radioimmunotherapy for B-cell non-Hodgkin's lymphoma.

Blood 104, 227-236.

(142) Rossi, E. A., Sharkey, R. M., McBride, W., Karacay, H., Zeng, L., Hansen, H. J., Goldenberg, D. M., and Chang, C. H. (2003) Development of new multivalent-bispecific agents for pretargeting tumor localization and therapy. *Clin Cancer Res 9*, 3886s-3896s.

(143) Sharkey, R. M., McBride, W. J., Karacay, H., Chang, K., Griffiths, G. L., Hansen, H. J., and Goldenberg, D. M. (2003) Sharkey, R.M., et al., A universal pretargeting system for cancer detection and therapy using bispecific antibody. *Cancer Res 63*, 354-363.

(144) Goodwin, D. A., Meares, C. F., McTigue, M., Chaovapong, W., Diamanti, C. I., Ransone, C. H., and McCall, M. J. (1992) Pretargeted immunoscintigraphy: effect of hapten valency on murine tumor uptake. *J Nucl Med 33*, 2006-2013.

(145) Boerman, O. C., Kranenborg, M. H., Oosterwijk, E., Griffiths, G. L., McBride, W. J., Oyen, W. J., de Weijert, M., Oosterwijk-Wakka, J., Hansen, H. J., and Corstens, F. H. (1999) Pretargeting of renal cell carcinoma: improved tumor targeting with a bivalent chelate. *Cancer Res 59*, 4400-4405.

(146) Karacay, H., Sharkey, R. M., McBride, W. J., Griffiths, G. L., Qu, Z., Chang, K., Hansen, H. J., and Goldenberg, D. M. (2002) Pretargeting for cancer radioimmunotherapy with bispecific antibodies: role of the bispecific antibody's valency for the tumor target antigen. *Bioconjug Chem 13*, 1054-1070.

(147) Rossi, E. A., Chang, C. H., Losman, M. J., Sharkey, R. M., Karacay, H., McBride, W., Cardillo, T. M., Hansen, H. J., Qu, Z., Horak, I. D., and Goldenberg, D. M. (2005) Pretargeting of carcinoembryonic antigen-expressing cancers with a trivalent bispecific fusion protein produced in myeloma cells. *Clin Cancer Res 11*, 7122s-7129s.

(148) Kuijpers, W. H., Bos, E. S., Kaspersen, F. M., Veeneman, G. H., and van Boeckel, C. A. (1993) Specific recognition of antibody-oligonucleotide conjugates by radiolabeled antisense nucleotides: a novel approach for two-step radioimmunotherapy of cancer. *Bioconjug Chem 4*, 94-102.

(149) Bos, E. S., Kuijpers, W. H., Meesters-Winters, M., Pham, D. T., de Haan, A. S., van Doornmalen, A. M., Kaspersen, F. M., van Boeckel, C. A., and Gougeon-Bertrand, F. (1994) In vitro evaluation of DNA-DNA hybridization as a two-step approach in radioimmunotherapy of cancer. *Cancer Res 54*, 3479-3486.

(150) Liu, G., Mang'era, K., Liu, N., Gupta, S., Rusckowski, M., and Hnatowich, D. J. (2002) Tumor pretargeting in mice using (99m)Tc-labeled morpholino, a DNA analog. *J Nucl Med 43*, 384-391.

(151) Summerton, J., and Weller, D. (1997) Morpholino antisense oligomers: design, preparation, and properties. *Antisense Nucleic Acid Drug Dev 7*, 187-195.

(152) Liu, G., Liu, C., Zhang, S., He, J., Liu, N., Gupta, S., Rusckowski, M., and Hnatowich, D. J. (2003) Investigations of (99m)Tc morpholino pretargeting in mice. *Nucl Med Commun 24*, 697-705.

(153) Liu, G., He, J., Dou, S., Gupta, S., Rusckowski, M., and Hnatowich, D. J. (2005) Further investigations of morpholino pretargeting in mice--establishing quantitative relations in tumor. *Eur J Nucl Med Mol Imaging 32*, 1115-1123.

(154) Liu, G., Dou, S., Mardirossian, G., He, J., Zhang, S., Liu, X., Rusckowski, M., and Hnatowich, D. J. (2006) Successful radiotherapy of tumor in pretargeted mice by 188Re-radiolabeled phosphorodiamidate morpholino oligomer, a synthetic DNA analogue. *Clin Cancer Res 12*, 4958-4964.

(155) Liu, G., Dou, S., He, J., Liu, X., Rusckowski, M. and Hnatowich, D. J. (2007) Predicting the biodistribution of radiolabeled cMORF effector in MORF-pretargeted mice. *Eur J Nucl Med Mol Imaging 34*, 237-246.

(156) Liu, G., Dou, S., Rusckowski, M., and Hnatowich, D. J. (2008) An experimental and theoretical evaluation of the influence of pretargeting antibody on the tumor accumulation of effector. *Mol Cancer Ther 7*, 1025-1032.

(157) Wang, Y., Chang, F., Zhang, Y., Liu, N., Liu, G., Gupta, S., Rusckowski, M., and Hnatowich, D. J. (2001) Pretargeting with amplification using polymeric peptide nucleic acid. *Bioconjug Chem 12*, 807-816.

(158) He, J., Liu, G., Gupta, S., Zhang, Y., Rusckowski, M., and Hnatowich, D. J. (2004) Amplification targeting: a modified pretargeting approach with potential for signal amplification-proof of a concept. *J Nucl Med 45*, 1087-1095.

(159) Xu, G., and McLeod, H. L. (2001) Strategies for enzyme/prodrug cancer therapy. *Clin Cancer Res 7*, 3314-3324.

(160) Chester, K., Pedley, B., Tolner, B., Violet, J., Mayer, A., Sharma, S., Boxer, G., Green, A., Nagl, S., and Begent, R. (2004) Engineering antibodies for clinical applications in cancer. *Tumour Biol 25*, 91-98.

(161) Francis, R. J., Sharma, S. K., Springer, C., Green, A. J., Hope-Stone, L. D., Sena, L., Martin, J., Adamson, K. L., Robbins, A., Gumbrell, L., O'Malley, D., Tsiompanou, E., Shahbakhti, H., Webley, S., Hochhauser, D., Hilson, A. J., Blakey, D., and Begent, R. H. (2002) A phase I trial of antibody directed enzyme prodrug therapy (ADEPT) in patients with advanced colorectal carcinoma or other CEA producing tumours. *Br J Cancer 87*, 600-607.

(162) Matsumura, Y., and Maeda, H. (1986) A new concept for macromolecular therapeutics in cancer chemotherapy: mechanism of tumoritropic accumulation of proteins and the antitumor agent smancs. *Cancer Res 46*, 6387-6892.

(163) Fang, J., Nakamura, H., and Maeda, H. (2010) The EPR effect: Unique features of tumor blood vessels for drug delivery, factors involved, and limitations and augmentation of the effect. *Adv Drug Deliv Rev*, doi: 10.1016/j.addr.2010.04.009.

(164) Vasey, P. A., Kaye, S. B., Morrison, R., Twelves, C., Wilson, P., Duncan, R., Thomson, A. H., Murray, L. S., Hilditch, T. E., Murray, T., Burtles, S., Fraier, D., Frigerio, E., and Cassidy, J. (1999) Phase I clinical and pharmacokinetic study of PK1 [*N*-(2-hydroxypropyl)methacrylamide copolymer doxorubicin]: first member of a new class of chemotherapeutic agents-drug-polymer conjugates. Cancer Research Campaign Phase I/II Committee. *Clin Cancer Res 5*, 83-94.

(165) Rejmanová, P., Kopeček, J., Duncan, R., and Lloyd, J. B. (1985) Stability in rat plasma and serum of lysosomally degradable oligopeptide sequences in *N*-(2-hydroxypropyl) methacrylamide copolymers. *Biomaterials 6*, 45-48.

(166) Duncan, R., Cable, H. C., Lloyd, J. B., Rejmanová, P., and Kopeček, J. (1982) Degradation of side-chains of *N*-(2-hydroxypropyl)methacrylamide copolymers by lysosomal thiol-proteinases. *Biosci Rep 2*, 1041-1046.

(167) Seymour, L. W., Ferry, D. R., Kerr, D. J., Rea, D., Whitlock, M., Poyner, R., Boivin, C., Hesslewood, S., Twelves, C., Blackie, R., Schatzlein, A., Jodrell, D., Bissett, D., Calvert, H., Lind, M., Robbins, A., Duncan, R., and Cassidy, J. (2009) Phase II studies of polymer-doxorubicin (PK1, FCE28068) in the treatment of breast, lung and colorectal cancer. *Int J Oncol 34*, 1629-1636.

(168) Hotchkiss, R. S., Strasser, A., McDunn, J. E., and Swanson, P. E. (2009) Cell death. *N Engl J Med 361*, 1570-1583.

(169) Kroemer, G., Galluzzi, L., Vandenabeele, P., Abrams, J., Alnemri, E. S., Baehrecke, E. H., Balgosklonny, M. V., El-Deiry, W. S., Golstein, P., Green, D. R., Hengartner, M., Knight, R. A., Kumar, S., Lipton, S. A., Malorni, W., Nunez, G., Petter, M. E., Tschopp, J., Yuan, J., Piacentini, M., Zhivotovsky, B., and Melino, G. (2009) Classification of cell death: recommendations of the Nomenclature Committee on Cell Death 2009. *Cell Death Differ 16*, 3-11.

(170) Zhivotovsky, B., and Orrenius, S. (2010) Cell death mechanisms: cross-talk and role in disease. *Exp Cell Res 316*, 1374-1383.

(171) Kerr, J. F., Wyllie, A. H., and Currie, A. R. (1972) Apoptosis: a basic biological phenomenon with wide-ranging implications in tissue kinetics. *Br J Cancer 26*, 239-257.

(172) Declercq, J., Hensen, K., Van De Ven, W. J., and Chavez, M. (2003) PLAG proteins: how they influence apoptosis and cell proliferation. *Ann N Y Acad Sci*

1010, 264-265.

(173) Hengartner, M. O. (2000) The biochemistry of apoptosis. *Nature 407*, 770-776.

(174) Kroemer, G. (1997) The proto-oncogene Bcl-2 and its role in regulating apoptosis. *Nat Med 3*, 614-620.

(175) Tawa, P., Tam, J., Cassady, R., Nicholson, D. W., and Xanthoudakis, S. (2001) Quantitative analysis of fluorescent caspase substrate cleavage in intact cells and identification of novel inhibitors of apoptosis. *Cell Death Differ 8*, 30-37.

(176) Gavrieli, Y., Sherman, Y., and Ben-Sasson, S. A. (1992) Identification of programmed cell death *in situ* via specific labeling of nuclear DNA fragmentation. *J Cell Biol 119*, 493-501.

(177) Watanabe, I., Toyoda, M., Okuda, J., Tenjo, T., Tanaka, K, Yamamoto, T., Kawasaki, H., Sugiyama, T., Kawarada, Y., and Tanigawa, N. (1999) Detection of apoptotic cells in human colorectal cancer by two different in situ methods: antibody against single-stranded DNA and terminal deoxynucleotidyl transferase-mediated dUTP-biotin nick end-labeling (TUNEL) methods. *Jpn J Cancer Res 90*, 188-193.

(178) Vermes, I., Haanen, C., Steffens-Nakken, H., and Reutelingsperger, C. (1995) A novel assay for apoptosis. Flow cytometric detection of phosphatidylserine expression on early apoptotic cells using fluorescein labelled Annexin V. *J Immunol Methods 184*, 39-51.

(179) Riccardi, C., and Nicoletti, I. (2006) Analysis of apoptosis by propidium iodide staining and flow cytometry. *Nat Protoc 1*, 1458-1461.

(180) Klionsky, D. J. (2007) Autophagy: from phenomenology to molecular understanding in less than a decade. *Nat Rev Mol Cell Biol 8*, 931-937.

(181) Eisenberg-Lerner, A., Bialik, S., Simon, H. U., and Kimchi, A. (2009) Life and death partners: apoptosis, autophagy and the cross-talk between them. *Cell Death Differ 16*, 966-975.

(182) Golstein, P., and Kroemer, G. (2007) Cell death by necrosis: towards a molecular definition. *Trends Biochem Sci 32*, 37-43.

(183) Druker, B. J. (2002) STI571 (Gleevec^{TM}) as a paradigm for cancer therapy. *Trends Mol Med 8*, S14-18.

(184) Kollmannsberger, C., Mross, K., Jakob, A., Kanz, L., and Bokemeyer, C. (1999) Topotecan - a novel topoisomerase I inhibitor: pharmacology and clinical experience. *Oncology 56*, 1-12.

(185) Gordon, A. N., Tonda, M., Sun, S., and Rackoff, W. (2004) Long-term survival advantage for women treated with pegylated liposomal doxorubicin compared with topotecan in a phase 3 randomized study of recurrent and refractory epithelial ovarian cancer. *Gynecol Oncol 95*, 1-8.

(186) Piot, C., Croisille, P., Staat, P., Thibault, H., Rioufol, G., Mewton, N., Elbelghiti, R., Cung, T. T., Bonnefoy, E., Angoulvant, D., Macia, C., Raczka, F., Sportouch, C., Gahide, G., Andre-Fouet, X., Revel, D., Kirkorian, G., Monassier, J. P., Derumeaux, G., and Ovize, M. (2008) Effect of cyclosporine on reperfusion injury in acute myocardial infarction. *N Engl J Med 359*, 473-481.

(187) American Cancer Society (2010) Cancer facts and figures 2010. *American Cancer Society*. Atlanta, GA.

(188) Altekruse S. F., Kosary, C., Krapcho, M., Neyman, N., Aminou, R., Waldron, W., Ruhl, J., Howlader, N., Tatalovich, Z., Cho, H., Maritto, A., Eisner, M. P., Lewis, D. R., Cronin, K., Chen, H. S., Feuer, E. J., Stinchcomb, D. G., and Edwards, B. K. (2010) SEER Cancer Statistics Review, 1975-2007. *National Cancer Institute*. Bethesda, MD.

(189) Good, D. J., and Gascoyne, R. D. (2008) Classification of non-Hodgkin's lymphoma. *Hematol Oncol Clin North Am 22*, 781-805.

(190) Jaffe, E. S. (2009) The 2008 WHO classification of lymphomas: implications for clinical practice and translational research. *Hematology Am Soc Hematol Educ Program*, 523-531.

(191) Yoon, S. S., Coit, D. G., Portlock, C. S., and Karpeh, M. S. (2004) The diminishing role of surgery in the treatment of gastric lymphoma. *Ann Surg 240*, 28-37.

(192) Fisher, R. I., Gaynor, E. R., Dahlberg, S., Oken, M. M., Grogan, T. M., Mize, E. M., Glick, J. H., Coltman, C. A. Jr., and Miller, T. P. (1993) Comparison of a standard regimen (CHOP) with three intensive chemotherapy regimens for advanced non-Hodgkin's lymphoma. *N Engl J Med 328*, 1002-1006.

(193) Palanca-Wessels, M. C., and Press, O. W. (2010) Improving the efficacy of radioimmunotherapy for non-Hodgkin lymphomas. *Cancer 16 (4s)*, 1126-1133.

(194) Tay, K., Dunleavy, K., and Wilson, W. H. (2010) Novel agents for B-cell non-Hodgkin lymphoma: science and the promise. *Blood Rev 24*, 69-82.

(195) Hurvitz, S. A., and Timmerman, J. M. (2005) Current status of therapeutic vaccines for non-Hodgkin's lymphoma. *Curr Opin Oncol 17*, 432-440.

(196) Ho, D. H., Brown, N. S., Yen, A., Holmes, R., Keating, M., Abuchowski, A., Newman, R. A., and Krakoff, I. H. (1986) Clinical pharmacology of polyethylene glycol-L-asparaginase. *Drug Metab Dispos 14*, 349-352.

(197) Abshire, T. C., Pollock, B. H., Billet, A. L., Bradley, P., and Buchanan, G. R. (2000) Weekly polyethylene glycol conjugated L-asparaginase compared with biweekly dosing produces superior induction remission rates in childhood relapsed acute lymphoblastic leukemia: a Pediatric Oncology Group Study. *Blood 96*, 1709-1715.

(198) Schluep, T., Cheng, J., Khin, K. T., and Davis, M. E. (2006) Pharmacokinetics and biodistribution of the camptothecin-polymer conjugate IT-101 in rats and tumor-bearing mice. *Cancer Chemother Pharmacol 57*, 654-662.

(199) Numbenjapon, T., Wang, J., Colcher, D., Schluep, T., Davis, M. E., Duringer, J., Kretzner, L., Yen, Y., Forman, S. J., and Raubitschek, A. (2009) Preclinical results of camptothecin-polymer conjugate (IT-101) in multiple human lymphoma xenograft models. *Clin Cancer Res 15*, 4365-4373.

(200) Wu, A. M., and Senter, P. D. (2005) Arming antibodies: prospects and challenges for immunoconjugates. *Nat Biotechnol 23*, 1137-1146.

(201) Ghetie, M. A., Bright, H., and Vitetta, E. S. (2001) Homodimers but not monomers of Rituxan (chimeric anti-CD20) induce apoptosis in human B-lymphoma cells and synergize with a chemotherapeutic agent and an immunotoxin. *Blood 97*, 1392-1398.

(202) Hernandez-Ilizaliturri, F. J., Jupudy, V., Ostberg, J., Oflazoglu, E., Huberman, A., Repasky, E., and Czuczman, M. S. (2003) Neutrophils contribute to the biological antitumor activity of rituximab in a non-Hodgkin's lymphoma severe combined immunodeficiency mouse model. *Clin Cancer Res 9*, 5866-5873.

(203) Zhang, N., Khawli, L. A., Hu, P., and Epstein, A. L. (2005) Generation of rituximab polymer may cause hyper-cross-linking-induced apoptosis in non-Hodgkin's lymphomas. *Clin Cancer Res 11*, 5971-5980.

(204) Tomita, A., Hiraga, J., Kiyoi, H., Ninomiya, M., Sugimoto, T., Ito, M., Kinoshita, T., and Naoe, T. (2007) Epigenetic regulation of CD20 protein expression in a novel B-cell lymphoma cell line, RRBL1, established from a patient treated repeatedly with rituximab-containing chemotherapy. *Int J Hematol 86*, 49-57.

(205) Chen, W. C., Completo, G. C., Sigal, D. S., Crocker, P. R., Saven, A. and Paulson, J. C. (2010) In vivo targeting of B-cell lymphoma with glycan ligands of CD22. *Blood 115*, 4778-4786.

(206) Ghetie, M. A., Tucker, K., Richardson, J., Uhr, J. W., and Vitetta, E. S. (1992) The antitumor activity of an anti-CD22 immunotoxin in SCID mice with disseminated Daudi lymphoma is enhanced by either an anti-CD19 antibody or an anti-CD19 immunotoxin. *Blood 80*, 2315-2320.

(207) Lapalombella, R., Zhao, X., Triantafillou, G., Yu, B., Jin, Y., Lozanski, G., Cheney, C., Heerema, N., Jarjoura, D., Lehman, A., Lee. L. J., Marcucci, G., Lee,

R. J., Caligiuri, M. A., and Byrd, J. C. (2008) A novel Raji-Burkitt's lymphoma model for preclinical and mechanistic evaluation of CD52-targeted immunotherapeutic agents. *Clin Cancer Res 14*, 569-578.

(208) Goldenberg, D. M., Rossi, E. A., Stein, R., Cardillo, T. M., Czuczman, M. S., Hernandez-Ilizaliturri, F. J., Hansen, H. J., and Chang, C. H. (2009) Properties and structure-function relationships of veltuzumab (hA20), a humanized anti-CD20 monoclonal antibody. *Blood 113*, 1062-1070.

(209) Hendrickson, E. A. (1993) The SCID mouse: relevance as an animal model system for studying human disease. *Am J Pathol 143*, 1511-1522.

(210) Tedder, T. F., and Engel, P. (1994) CD20: a regulator of cell-cycle progression of B lymphocytes. *Immunol Today 15*, 450-454.

(211) Ishibashi, K., Suzuki, M., Sasaki, S., and Imai, M. (2001) Identification of a new multigene four-transmembrane family (MS4A) related to CD20, HTm4 and beta subunit of the high-affinity IgE receptor. *Gene 264*, 87-93.

(212) Stashenko, P., Nadler, L. M., Hardy, R., and Schlossman, S. F. (1980) Characterization of a human B lymphocyte-specific antigen. *J Immunol 125*, 1678-1685.

(213) Reff, M. E., Carner, K., Chambers, K. S., Chinn, P. C., Leonard, J. E., Raab, R., Newman, R. A., Hanna, N., and Anderson, D. R. (1994) Depletion of B cells in vivo by a chimeric mouse human monoclonal antibody to CD20. *Blood 83*, 435-445.

(214) Anderson, K. C., Bates, M. P., Slaughenhoupt, B. L., Pinkus, G. S., Schlossman, S. F., and Nadler, L. M. (1984) Expression of human B cell-associated antigens on leukemias and lymphomas: a model of human B cell differentiation. *Blood 63*, 1424-1433.

(215) Pescovitz, M. D. (2006) Rituximab, an anti-CD20 monoclonal antibody: history and mechanism of action. *Am J Transplant 6*, 859-866.

(216) Kosmas, C., Stamatopoulos, K., Stavroyianni, N., Tsavaris, N., and Papadaki, T. (2002) Anti-CD20-based therapy of B cell lymphoma: state of the art. *Leukemia 16*, 2004-2015.

(217) Deans, J.P., Li, H., and Polyak, M. J. (2002) CD20-mediated apoptosis: signaling through lipid rafts. *Immunology 107*, 176-182.

(218) Smith, M. R. (2003) Rituximab (monoclonal anti-CD20 antibody): mechanisms of action and resistance. *Oncogene 22*, 7359-7368.

(219) Bubien, J. K., Zhou, L. J., Bell, P. D., Frizzell, R. A., and Tedder, T. F. (1993) Transfection of the CD20 cell surface molecule into ectopic cell types generates a

Ca^{2+} conductance found constitutively in B lymphocytes. *J Cell Biol 121*, 1121-1132.

(220) Polyak, M. J., Li, H., Shariat, N., and Deans, J. P. (2008) CD20 homo-oligomers physically associate with the B cell antigen receptor. Dissociation upon receptor engagement and recruitment of phosphoproteins and calmodulin-binding proteins. *J Biol Chem 283*, 18545-18552.

(221) Deans, J. P., Schieven, G. L., Shu, G. L., Valentine, M. A., Gilliland, L. A., Aruffo, A., Clark, E. A., and Ledbetter, J. A. (1993) Association of tyrosine and serine kinases with the B cell surface antigen CD20. Induction via CD20 of tyrosine phosphorylation and activation of phospholipase C-gamma 1 and PLC phospholipase C-gamma 2. *J Immunol 151*, 4494-4504.

(222) Deans, J. P., Kalt, L., Ledbetter, J. A., Schieven, G. L., Bolen, J. B., and Johnson, P. (1995) Association of 75/80-kDa phosphoproteins and the tyrosine kinases Lyn, Fyn, and Lck with the B cell molecule CD20. Evidence against involvement of the cytoplasmic regions of CD20. *J Biol Chem 270*, 22632-22638.

(223) Deans, J. P., Robbins, S. M., Polyak, M. J., and Savage, J. A. (1998) Rapid redistribution of CD20 to a low density detergent-insoluble membrane compartment. *J Biol Chem 273*, 344-348.

(224) Polyak, M. J., Tailor, S. H., and Deans, J. P. (1998) Identification of a cytoplasmic region of CD20 required for its redistribution to a detergent-insoluble membrane compartment. *J Immunol 161*, 3242-3248.

(225) Cragg, M. S., Morgan, S. M., Chan, H. T., Morgan, B. P., Filatov, A. V., Johnson, P. W., French, R. R., and Glennie, M. J. (2003) Complement-mediated lysis by anti-CD20 mAb correlates with segregation into lipid rafts. *Blood 101*, 1045-1052.

(226) Kanzaki, M., Shibata, H., Mogami, H., and Kojima, I. (1995) Expression of calcium-permeable cation channel CD20 accelerates progression through the G_1 phase in Balb/c 3T3 cells. *J Biol Chem 270*, 13099-13104.

(227) Li, H., Ayer, L. M., Lytton, J., and Deans, J. P. (2003) Store-operated cation entry mediated by CD20 in membrane rafts. *J Biol Chem 278*, 42427-42434.

(228) Walshe, C. A., Beers, S. A., French, R. R., Chan, C. H., Johnson, P. W., Packham, G. K., Glennie, M. J., and Cragg, M. S. (2008) Induction of cytosolic calcium flux by CD20 is dependent upon B Cell antigen receptor signaling. *J Biol Chem 283*, 16971-16984.

(229) Pierce, S. K. (2002) Lipid rafts and B-cell activation. *Nat Rev Immunol 2*, 96-105.

(230) Clark, E. A., Shu, G., and Ledbetter, J. A. (1985) Role of the Bp35 cell surface polypeptide in human B-cell activation. *Proc Natl Acad Sci USA 82*, 1766-1770.

(231) Golay, J. T., Clark, E. A., and Beverley, P. C. (1985) The CD20 (Bp35) antigen is involved in activation of B cells from the G_0 to the G_1 phase of the cell cycle. *J Immunol 135*, 3795-3801.

(232) Mattson, M. P., and Chan, S. L. (2003) Calcium orchestrates apoptosis. *Nat Cell Biol 5*, 1041-1043.

(233) Einfeld, D. A., Brown, J. P., Valentine, M. A., Clark, E. A., and Ledbetter, J. A. (1988) Molecular cloning of the human B cell CD20 receptor predicts a hydrophobic protein with multiple transmembrane domains. *EMBO J 7*, 711-717.

(234) Polyak, M. J., and Deans, J. P. (2002) Alanine-170 and proline-172 are critical determinants for extracellular CD20 epitopes; heterogeneity in the fine specificity of CD20 monoclonal antibodies is defined by additional requirements imposed by both amino acid sequence and quaternary structure. *Blood 99*, 3256-3262.

(235) Glennie, M. J., French, R. R., Cragg, M. S., and Taylor, R. P. (2007) Mechanisms of killing by anti-CD20 monoclonal antibodies. *Mol Immunol 44*, 3823-3837.

(236) Lim, S. H., Beers, S. A., French, R. R., Johnson, P. W., Glennie, M. J., and Cragg, M. S. (2010) Anti-CD20 monoclonal antibodies: historical and future perspectives. *Haematologica 95*, 135-143.

(237) Fanale, M. A., and Younes, A. (2007) Monoclonal antibodies in the treatment of non-Hodgkin's lymphoma. *Drugs 67*, 333-350.

(238) Press, O. W., Appelbaum, F., Ledbetter, J. A., Martin, P. J., Zarling, J., Kidd, P., and Thomas, E. D. (1987) Monoclonal antibody 1F5 (anti-CD20) serotherapy of human B cell lymphomas. *Blood 69*, 584-591.

(239) Jacene, H. A., Filice, R., Kasecamp, W., and Wahl, R. L. (2007) Comparison of ^{90}Y-ibritumomab tiuxetan and ^{131}I-tositumomab in clinical practice. *J Nucl Med 48*, 1767-1776.

(240) Stein, R., Qu, Z., Chen, S., Rosario, A., Shi, V., Hayes, M., Horak, I. D., Hansen, H. J., and Goldernberg, D. M. (2004) Characterization of a new humanized anti-CD20 monoclonal antibody, IMMU-106, and its use in combination with the humanized anti-CD22 antibody, epratuzumab, for the therapy of non-Hodgkin's lymphoma. *Clin Cancer Res 10*, 2868-2878.

(241) Morschhauser, F., Leonard, J. P., Fayad, L., Coiffier, B., Petillon, M. O., Coleman, M., Schuster, S. J., Dyer, M. J., Horne, H., Teoh, N., Wegener, W. A., and Goldernberg, D. M. (2009) Humanized anti-CD20 antibody, veltuzumab, in refractory/recurrent non-Hodgkin's lymphoma: phase I/II results. *J Clin Oncol 27*, 3346-3353.

(242) Morschhauser, F., Marlton, P., Vitolo, U., Linden, O., Seymour, J. F., Crump, M., Coiffier, B., Foa, R., Wassner, E., Burger, H. U., Brennan, B., and Mendila, M.

(2010) Results of a phase I/II study of ocrelizumab, a fully humanized anti-CD20 mAb, in patients with relapsed/refractory follicular lymphoma. *Ann Oncol*, doi:10.1093/annonc/mdq027.

(243) Keating, M. J., Dritselis, A., Yasothan, U., and Kirkpatrick, P. (2010) Ofatumumab. *Nat Rev Drug Discov 9*, 101-102.

(244) Mossner, E., Brunker, P., Moser, S., Puntener, U., Schmidt, C., Herter, S., Grau, R., Gerdes, C., Nopora, A., van Puijenbroek, E., Ferrara, C., Sondermann, P., Jager, C., Strein, P., Fertig, G., Friess, T., Schull, C., Bauer, S., Dal Porto, J., Del Nagro, C., Dabbagh, K., Dyer, M. J., Poppema, S., Klein, C., and Umana, P. (2010) Increasing the efficacy of CD20 antibody therapy through the engineering of a new type II anti-CD20 antibody with enhanced direct and immune effector cell-mediated B-cell cytotoxicity. *Blood 115*, 4393-4402.

(245) Oflazoglu, E., and Audoly, L. P. (2010) Evolution of anti-CD20 monoclonal antibody therapeutics in oncology. *MAbs 2*, 14-19.

(246) Bello, C., and Sotomayor, E. M. (2007) Monoclonal antibodies for B-cell lymphomas: rituximab and beyond. *Hematology Am Soc Hematol Educ Program*, 233-242.

(247) Cochlovius, B., Braunagel, M., and Welschof, M. (2003) Therapeutic antibodies. *Mod Drug Discovery October*, 33-38.

(248) Major, E. O., Amemiya, K., Tornatore, C. S., Houff, S. A., and Berger, J. R. (1992) Pathogenesis and molecular biology of progressive multifocal leukoencephalopathy, the JC virus-induced demyelinating disease of the human brain. *Clin Microbiol Rev 5*, 49-73.

(249) Major, E. O. (2009) Reemergence of PML in natalizumab-treated patients – new cases, same concerns. *N Engl J Med 361*, 1041-1043.

(250) Allison, M. (2010) PML problems loom for Rituxan. *Nat Biotechnol 28*, 105-106.

(251) Browning, J. L. (2006) B cells move to centre stage: novel opportunities for autoimmune disease treatment. *Nat Rev Drug Discov 5*, 564-576.

(252) van der Kolk, L. E., Grillo-Lopez, A. J., Baars, J. W., Hack, C. E., and van Oers, M. H. (2001) Complement activation plays a key role in the side-effects of rituximab treatment. *Br J Haematol 115*, 807-811.

(253) Law, C. L., Cerveny, C. G., Gordon, K. A., Klussman, K., Mixan, B. J., Chace, D. F., Meyer, D. L., Doronina, S. O., Siegall, C. B., Francisco, J. A., Senter, P. D., and Wahl, A. F. (2004) Efficient elimination of B-lineage lymphomas by anti-CD20-auristatin conjugates. *Clin Cancer Res 10*, 7842-7851.

CHAPTER 2

NOVEL SYNTHESIS OF HPMA COPOLYMERS CONTAINING PEPTIDE GRAFTS AND THEIR SELF-ASSEMBLY INTO HYBRID HYDROGELS

2.1. Summary

A new pathway for the synthesis of *N*-(2-hydroxypropyl)methacrylamide (HPMA) copolymers containing coiled-coil forming motifs of different sequences was developed and their self-assembly into hybrid hydrogels was investigated. Linear water-soluble polyHPMA was chosen as the polymer backbone due to its excellent biocompatibility. Upon macromonomer copolymerization, coiled-coil motifs were covalently attached onto the polymeric backbone forming the grafts. Peptide chain length was one of the major factors examined in this study regarding its influence on gelation ability of the resulted graft copolymers. Results showed that at least four heptads were needed to facilitate the hybrid system to form hydrogels under the experimental conditions tested. Other possible

---

Note: This chapter is reprinted with permission from the following publication: Wu, K., Yang, J., Koňák, Č., Kopečková, P., and Kopeček, J. (2008) Novel synthesis of HPMA copolymers containing peptide grafts and their self-assembly into hybrid hydrogels. *Macromol Chem Phys 209*, 467-475.

factors affecting the kinetics of hydrogel self-assembly were also scrutinized: concentration and temperature. These factors played a critical role in the process of self-assembly and gel formation, as demonstrated in this study.

2.2. Introduction

Hybrid hydrogels are usually referred to as hydrogel systems with components from at least two distinct classes of molecules, for example, synthetic polymers and biological macromolecules, interconnected either covalently or noncovalently *(1, 2)*. Peptide and/or protein segments have been used to introduce degradability *(3-5)*, temperature-dependent phase responsiveness *(6, 7)* and sensitivity to the presence of active biomolecules *(8, 9)* into the hybrid hydrogel structure. Water-soluble synthetic polymers have been cross-linked with molecules of biological origin, such as oligopeptides *(3-5)*, oligodeoxyribo-nucleotides *(10)*, cross-linking agents containing oligolactate esters or oligoglycolate esters *(11)*, stereospecific D,L-lactic acid oligomers *(12)* or antigen-antibody binding *(8)*.

Numerous protein motifs have been combined with synthetic polymers to produce macromolecules whose self-assembly into hydrogels is mediated by protein domains *(6, 13-18)*. One of the frequently used protein folding motifs is the coiled-coil. It consists of two or more α-helices wound together forming a super-helix *(19)*. Its primary structure is featured by repeats of heptad, seven amino acid sequence designated as $(abcdefg)_n$, where *a* and *d* positions are usually taken by hydrophobic residues. The formation and stability of coiled-coils depend on the structure and the number of heptad repeats *(20)*. The distinctive feature of coiled-coils is the specific spatial recognition, association and dissociation of the helices, making it an ideal model for protein biomaterials in which the

higher structure may be pre-determined by the primary amino acid sequence *(21, 22)*.

Recently, *N*-(2-hydroxypropyl)methacrylamide (HPMA) graft copolymers containing coiled-coil sequences were designed and their self-assembly into hydrogels evaluated *(13, 14)*. One of the designs was composed of a linear, water-soluble polyHPMA as polymer backbone, and coiled-coil forming peptides as grafts. Three peptides of different chain lengths [$(VSKLESK)_n$-(KSKLESK)-(VSKLESK)GYC, n=1-3] were attached to an HPMA copolymer precursor by a polymer-analogous reaction of SH groups with maleimido groups at the termini of the copolymer side chains *(13)*. The results revealed that the length and number of coiled-coil grafts per macromolecule had a significant impact on the gelation process.

Alternatively, peptide grafts can be incorporated into water-soluble polymers by radical copolymerization of a peptide-containing macromonomer and a primary chain-forming monomer, such as HPMA or acrylamide. For instance, synthetic peptide vaccines were prepared by copolymerization of acrylamide with peptides capped at the *N*-terminus with *N*-acryloylaminohexanoyl groups *(23)*. Targetable HPMA copolymer-photosensitizer conjugates were prepared, in a one-step process, by copolymerization of HPMA, a polymerizable derivative of mesochlorin e_6 (photosensitizer) and a polymerizable Fab' antibody fragment *(24)*.

Here, three macromonomers, containing coiled-coil forming peptides of the structure [$(VSKLESK)_n$-(KSKLESK)-(VSKLESK), n=1-3], and capped at the *N*-terminus with an *N*-methacryloylglycylglycyltryptophan spacer, were synthesized by solid phase peptide synthesis and copolymerized with HPMA. The influence of graft length, concentration and temperature on the self-assembly of graft copolymers into

hydrogels was evaluated by physicochemical methods, including circular dichroism (CD) spectroscopy, microrheology and dynamic light scattering (DLS).

2.3. Materials and methods

2.3.1. Materials

Side-chain protected Fmoc-amino acids, 2-chlorotrityl resin, 1-hydroxy-benzo-triazole (HOBt), and benzotriazole-1-yl-oxy-tris-pyrrolidino-phosphonium hexafluoro-phosphate (PyBOP) were purchased from Novabiochem (San Diego, CA). *N,N*-dimethyl-formamide (DMSO) was purchased from EMD Chemicals, Inc. (Gibbstown, NJ). 2,2,2-trifluorothanol (TFE), DMF, trifluoroacetic acid (TFA), methanol and piperidine were purchased from VWR International (West Chester, PA). HPMA *(25)* and *N*-methyacryl-oylglyglycine (MaGG-OH) *(26)* were synthesized as previously reported. The water-soluble azo-initiator, VA044, was obtained from Wako Chemicals (Richmond, VA).

2.3.2. Macromonomer synthesis and purification

Macromonomers containing 24, 31 and 38 amino acids (Table 2.1) were synthesized using a solid phase method and a manual Fmoc/tBu strategy on 2-chlorotrityl resin, as described previously *(13, 27)*. The peptides contained 3, 4 and 5 coiled-coil forming heptads (Figure 2.1) and *N*-termini capped with a *N*-methacryloylglycylglycyltryptophan spacer. A fragment condensation strategy was adopted. After the attachment of 14 amino acid residues, corresponding number of side-chain protected VSKLESK segments were coupled. Finally, peptides were cleaved and side-chains deprotected from the resin using a TFA/H_2O/triisopropylsilane (95:2.5:2.5)mixture for 2 h under constant shaking.

Table 2.1. Macromonomer structures.

Macromonomer	Structure	# of amino acids	Molecular Weight	
			Theoretical	Measured[a)]
MaCC3[b)]	Ma-GGW(VSLKESK)$_1$ KSKLESKVSKLESK	24	2731.2	2731.6
MaCC4	Ma-GGW(VSLKESK)$_2$ KSKLESKVSKLESK	31	2504.0	2504.1
MaCC5	Ma-GGW(VSLKESK)$_3$ KSKLESKVSKLESK	38	4275.4	4275.6

a) molecular weight measured using MALDI-TOF MS; b) Ma, methacryloyl; CC, coiled-coil; 3 (4 or 5), number of heptads.

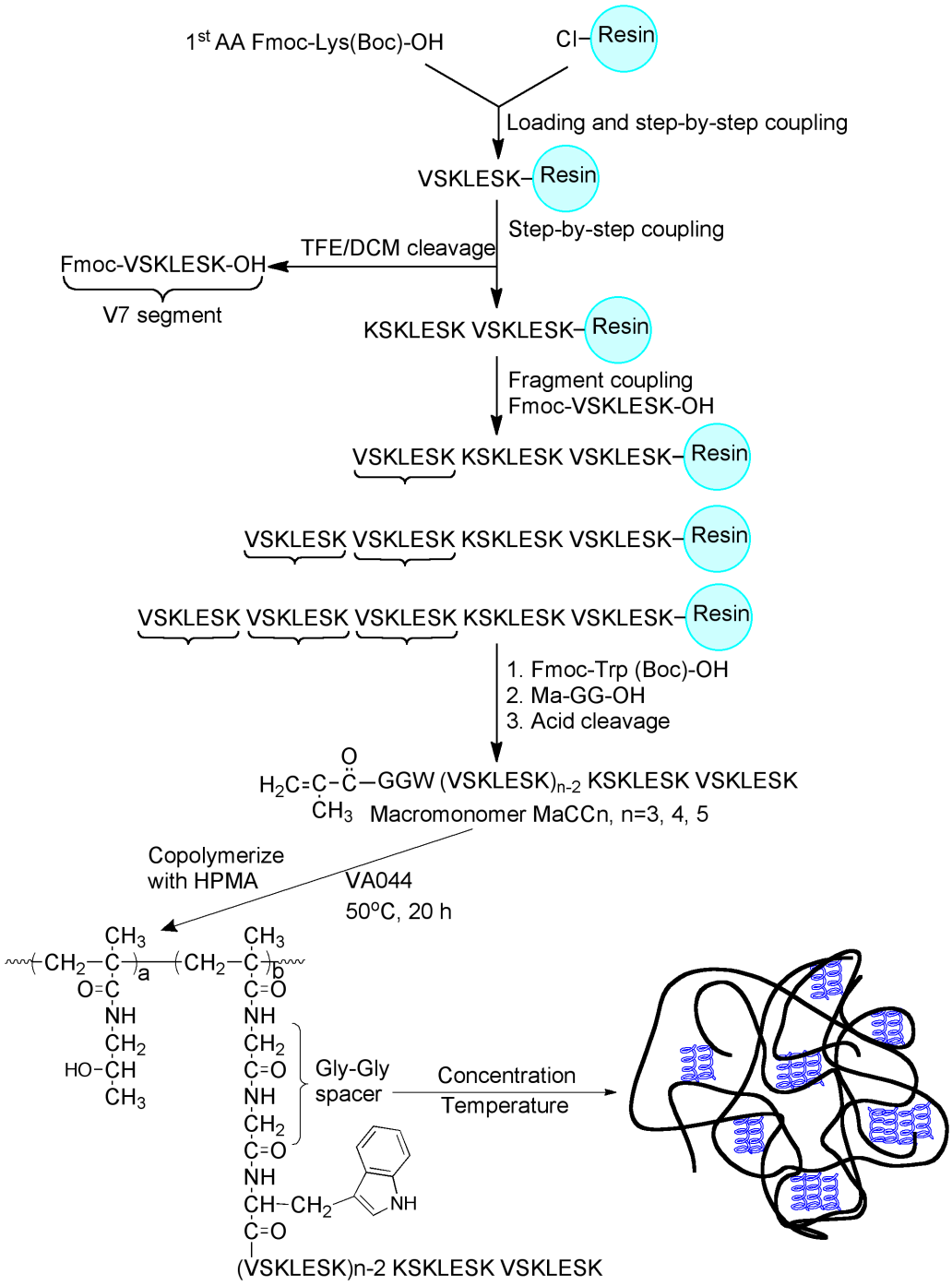

Figure 2.1. Schemes for macromonomers synthesis, free radical copolymerization, and self-assembly of the graft copolymers into hybrid hydrogels.

Crude macromonomers were purified using RP-HPLC (Agilent Technologies, Zorbax 300SB-CN, 9.4×250 mm, 5 μm, flow rate of 3 mL·min^{-1}) with a gradient from 20 to 40% of buffer B within 40 min. Buffer A was 0.1% TFA in water and buffer B 0.1% TFA in acetonitrile. Yields of macromonomers were 5–15%. Macromonomer structures were validated using matrix-assisted laser desorption-ionization time-of-flight mass spectroscopy (MALDI-TOF MS) (Voyager-DE STR Biospectrometry Workstation, Perseptive Biosystems).

2.3.3. Graft copolymer synthesis and purification

HPMA and corresponding macromonomers were copolymerized by free radical copolymerization (Figure 2.1) in water using VA044 as the initiator. For example, HPMA (2.86 mg, 2×10^{-5} mol) and MaCC3 (2.87 mg, 10^{-6} mol) were mixed in an Eppendorf tube and purged with N_2 for at least 10 min; then 23 μL VA044 (0.206 mg, 6.4×10^{-7} mol) aqueous solution, prebubbled with N_2 for 5 min, was added to dissolve the particles. The reaction solution was transferred and sealed in a capillary tube, and maintained at 50 ^{o}C for 20 h. Crude graft copolymers were collected by precipitation into an excess of acetone and further purified by size exclusion chromatography (SEC) (ÄKTA, Amersham Pharmacia Biotech; Superose 12 column) using phosphate-buffered saline (PBS, pH=7.4) as mobile phase. Fractions containing target copolymers were pooled, dialyzed against distilled water to remove salts and then freeze-dried. Final yields of copolymers were 40–60%. The molecular weight and molecular weight distribution of the copolymers were measured by SEC using ÄKTA system equipped with ultraviolet (UV) and refractive index (RI) detectors on a Superose 6 HR10/30 column eluted with

PBS (pH=7.4). The average molecular weights were calculated against a calibration with polyHPMA fractions. Graft contents in copolymers were determined by UV spectrophotometry (tryptophan: ε=5,580 L·mol^{-1}·cm^{-1} at 280 nm in PBS) *(28, 29)*. Key features of the graft copolymers are summarized in Table 2.2.

2.3.4. Circular dichroism (CD) spectroscopy

Circular dichroism (CD) spectra were collected on an Aviv 62DS CD spectrometer with a thermoelectric temperature control system. All samples were dissolved and dialyzed against benign buffer (5×10^{-2} M Na_2HPO_4/NaH_2PO_4/0.1 M KCl, pH=7.0) for 6 h using a dialysis membrane with a molecular weight cut-off of 2 kDa. Final concentrations of the peptides were determined by UV spectroscopy at 280 nm ($\approx10^{-4}$ M). Wavelength scans were recorded at a step-width of 1 nm with a 5 sec averaging time at each step from 200 to 250 nm using a 0.1 cm path length quartz cuvette. The spectra acquired were averaged from three consecutive scans and subtracted from the background. Ellipticity was reported as the mean residue ellipticity ([θ], in deg·cm^2·dmol^{-1}) calculated using function 2.1:

$$[\theta]_{222} = [\theta]_{obs} \times (MRW/10lc) \qquad (2.1)$$

where $[\theta]_{obs}$ is the ellipticity measured in millidegrees, *MRW* is the mean residue molecular weight of the polypeptide (molecular weight of the peptide divided by the number of amino acid residues), *l* is the optical path length of the cell in cm (0.1 cm), and *c* is the peptide concentration in mg·mL^{-1}.

Table 2.2. Key features of HPMA graft copolymers.

Copolymer	$\overline{M}_n$(kDa)	$\overline{M}_w / \overline{M}_n$	# of grafts per copolymer
PMaCC3	55.2	1.6	6.0
PMaCC4	57.8	1.5	6.7
PMaCC5	41.9	1.3	8.1

P, polymer.

2.3.5. Microrheology

Microrheology measures the mechanical properties of a material by monitoring the motion of micrometer-sized tracer particles in small sample volumes (usually less than 10 μL). In passive microrheology, there is no external driving force applied to the tracer particles; the intrinsic Brownian motion of the particles is used, driven by thermal energy (k_BT). The theoretical basis for passive microrheology is a generalized Stokes-Einstein relation (GSER) for materials with viscoelastic properties *(30, 31)*, and can be presented in the following form:

$$\left\langle \Delta\tilde{r}^2(s) \right\rangle = \frac{dk_BT}{3\pi as\tilde{G}(s)} \tag{2.2}$$

where $\left\langle \Delta\tilde{r}^2(s) \right\rangle$ is the Laplace transform of the tracer particles' mean-squared displacement (MSD) $\left\langle (r(t+\tau)-r(t))^2 \right\rangle$, d is the dimensionality of the displacement vector (usually 2 in video-microscopy), s is the Laplace frequency, a is the radius of the particles and $\tilde{G}(s)$ is the Laplace representation of the complex modulus, which encompasses the storage G' and loss G'' moduli.

Self-assembly of hydrogels (Figure 2.1) was examined in the presence of a suspension of fluorescently labeled latex beads (radius 0.5 μm, surfactant-free yellow-green fluorescent amidine-modified microspheres). The copolymer (10% w/v) was dissolved in DMSO/H_2O (50 vol.%), and latex beads were added and evenly mixed, then the sample was sealed between a microscope slide and a No. 1.5 glass cover slip with Cytoseal™ 60. Brownian motion of the embedded particles under particular experimental conditions (concentration, temperature and pH) was monitored with an epifluorescence optical microscope (Nikon Eclipse E800) using a 100×, NA=1.3, oil-immersion objective

and a CCD camera (Dage-MTI, DC330) with an exposure time of 2 msec. To avoid wall effects, the focus plane was set at least 20 μm into the sample chambers. For each sample, 3,000 images were recorded using StreamPix software (Norpix Inc.) at intervals of 33 ms. Images then were analyzed with IDL image analysis software (Research Systems Inc, Boulder, CO) and the trajectories of the particles were extracted using algorithms developed and kindly provided by Crocker and co-workers *(32)*.

2.3.6. Dynamic light scattering (DLS)

DLS studies were conducted using a Brookhaven BI-200SM goniometer and BI-9000AT digital correlator equipped with a He-Ne laser (λ=633 nm). Different concentrations of PMaCC5 in deionized (DI) water were measured at 10 ^{o}C and selected samples were then measured at different temperatures (4-62 ^{o}C) to elucidate the temperature dependence of gel cluster formation. The time correlation functions of the scattered intensity $G^{(2)}(t)$, where t is the delay time, were analyzed using the inverse Laplace transformation technique (the REPES *(33)* analysis in the program GENDIST in this case) to calculate the distribution function of relaxation times, τ.

Since the REPES analysis has a tendency to split broad distributions into two or more contributions (overfitting), the correlation functions were also fitted to a stretched exponential function with an exponent β. The exponent β ($0 \leq \beta \leq 1$) is interpreted as a measure of the width of the corresponding distribution of relaxation times, τ: the smaller is the value of β, the broader is the distribution. The mean relaxation time is given by, $\tau_c=(\tau_0/\beta)\Gamma(1/\beta)$, where τ_0 is the effective relaxation time obtained from force fitting to a stretched exponential function and $\Gamma(1/\beta)$ is the gamma function. DLS results were

presented using a plot of normalized intensity correlation function, $g^{(2)}(t)$-1 versus log(t). The apparent hydrodynamic radius (Rh) was calculated from the mean relaxation time τ_c via the Stokes-Einstein equation:

$$R_h = k_B T q^2 \tau_c / 6\pi\eta \quad (2.3)$$

where k_B is the Boltzmann constant, T is the absolute temperature, q is the scattering vector ($q=4\pi n_s \cdot \sin(\theta/2)/\lambda$, where n_s is the refractive index of the solvent, θ is the scattering angle, and λ is the wavelength of incident laser light in vacuum), and η is the solvent viscosity. Repeated measurements were undertaken for each sample in order to calculate an average hydrodynamic radius.

Since the position of $g^{(2)}(t)$-1plot on the x axis depends not only on the R_h of particles but also on temperature T and solvent viscosity $\eta_{(T)}$, we used a comparison of time correlation functions measured at different temperatures, a new variable $t'=t\mathrm{T}/\eta$, to replace the delay time t. In this new plot, the position of $g^{(2)}(t')$-1 on the x axis (t') is only related to temperature-induced variations of the mean R_h of particles.

2.4. Results and discussion

HPMA copolymers composed of various macromonomers, such as methacryloylated α-methoxypoly(ethylene glycol) *(34)* and polymerizable antibody fragments *(24)* have been reported previously. Here, new macromonomers containing 3, 4 and 5 coiled-coil forming haptads were synthesized. The fact that both HPMA and the macromonomers contain methacryloyl groups as polymerizable components ensures the compatibility of comonomers in free radical copolymerization.

2.4.1. Design, synthesis and copolymerization of macromonomers

The design of macromonomers was based on the well-characterized heptad VSSLESK. A model peptide (EK42), composed of six VSSLESK heptads, forms parallel homodimers at room temperature and neutral pH *(35)*. To reveal the structure-property relationship, peptides containing 3, 4 and 5 heptads were chosen for evaluation. Two structural modifications were exercised to the EK42 structure *(13)*. To promote "in-register" alignment of the peptide domains, valine in position *a* of the second heptad was substituted with lysine. In addition, serine residues in all *c* positions were replaced by lysine. The latter might destabilize the coiled-coil by electrostatic repulsion between the *c* and *g* positions on the same strand to achieve better responsiveness of hydrogels to temperature change.

In a previous publication, the peptides were capped at *N*-termini with CGG *(13)*. This permitted their attachment to HPMA copolymers containing maleimido end-groups on side chains. To create macromonomers, *N*-termini of the peptides were capped with *N*-methacryloylglycylglycyltryptophan (MaGGW, Table 2.1).

HPMA graft copolymers, PMaCC3, PMaCC4 and PMaCC5, were prepared by radical polymerization using a water-soluble azoinitiator, VA044. The copolymerization proceeded to a high conversion and yield (70–80%) of the copolymers. Although the macromonomers contained peptides of different lengths (3, 4 or 5 heptads), a similar content of grafts per copolymer was observed. This seems to indicate that the impact of the length of the oligopeptide sequence on the polymerization process was minor. However, the content of grafts in the final copolymer was lower than that in the feeding. Due to the reactivity difference between HPMA and macromonomers, the graft

copolymers may possess two levels of heterogeneity: a distribution of molecular weights and distribution of chemical composition.

2.4.2. Secondary structure of peptides in macromonomers and HPMA copolymers

Secondary structure of peptides in macromonomers and copolymers was evaluated by CD spectrometry under benign conditions (5×10^{-2} M Na_2HPO_4/ NaH_2PO_4, 0.1 M KCl, pH=7). CD spectrum of interacting coiled-coil motifs has a characteristic feature of double negative peaks at 208 and 222 nm respectively, demonstrating an α-helical secondary structure *(36)*. The molar ellipticity at 222 nm can be used to estimate the content of the helical structure present in a peptide *(37)*. A ratio of ellipticity at 222 versus 208 nm ($[\theta]_{222}/[\theta]_{208}$) close to 1 is an indication of strong interaction of α-helices, which leads to coiled-coil formation in our case *(13)*. Wavelength scans indicated that the helical content of MaCC3, MaCC4 and MaCC5 were 6.62, 8.02 and 8.51%, respectively *(38)*. As the chain length increased, the ellipticity at 222 nm tended to gradually increase. This suggested that all three peptides were essentially in the unfolded state under benign conditions at room temperature (Figure 2.2). This proved the contribution of the sequence modification that described above, as the secondary structure of $(VSSLESK)_x$ showed a typical pattern of α-helical structure when x was 5. To investigate whether these peptides had the potential to fold into α-helices (or the maximum possible helical content), CD spectra of macromonomers were also examined in the presence of 50% TFE. TFE has been shown to disrupt tertiary and quaternary structure but promote α-helix formation as a monomeric molecule. Corresponding spectra showed that their molar ellipticity at 222

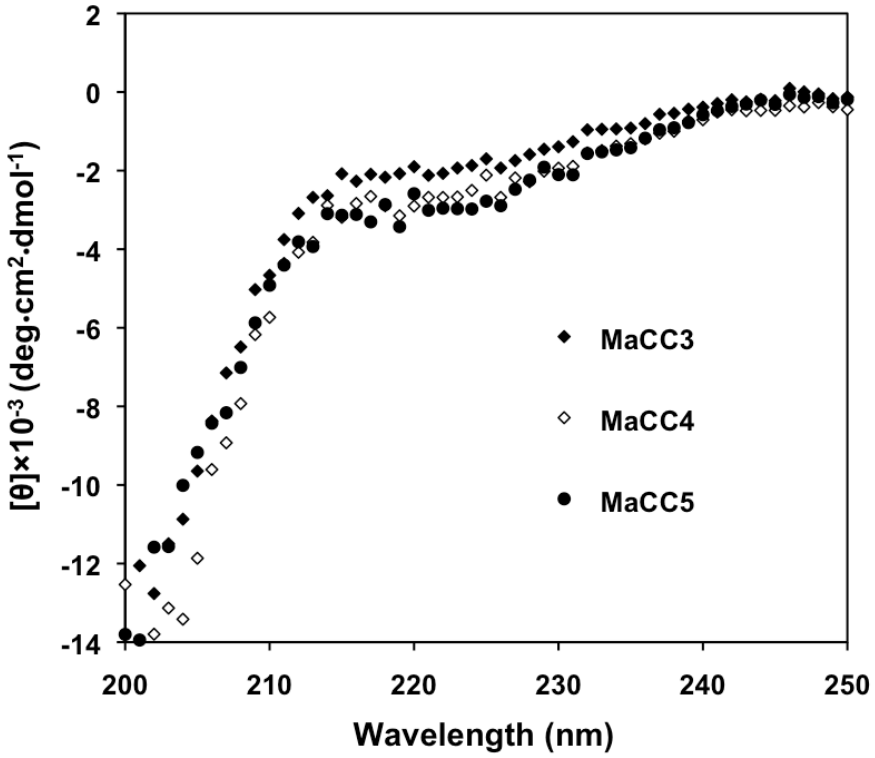

Figure 2.2. CD spectra of macromonomers under benign conditions. The spectra were recorded at 25 ^{o}C in 5×10^{-2} M Na_2HPO_4/NaH_2PO_4, 0.1 M KCl, pH=7.0. Peptide concentrations were approximately 10^{-4} M.

nm became considerably more negative (Figure 2.3), a phenomenon suggested that the peptides are capable of forming highly helical structures (e.g., MaCC5 28.8%). Incorporation of the macromonomers into HPMA graft copolymers resulted in an increase of α-helical content, especially in the case of PMaCC5, compared to free peptides (Figure 2.4). Addition of 50% of TFE could further enhance this effect. This result is in a good agreement with the observed secondary structure of (VSSLESK)x and PEG_{2000}-(VSSLESK)x diblock copolymers *(27)*. Moreover, HPMA graft copolymers prepared by two different methods, polymer-analogous reaction *(13)* and macromonomer copolymerization, possessed similar properties. This implied that the distribution of grafts along the polymer backbone is similar for graft copolymers constructed from either synthetic pathway. Alternatively, the techniques used for the analysis of copolymer properties may not be sensitive enough to detect minor changes in the distribution of grafts along the HPMA copolymer backbone.

2.4.3. Self-assembly of HPMA graft copolymers into hydrogels

The impact of heptad number on the self-assembly of HPMA graft copolymers into hydrogels was evaluated by microrheology and dynamic light scattering. Microrheology relies on the measurement of thermally induced Brownian motion of micrometer-size tracer particles dispersed in the samples. MSD of tracer particles increases linearly with time in a viscous solution. In a hydrogel, the motion of the embedded tracer particles is confined, which results in constant MSDs, independent of lag time.

The number of heptads in PMaCC3 was too low to mediate the self-assembly of the copolymer into three-dimensional structures; the MSD continuously increased with time

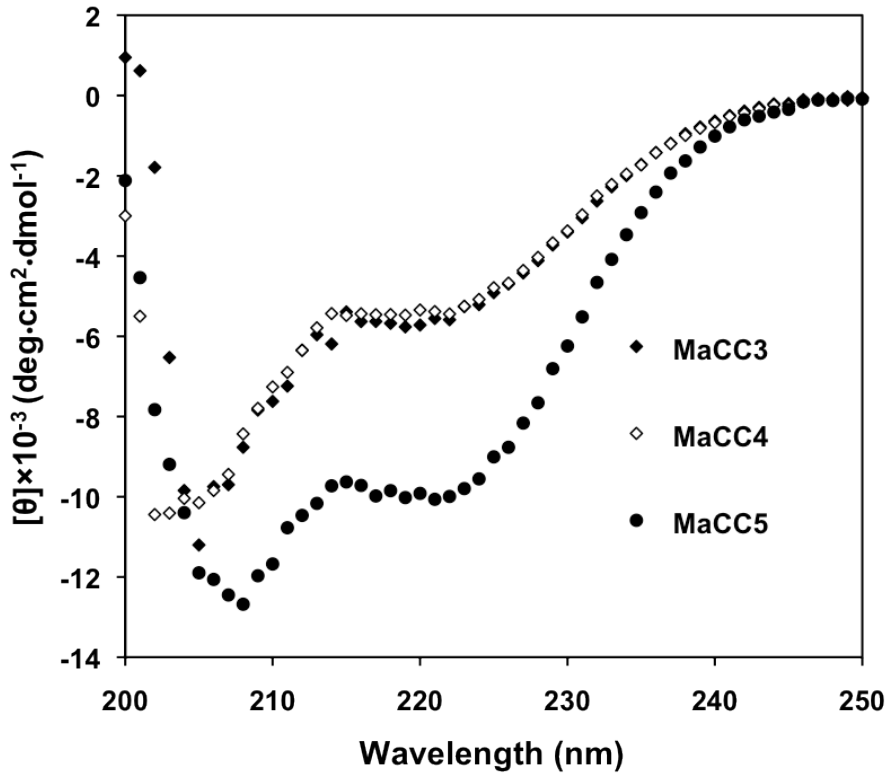

Figure 2.3. CD spectra of macromonomers in 50% of the α-helix enhancing agent TFE. The spectra were recorded at 25 ^{o}C in 5×10^{-2} M Na_2HPO_4/NaH_2PO_4, 0.1 M KCl, pH=7.0. Peptide concentrations were approximately 10^{-4} M. TFE, trifluoroethanol.

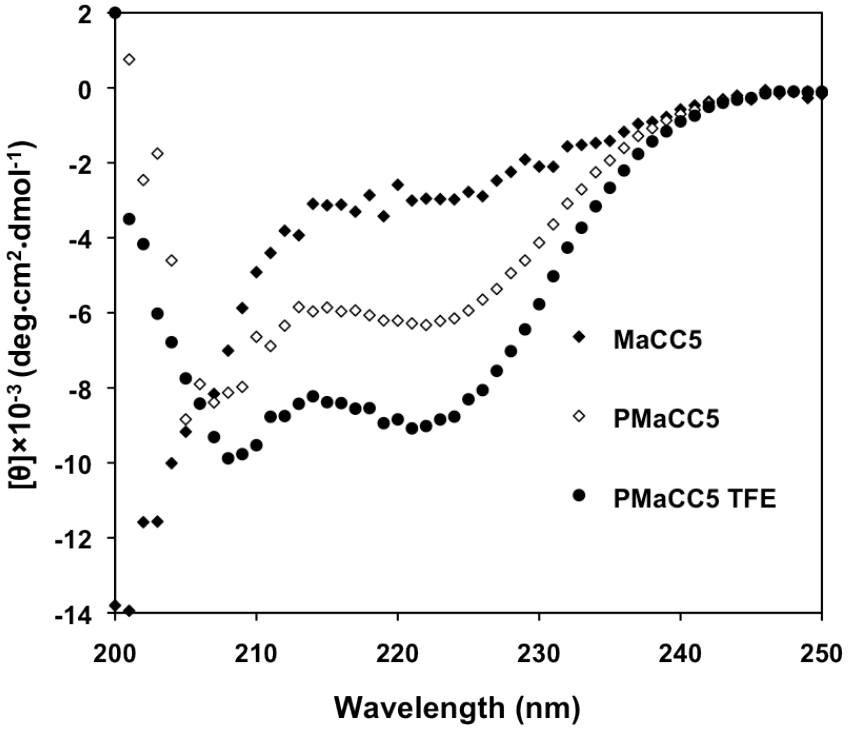

Figure 2.4. Comparison of CD profiles: MaCC5, PMaCC5 and PMaCC5 50% of the α-helix inducing solvent TFE. The spectra were recorded at 25 ^{o}C in 5×10^{-2} M Na_2HPO_4 /NaH_2PO_4, 0.1 M KCl, pH=7.0. Peptide concentrations were approximately 10^{-4} M. TFE, trifluoroethanol.

(Figure 2.5). However, the MSD of PMaCC4 and PMaCC5 were found to become constant with time, indicating self-assembly into hydrogels. The results of CD measurements (Figure 2.4) suggested that only for PMaCC5 was the self-assembly mediated by coiled-coil formation. In PMaCC4, non-specific interactions probably led to the self-assembly since there was no α-helical structure in the peptide domain observed by CD. As discussed before, the structure of the hydrogels is delicate, the oligopeptide sequences may form inter- and intra-molecular parallel homodimers. Cross-linking would then occur by the formation of tetramers and higher order aggregates *(6)*. For these structures, the steric hindrance of the polymer backbone on self-assembly becomes an important factor. Recently, it was shown that the design of HPMA copolymers containing oppositely charged sequences forming anti-parallel heterodimers could minimize steric hindrance *(14)*.

Dynamic light scattering is a method suitable for the characterization of nanoparticles and the evaluation of the time-dependence of the self-assembly. Therefore, the effect of temperature and polymer concentration on the self-assembly of PMaCC5 into hydrogel clusters (nanoparticles, aggregates) was investigated by DLS. The normalized intensity autocorrelation function, $g^{(2)}(t)$, for solutions of PMaCC5 was plotted as a function of $\log(t)$ for different graft copolymer concentrations, c=1.38, 2.76, 5.52, 8.00 and 9.20 $mg{\cdot}mL^{-1}$, in Figure 2.6a. All samples used for the measurement of concentration dependence were not filtered in order to keep them comparable since there was a small portion of large particles present in high concentration sample solutions (i.e., 8.00 and 9.20 $mg{\cdot}mL^{-1}$). Correlation function profiles changed with increasing concentrations from sharp ones at low concentrations to a broad one, extending over

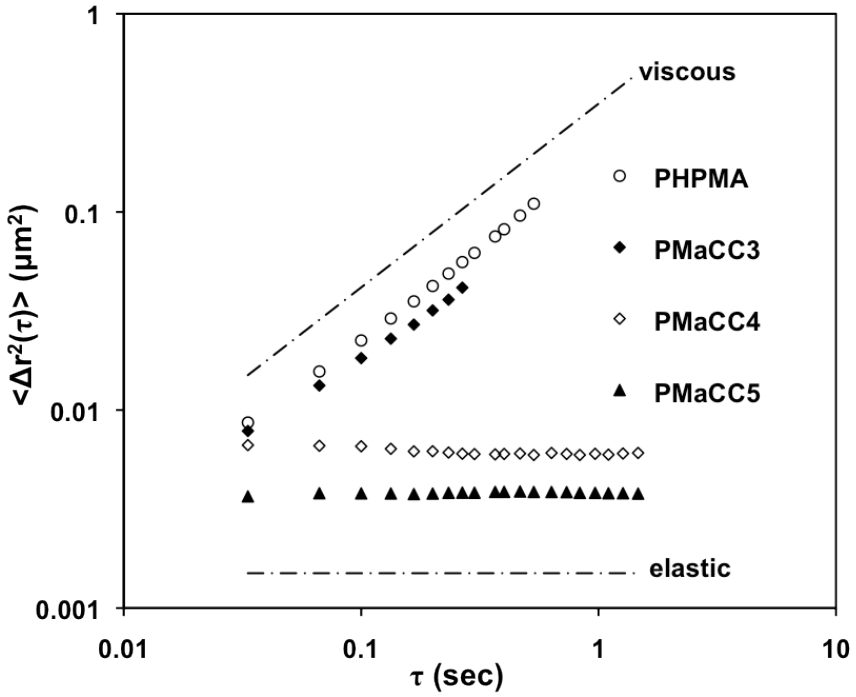

Figure 2.5. Mean-square displacement (MSD) as a function of lag time for 0.5 μm amidine-modified latex beads in 50 vol.% DMSO/H_2O. Also shown is a control solution of polyHPMA (o).

several orders of magnitude of t, at the highest concentration. The mean hydrodynamic radii of the polymer clusters, R_h, as calculated from results obtained by fitting of the time correlation functions in Figure 2.6a to a stretched exponential function were shown in Figure 2.6b. The particle size was independent of concentration at low concentrations and dramatically increased as concentration increased above 5.52 mg·mL^{-1}. The β value was about 0.90 at low concentrations and decreased to 0.75 at c=9.20 mg·mL^{-1}. These results strongly indicated the self-assembly of copolymers into clusters and underscored the importance of polymer concentration in this process. A formation of large aggregates (about 1 μm) was observed at c=9.20 mg·mL^{-1}. These data are in agreement with the results of the random association of synthetic block copolymers in selective solvents *(39)*, and with the self-assembly of graft copolymers containing sequences forming anti-parallel heterodimers *(40)*.

The normalized intensity autocorrelation functions were also measured for 5.52 mg·mL^{-1} PMaCC5 at temperatures ranging from 4 to 62 ^{o}C and $g^{(2)}(t')$ results were plotted as a function of $\log(tT/\eta)$ (Figure 2.7a). The autocorrelation functions shifted gradually as temperature increased to higher t' values reflecting the increase of R_h with increasing temperature. This demonstrated the effect of temperature on the association: as temperature went up, the collision probability of grafts also increased, so that the self-assembly of copolymers was more effective at higher temperatures. The temperature dependence of average R_h values, as obtained by the force fitting of the correlation functions from Figure 2.7a to a stretched exponential function, was shown in Figure 2.7b. R_h increased with increasing temperature while β values were practically independent of temperature, β=0.7±0.02.

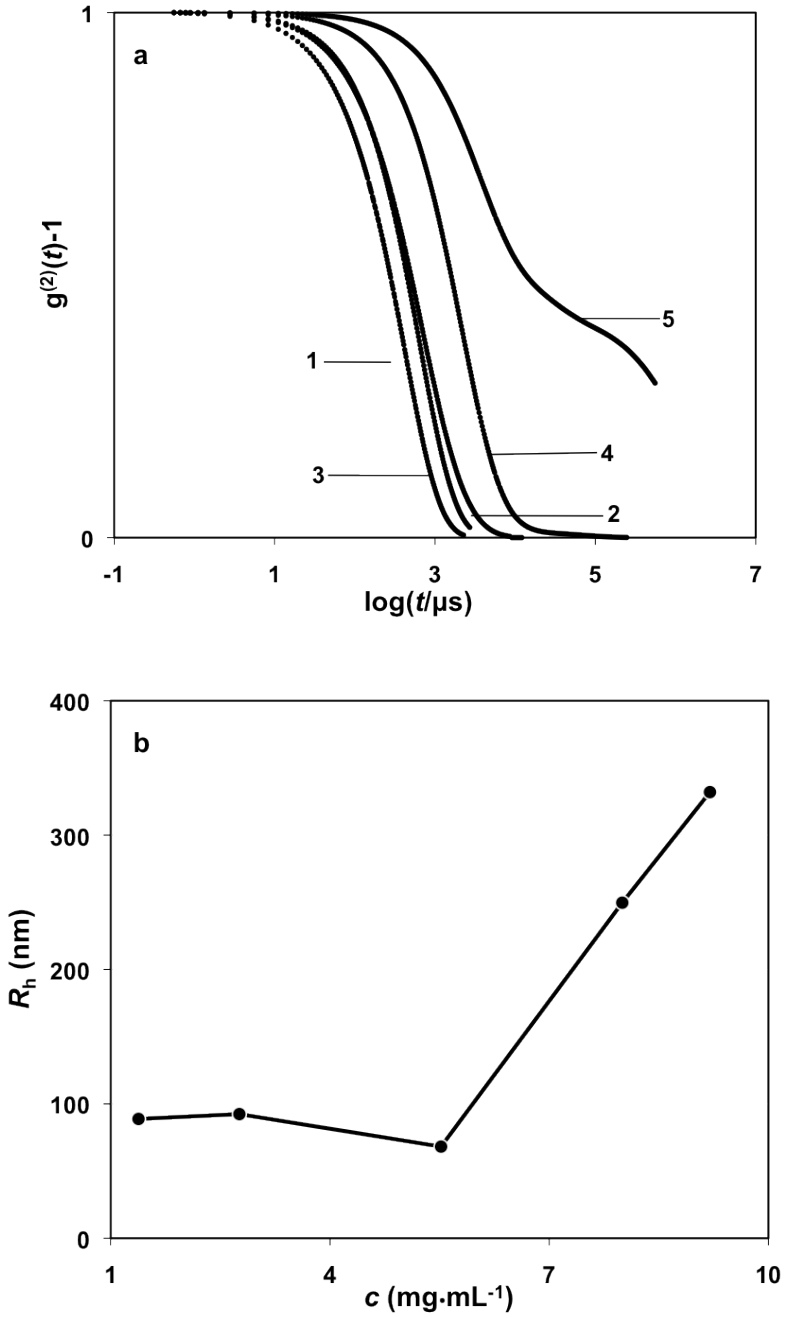

Figure 2.6. Concentration-dependence of PMaCC5 gel formation. a) Normalized intensity autocorrelation functions, $g^{(2)}(t)$-1, at a scattering angle of 90°, for aqueous solutions of PMaCC5 at 10 °C. Concentrations of graft co-polymer were: (1) 1.38, (2) 2.76, (3) 5.52, (4) 8.00, (5) 9.20 mg·mL^{-1}. b) Concentration dependence of the hydrodynamic radii R_h of polymer clusters. R_h values were obtained from correlation functions in a) by force fitting to a stretched exponential function.

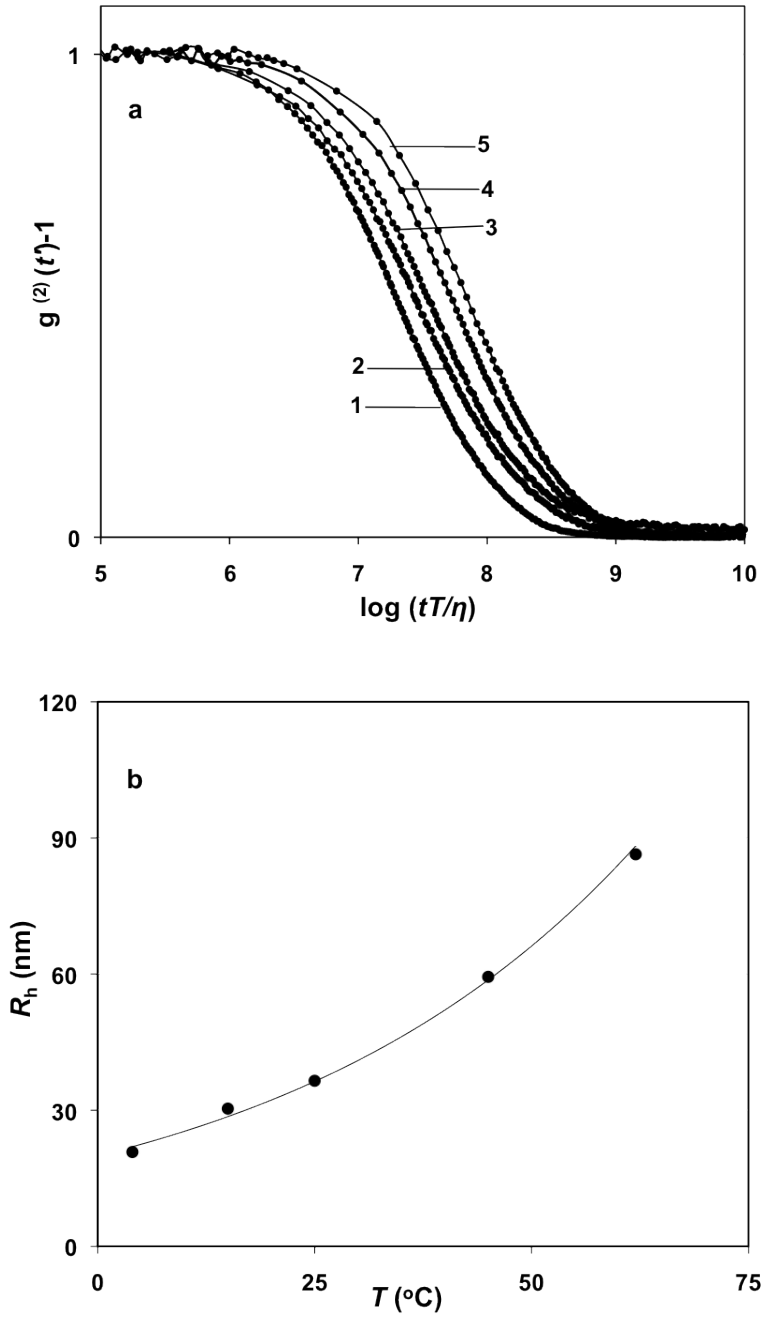

Figure 2.7. Temperature-dependence of PMaCC5 gel formation. a) Normalized intensity autocorrelation functions, $g^{(2)}(t')$-1, at scattering angle of 90°, for aqueous solution of PMaCC5 (5.54 mg·mL^{-1}) at different temperatures: (1) 4, (2) 15, (3) 25, (4) 45, (5) 62 °C. b) Temperature dependence of the hydrodynamic radii R_h of polymer clusters. R_h values were deduced from correlation functions in a) by force fitting to a stretched exponential function.

By comparing the R_h and β values acquired from concentration and temperature measurements via DLS, we observed a minor discrepancy. This could be the result of sample preparation during the experiments. The solutions used for the concentration-dependence measurement were not filtered as pointed out above; while the one for temperature-dependence measurement was filtered through a 0.45 μm membrane. Nevertheless, this would not influence the trends observed in the experiments.

2.5. Conclusion

New macromonomers, containing 3, 4 and 5 heptads of coiled-coil forming motifs, were designed and synthesized. Free radical macromonomer copolymerization with HPMA produced hybrid graft copolymers composed of a linear HPMA copolymer backbone and coiled-coil motifs as grafts. The self-assembly of graft copolymers was evaluated by microrheology and DLS. Results showed that four heptads were the minimum for sufficient self-assembly. CD spectra of graft copolymer solutions and self-assembly data indicated that five heptads were required for self-assembly mediated by coiled-coil formation. DLS data on self-assembly of PMaCC5 demonstrated the impact of graft copolymer concentration and temperature on self-assembly.

2.6. Acknowledgements

K. Wu would like to thank American Foundation for Pharmaceutical Education (AFPE) for the generous financial support. This research was supported in part by NIH grant EB005288. Č. Koňák acknowledges the financial support of the Grant Agency of the Czech Republic (SON/06/E005).

2.7. References

(1) Kopeček, J., Tang, A., Wang, C., and Stewart, R. J. (2001) De novo design of biomedical polymers: hybrids from synthetic macromolecules and genetically engineered protein domains. *Macromol Symp 174*, 31-42.

(2) Vandermeulen, G. W., and Klok, H. A. (2004) Peptide/protein hybrid materials: enhanced control of structure and improved performance through conjugation of biological and synthetic polymers. *Macromol Biosci 4*, 383-398.

(3) Ulbrich, K., Strohalm, J., and Kopeček, J. (1982) Polymers containing enzymatically degradable bonds. VI. Hydrophilic gels cleavable by chymotrypsin. *Biomaterials 3*,150-154.

(4) Rejmanová, P., Kopeček, J., Pohl, J., Baudyš, M., and Kostka, V. (1983) Polymers containing enzymatically degradable bonds, 8. Degradation of oligopeptide sequences in *N*-(2-hydroxypropyl)methacrylamide copolymers by bovine spleen cathepsin B. *Macromol Chem 184*, 2009-2020.

(5) Šubr, V., Duncan, R., and Kopeček, J. (1990) Release of macromolecules and daunomycin from hydrophilic gels containing enzymatically degradable bonds. *J Biomater Sci Polym Ed 1*, 261-278.

(6) Wang, C., Stewart, R. J., and Kopeček, J. (1999) Hybrid hydrogels assembled from synthetic polymers and coiled-coil protein domains. *Nature 397*, 417-420.

(7) Wang, C., Stewart, R. J., and Kopeček, J. (2001) "Genetically engineered protein domains as crosslinks in hydrogels", in: *Polymeric Drugs and Drug Delivery Systems*, Ottenbrite, R. M., and Kim, S. W. Eds., Technomics Publishing, Lancaster, PA. page 131.

(8) Miyata, T., Asami, N., and Uragami, T. (1999) A reversibly antigen-responsive hydrogel. *Nature 399,* 766-769.

(9) Lu, Z.-R., Kopečková, P., and Kopeček, J. (2003) Antigen responsive hydrogels based on polymerizable antibody Fab' fragment. *Macromol Biosci 3*, 296-300.

(10) Nagahara, S., and Matsuda, T. (1996) Hydrogel formation via hybridization of oligonucleotides derivatized in water-soluble vinyl polymers. *Polym Gels Networks 4*, 111-127.

(11) Thomas, A.A., Kim, I.T., and Kiser, P.F. (2005) Symmetrical biodegradable crosslinkers for use in polymeric devices. *Tetrahedron Lett 46*, 8921-8925.

(12) de Jong, S. J., De Smedt, S. C., Wahls, M. W. C., Demeester, J., Ketteres-van den Bosch, J. J., and Hennink, W. E. (2000) Novel self-assembled hydrogels by

stereocomple formation in aqueous solution of enantiomeric lactic acid oligomers grafted to destran. *Macromolecules 33*, 3680-3686.

(13) Yang, J., Xu, C., Kopečková, P., and Kopeček, J. (2006) Hybrid hydrogels self-assembled from HPMA copolymers containing peptide grafts. *Macromol Biosci 6*, 201-209.

(14) Yang, J., Xu, C., Wang, C., and Kopeček, J. (2006) Refolding hydrogels self-assembled from *N*-(2-hydroxypropyl)methacrylamide graft copolymers by antiparallel coiled-coil formation. *Biomacromolecules 7*, 1187-1195.

(15) Collier, J. H., and Messersmith, P. B. (2004) Self-assembling polymer-peptide conjugates: nanostructural tailoring. *Adv Mater 16*, 907-910.

(16) Ehrick, J.D., Deo, S. K., Browning, T. W., Bachas, L. G., Madou, M. J., and Daunert, S. (2005) Genetically engineered protein in hydrogels tailors stimuli-responsive characteristics. *Nat Mater 4*, 298-302.

(17) Chen, L., Kopeček, J., and Stewart, R. J. (2000) Responsive hybrid hydrogels with volume transitions modulated by a titin immunoglobulin module. *Bioconjug Chem 11*, 734-40.

(18) Rizzi, S. C., and Hubbell, J. A. (2005) Recombinant protein-co-PEG networks as cell-adhesive and proteolytically degradable hydrogel matrixes. Part I: Development and physicochemical characteristics. *Biomacromolecules 6*, 1226-1238.

(19) Lupas, A. (1996) Coiled coils: new structures and new functions. *Trends Biochem Sci 21*, 375-382.

(20) Su, J. Y., Hodges, R. S., and Kay, C.M. (1994) Effect of chain length on the formation and stability of synthetic alpha-helical coiled coils. *Biochemistry 33*, 15501-15510.

(21) Yu, Y. B. (2002) Coiled-coils: stability, specificity, and drug delivery potential. *Adv Drug Deliv Rev 54*, 1113-1129.

(22) Mason, J. M., Schmitz, M. A., Muller, K. M., and Arndt, K. M. (2006) Semirational design of Jun-Fos coiled coils with increased affinity: Universal implications for leucine zipper prediction and design. *Proc Natl Acad Sci USA 103*, 8989-8994.

(23) O'Brien-Simpson, N. M., Ede, N. J., Brown, L. E., Swan, J., and Jackson, D. C. (1997) Polymerization of unprotected synthetic peptides: a view toward synthetic peptide vaccines. *J Am Chem Soc 119*, 1183-1188.

(24) Lu, Z.-R., Kopečková, P., and Kopeček, J. (1999) Polymerizable Fab' antibody fragments for targeting of anticancer drugs. *Nat Biotechnol 17*, 1101-1104.

(25) Kopeček, J., and Bažilová, H. (1973) Poly[*N*-(2-hydroxypropyl)methacrylamide]-I. Radical polymerization and copolymerization. *Eur Polym J 9*, 7-14.

(26) Drobník, J., Kopeček, J., Labský, J., Rejmanová, P., Exner, J., Saudek, V., and Kálal, J. (1976) Enzymatic cleavage of side chains of synthetic water-soluble polymers. *Makromol Chem 177*, 2833-2848.

(27) Pechar, M., Kopečková, P., Joss, L., and Kopeček, J. (2002) Associative Diblock Copolymers of Poly(ethylene glycol) and Coiled-Coil Peptides. *Macromol Biosci 2*, 199-206.

(28) Edelhoch, H. (1967) Spectroscopic determination of tryptophan and tyrosine in proteins. *Biochemistry 6*, 1948-1954.

(29) Lumb, K. J., and Kim, P. S. (1995) A buried polar interaction imparts structural uniqueness in a designed heterodimeric coiled coil. *Biochemistry 34*, 8642-8648.

(30) Mason, T. G., and Weitz, D. A. (1995) Optical measurements of frequency-dependent linear viscoelastic moduli of complex fluids. *Phys Rev Lett 74*, 1250-1253.

(31) Levine, A. J., and Lubensky, T.C. (2000) One- and two-particle microrheology. *Phys Rev Lett 85*, 1774-1777.

(32) Crocker, J. C., Valentine, M. T., Weeks, E. R., Gisler, T., Kaplan, P. D., Yodh, A. G., and Weitz, D. A. (2000) Two-point microrheology of inhomogeneous soft materials. *Phys Rev Lett 85*, 888-891.

(33) Jakeš, J. (1995) Regularized positive exponential sum (REPES) program - a way of inverting laplace transform data obtained by dynamic light scattering. *Collect Czech Chem Commun 60*, 1781-1797.

(34) Lee, J. H., Kopečková, P., Kopeček, J., and Andrade, J. D. (1990) Surface properties of copolymers of alkyl methacrylates with methoxy (polyethylene oxide) methacrylates and their application as protein-resistant coatings. *Biomaterials 11*, 455-464.

(35) Graddis, T. J., Myszka, D. G., and Chaiken, I. M. (1993) Controlled formation of model homo- and heterodimer coiled coil polypeptides. *Biochemistry 32*, 12664-12671.

(36) Woody, R. W. (1995) Circular dichroism. *Methods Enzymol 246*, 34-71.

(37) Gans, P. J., Lyu, P. C., Manning, M. C., Woody, R. W., and Kallenbach, N. R. (1991) The helix-coil transition in heterogeneous peptides with specific side-chain interactions: theory and comparison with CD spectral data. *Biopolymers 31*, 1605-1614.

(38) Chen, Y. H., Yang, J. T., and Chau, K. H. (1974) Determination of the helix and beta form of proteins in aqueous solution by circular dichroism. *Biochemistry 13*, 3350-3359.

(39) Koňák, Č., Fleischer, G., Tuzar, Z., and Bansil, R. (2000) Dynamics of solutions of triblock copolymers in a selective solvent: Effect of varying copolymer concentration. *J Polym Sci Part B: Polym Phys 38*, 1312-1322.

(40) Yang, J., Wu, K., Koňák, Č., and Kopeček, J. (2008) Dynamic light scattering study of self-assembly of HPMA hybrid graft copolymers. *Biomacromolecules 9*, 510-517.

CHAPTER 3

DRUG-FREE MACROMOLECULAR THERAPEUTICS: INDUCTION OF APOPTOSIS BY COILED-COIL-MEDIATED CROSS-LINKING OF ANTIGENS ON CELL SURFACE

3.1. Summary

Molecular biorecognition is at the heart of all biological processes and the design of precisely defined smart systems. Here we hypothesized that a unique biorecognition of two complementary coiled-coil motifs, CCE and CCK, could be employed to mediate a therapeutic effect for B-cell NHL. To this end, a binary system was designed, composed of polyHPMA copolymer grafted with multiple copies of CCK and Fab' fragment of 1F5 anti-CD20 antibody conjugated with CCE. Both conjugates were well characterized using various biophysical techniques and their in vitro efficacy was evaluated on Raji B cells. The multivalent effect during the heterodimerization of CCE and CCK and subsequent cross-linking of CD20 antigens led to a clinically relevant magnitude of B-cell apoptosis. This bodes well for the development of novel drug-free macromolecular therapeutics.

Note: This chapter is reprinted with permission from the following publication: Wu, K., Liu, J., Johnson, R. N., Yang, J., and Kopeček, J. (2010) Drug-free macromolecular therapeutics: Induction of apoptosis by coiled-coil mediated cross-linking of antigens on the cell surface. *Angew Chem Int Ed 49*, 1451-1455.

3.2. Introduction

Molecular biorecognition is at the center of all biological processes and forms the basis for the design of precisely defined smart systems, including targeted therapeutics, imaging agents, biosensors, and stimuli-sensitive and self-assembled biomaterials. The self-assembly of hybrid materials composed of synthetic and biological macromolecules is mediated by the biorecognition of biological motifs *(1-4)*. We have previously designed self-assembling hybrid hydrogel systems composed of a synthetic *N*-(2-hydroxypropyl)methacrylamide (HPMA) copolymer backbone and coiled-coil peptide motifs; our results showed that it is possible to impose properties of a well-defined coiled-coil peptide on a whole hybrid hydrogel *(5)*. Recently, we designed a pair of oppositely charged pentaheptad peptides (CCE and CCK) that formed anti-parallel coiled-coil heterodimers and served as physical cross-linkers *(6)*. HPMA graft copolymers CCE–P and CCK–P (P is the HPMA copolymer backbone) self-assembled into hybrid hydrogels with a high degree of biorecognition *(6, 7)*.

We hypothesized that this unique biorecognition of CCK and CCE peptide motifs could be extended beyond biomaterials design and applied to a living system to mediate a biological process. This approach would provide a bridge between the design of biomaterials and the design of macromolecular therapeutics.

To verify this hypothesis, we chose to study the induction of apoptosis in CD20-positive cells. CD20 is one of the most reliable biomarkers for B-cell non-Hodgkin's lymphoma (NHL) *(8, 9)*. It functions as a cell-cycle-regulatory protein *(10)* that either controls or behaves as a store-operated calcium channel *(11-13)*. CD20 also forms dimers and tetramers *(11)* constitutively associated with lipid rafts of the cell membrane *(9)*. It is

a non-internalizing antigen that remains on the cell surface when bound to a complementary antibody (Ab) *(14)*. However, the cross-linking of CD20-bound antibodies with a secondary antibody results in apoptosis *(15)*. To exploit this phenomenon, we designed a system composed of CCE and CCK peptides, the Fab' fragment of the 1F5 anti-CD20 antibody, and HPMA copolymer (Figure 3.1). The exposure of CD20+ Raji B cells to Fab'-CCE resulted in the decoration of the cell surface with multiple copies of the CCE peptide through antigen-antibody-fragment biorecognition. Further exposure of the decorated cells to HPMA copolymer grafted with multiple copies of CCK resulted in the formation of CCE–CCK coiled-coil heterodimers on the cell surface. This second biorecognition event induced the cross-linking of CD20 receptors and triggered the apoptosis of Raji B cells.

3.3. Materials and methods

3.3.1. Materials

Side-chain protected Fmoc-amino acids, 2-chlorotrityl resin, 2-(1H-benzotriazol-1-yl)-1,1,3,3-tetramethyluronium hexafluorophosphate (HBTU), and ethanedithiol (EDT) were purchased from Novabiochem (San Diego, CA). Dimethyl sulfoxide (DMSO) was purchased from EMD Chemicals, Inc. (Gibbstown, NJ). Dimethylformamide (DMF), trifluoroacetic acid (TFA), and methanol were purchased from VWR International (West Chester, PA). 2,2'-azobisisobutyronitrile (AIBN) and succinimidyl-4-(*N*-maleimido-methyl)cyclohexane-1-carboxylate (SMCC) were purchased from Soltec Ventures (Beverly, MA). Tris(2-carboxyethyl) phosphine hydrochloride (TCEP) was purchased from Thermo Scientific (Waltham, MA). *N,N*-diisopropylethylamine (DIPEA), peridine,

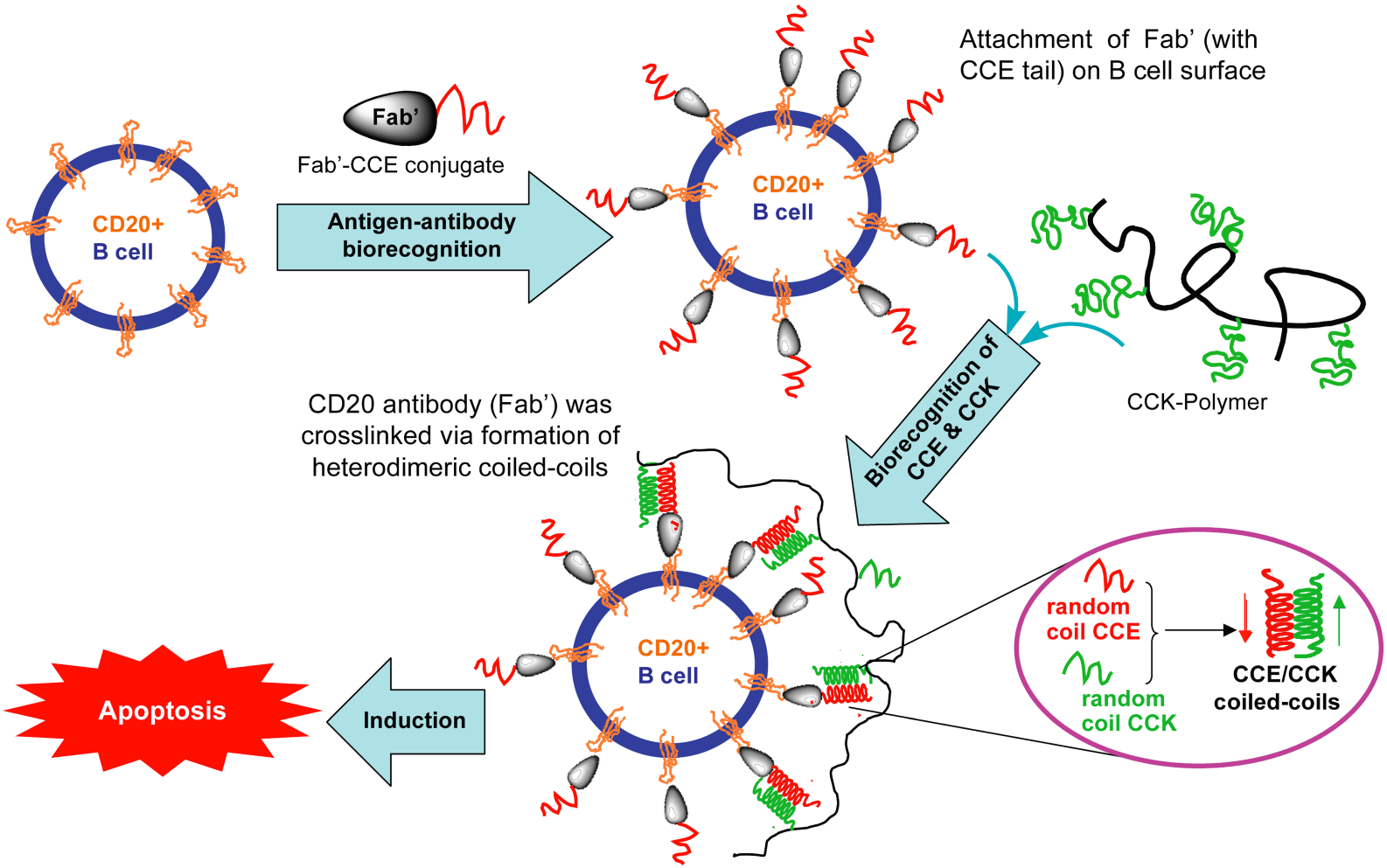

Figure 3.1. Induction of apoptosis in human Burkitt's NHL Raji B cells by cross-linking of its CD20 antigens mediated by coiled-coil formation on the cell surface.

O-phthaldialdehyde (OPA), triisopropylsilane (TIS) and 3-mercaptopropionic acid (MPA) were purchased from Sigma Aldrich (St. Louis, MO). Dichloromethane (DCM) was purchase from Mallinckrodt Chemicals (Phillipsburg, NJ). HPMA *(16)* and *N*-methacryloylaminopropyl fluorescein thiourea (MA-FITC) *(17)* were synthesized as previously reported.

3.3.2. Sequence design and synthesis of CCE and CCK

3.3.2.1. Sequence design

We recently designed two oppositely charged pentaheptad peptides, CCE and CCK (Figure 3.2), that self-assembled into anti-parallel coiled-coil heterodimers *(6)*. Three major stabilizing interactions were the hallmarks of the design: the hydrophobic interactions in the core, electrostatic interactions across the interface, and helical propensity effects *(6)*. The coiled-coil sequences were extended at the *N*-terminus: a) the CCK peptide with a tetrapeptide spacer, CYGG, to permit its attachment as graft to *N*-(2-hydropxypropyl)methacrylamide (HPMA) copolymer containing side chains terminated with maleimido groups via thioether bonds; b) the CCE peptide with maleimide-YGG to allow for the conjugation to SH groups of the Fab' fragment. In addition, the insertion of spacers to both sequences would decrease the steric hindrance of the HPMA copolymer backbone and of the Fab' fragment on the "in-register" arrangement of CCK-CCE anti-parallel coiled-coil heterodimers.

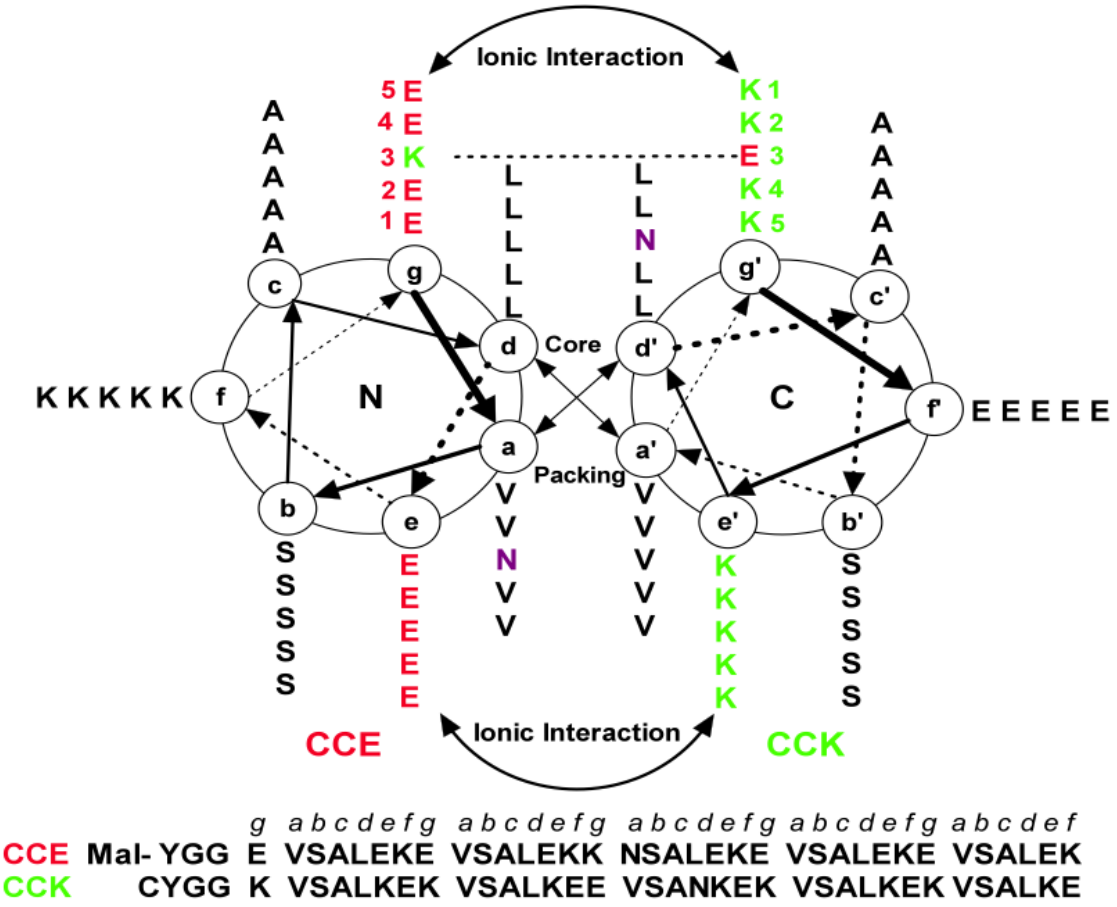

Figure 3.2. Helical wheel representation of CCE/CCK coiled-coil anti-parellel heterodimers. The view was shown looking down the super-helical axis from the *N*-terminus of CCE and from the *C*-terminus of CCK. The primary structure of the coiled-coil motif is characterized by a heptad repeating sequence of amino acids designated as *a*-*g*. CC, coiled-coil; E and K sequences whose *g* positions are mainly occupied by glutamic acid (E) and lysine (K), respectively; Mal, maleimido group. Adapted from reference *(6)*.

3.3.2.2. Peptide synthesis

CCE and CCK peptides were synthesized using solid-phase method following a manual Fmoc/tBu strategy on 2-chlorotrityl resin as described previously *(6, 18)*. Synthesis of CCK: 2-chlorotrityl resin (500 mg, 1.3 mmol·g^{-1} resin) was weighed and put into a 20 mL polypropylene syringe equipped with a bottom 20 μm polyethylene filter. The first residue (Fmoc-Glu(OtBu)-OH, 0.325 mmol, 138 mg, 50% loading) was dissolved in 10 mL DCM, followed by the addition of *N,N*-diisopropylethylamine (DIPEA; 4×, 1.30 mmol, 0.224 mL). This solution was added to the resin and the suspension was gently shaken for 1 h. The loaded resin was washed three times with DCM/MeOH/DIPEA (17:2:1), DCM, and DMF, respectively. After DMF was drained in vacuum, the loaded resin was deprotected twice with 2.5 mL of 20% piperidine in DMF for 10 min to remove the Fmoc protecting grop. Then the resin was washed thoroughly with DMF (3 times) and confirmed via positive Kaiser test. The second residue (Fmoc-Lys(Boc)-OH, 2.5×1^{st} residue, 0.81 mmol, 380.6 mg) and HBTU (0.9 × 2^{nd} residue, 0.729 mmol, 277 mg) were dissolved in 5 mL DMF, followed by DIPEA (4×, 3.25 mmol, 560 μL). The mixture was added into the resin and gently shaken for 2-3 h at room temperature. The completeness of coupling was monitored also by the Kaiser test. The resin was then washed with DMF and deprotected as described above. The coupling reaction was repeated likewise untill the last amino acid residue, Fmoc-Cys(Trt)-OH. Cleavage of the peptide from the resin and deprotection of side-chain protecting groups was achieved simultaneously by incubating the resin with a cleavage cocktail (94.5% TFA, 2.5% H_2O, 2.5% EDT and 1% TIS) for 2.5 h at room temperature under constant shaking. Upon removal of the cleaved resin, solvents were evaporated under reduced

pressure and the product was precipitated into cold ether. The crude peptide was retrieved after centrifugation at 3,000 rpm for 20 min and dried in vacuum. The CCK peptide was purified by preparative reversed-phase HPLC (RP-HPLC) and lyophilized.

CCE was synthesized following a similar protocol as CCK. To introduce the maleimido functional group to the *N*-terminus of CCE, SMCC, a hetero-bifunctional cross-linking agent, was coupled at the last step. A solution of SMCC (0.65 mmol, 217 mg) and DIPEA (1.3 mmol, 224 μL) in 2.5 ml DMF was added to the peptide-bound resin (0.65mmol, 500 mg). The suspension was kept at room temperature for 6-12 h to allow for complete coupling under constant shaking. Then the peptide was cleaved from the resin using a TFA/TIS/H_2O cocktail solution (95:2.5:2.5, vol.%), and the product was processed as described above.

3.3.2.3. Peptide characterization

Crude peptides were purified by RP-HPLC equipped with a semi-preparative Zorbax 300SB-C18 column (250×9.4 mm, 5 μm particle size, 300 Å pore size) from Agilent Technologies (Santa Clara, CA). The peptides were eluted with a linear gradient at a flow rate of 2 $mL \cdot min^{-1}$ with buffer A as 0.1% TFA in water and B as 0.1% TFA in 90/10 (v/v) methanol/H_2O. The peptide structures were confirmed by MALDI-TOF mass spectrometry (Voyager-DE STR Biospectrometry Workstation, Perseptive Biosystems, Framingham, MA).

3.3.3. Synthesis of Fab'-$(CCE)_1$ conjugate labeled with Rhodamine Red-X (RRX)

3.3.3.1. Preparation of RRX labeled $F(ab')_2$

The murine 1F5 anti-CD20 IgG2a antibody (Ab) was prepared using the anti-CD20 hybridoma clone 1F5 *(19)*. The hybridoma clone (ATCC, Bethesda, MD) was initially cultured and recloned through limiting dilution in RPMI 1640 medium supplemented with 10% fetal bovine serum (FBS; Hyclone Laboratories, Logan, UT) in a humidified environment with 5% CO_2 in air. The selected clone was adapted to chemically defined, serum-free media (Invitrogen, Carlsbad, CA). Adapted cells were used to seed a CellMax© bioreactor (Spectrum Laboratories, Rancho Dominguez, CA) according to the manufacturer's instructions. Anti-CD20 mAb 1F5 was purified on a Protein G Sepharose 4 Fast Flow column (GE Healthcare, Piscataway, NJ) from bioreactor harvest supernatant *(20, 21)*.

As shown in Figure 3.3a, the 1F5 antibody was digested into $F(ab)_2$ with lysyl endopeptidase (Wako Chemicals USA, Richmond, VA) as previously described. $F(ab')_2$ was then labeled with RRX succinimidyl ester (Invitrogen, Carlsbad, CA) to introduce a fluorophore to facilitate the fluorescence microscopy investigation. Briefly, 40 μL of RRX succinimidyl ester solution (5 mM) in DMF was added into 3 mL of $F(ab')_2$ solution (3 $mg{\cdot}mL^{-1}$) in PBS (pH 7.4). Then the pH of the labeling mixture was gradually adjusted to 8.3 using 0.1 N NaOH under constant stirring. Additional 30 min were allowed to complete the labeling reaction. The labeled $F(ab')_2$ was then purified twice using a PD10 column (GE Healthcare, Buckinghamshire, UK) to remove the unreacted ester. To estimate the degree of labeling, a 10× diluted sample was scanned from 250-650

nm on Varian UV-Vis spectrophotometer (Varian Inc., Palo Alto, CA). The concentration of RRX was calculated using the absorbance at 585 nm with an extinction coefficient of 63,000 $cm^{-1} \cdot M^{-1}$ in PBS; absorbance at 280 nm was used to deduce the molar concentration of $F(ab')_2$ using an empirical equation ($c\ (mg \cdot mL^{-1}) = A_{280nm}/1.35$) together with molecular weight. The ratio of these two molar concentrations gave a labeling degree of two RRX probes per $F(ab')_2$ molecule.

3.3.3.2. Synthesis of Fab'-$(CCE)_1$

Fab'-$(CCE)_1$ was obtained by conjugation of Fab' with CCE using maleimide-thiol chemistry. Immediately prior to use, the RRX labeled $F(ab')_2$ was reduced to Fab' with 10 mM TCEP in PBS (pH 7.4) containing 5 mM EDTA for 1 h at 37 ^oC in the dark. CCE (1.5× in excess to Fab') was added and the coupling reaction proceeded at 4 ^oC in the dark overnight. The crude product was then purified twice using a PD10 column. As reported *(22)*, this coupling reaction follows a 1:1 stoichiometry. Thus the resulting conjugate was named Fab'-$(CCE)_1$.

3.3.4. Synthesis of HPMA copolymer grafted with CCK ($(CCK)_9$-P)*(6)*

The synthetic procedure consisted of three steps: first, a copolymer of HPMA and *N*-(3-aminopropyl)methacrylamide ($MA\text{-}NH_2$) was prepared by radical copolymerization in methanol at 50 ^oC with AIBN as the initiator. Then the amino groups at side-chain termini were converted to maleimido groups (polymer precursor) by reaction using SMCC. Finally, the CCK peptide flanked with a cysteine residue at the *N*-terminus was attached to the polymer precursor side-chains via thioether bonds (Figure 3.3b).

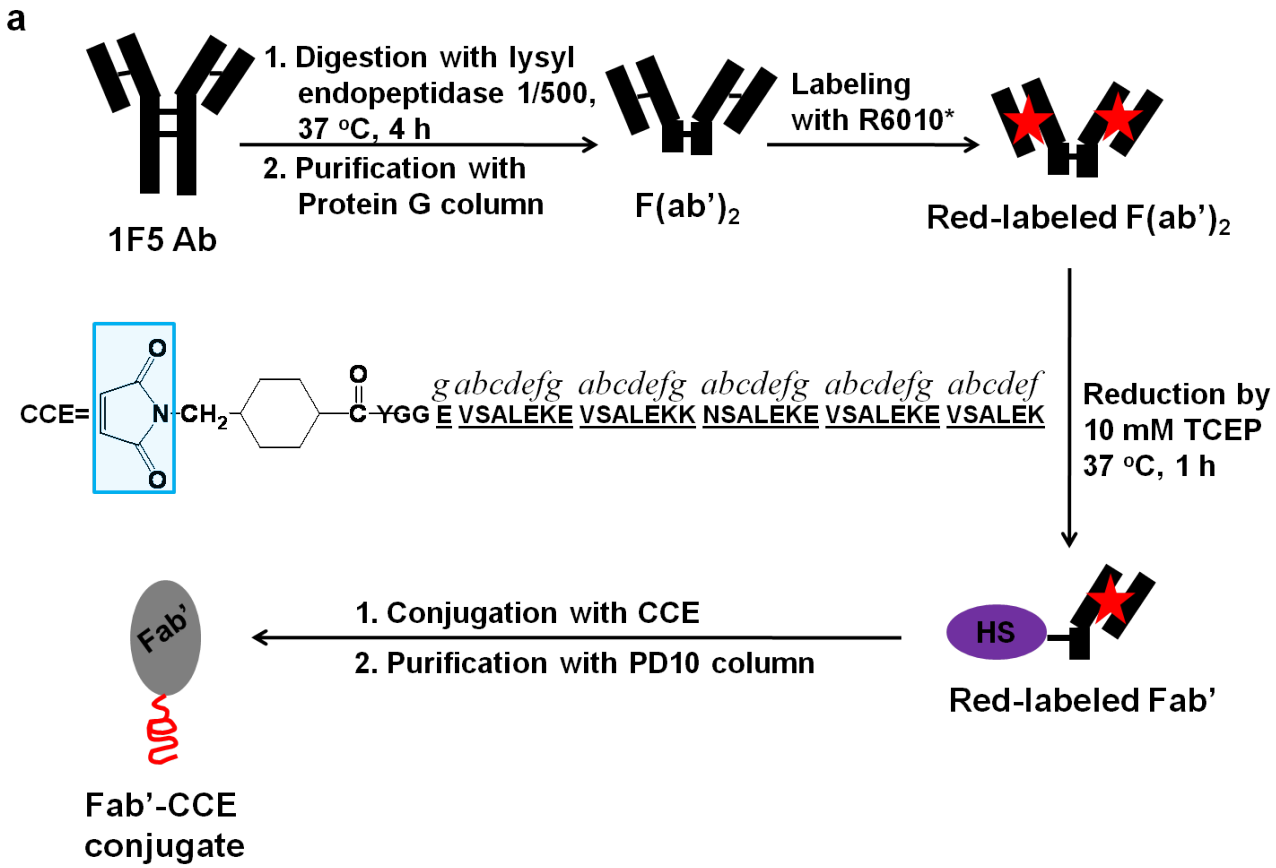

Figure 3.3. Synthetic schemes for the conjugates. a) Fab'-CCE and b) CCK-P.

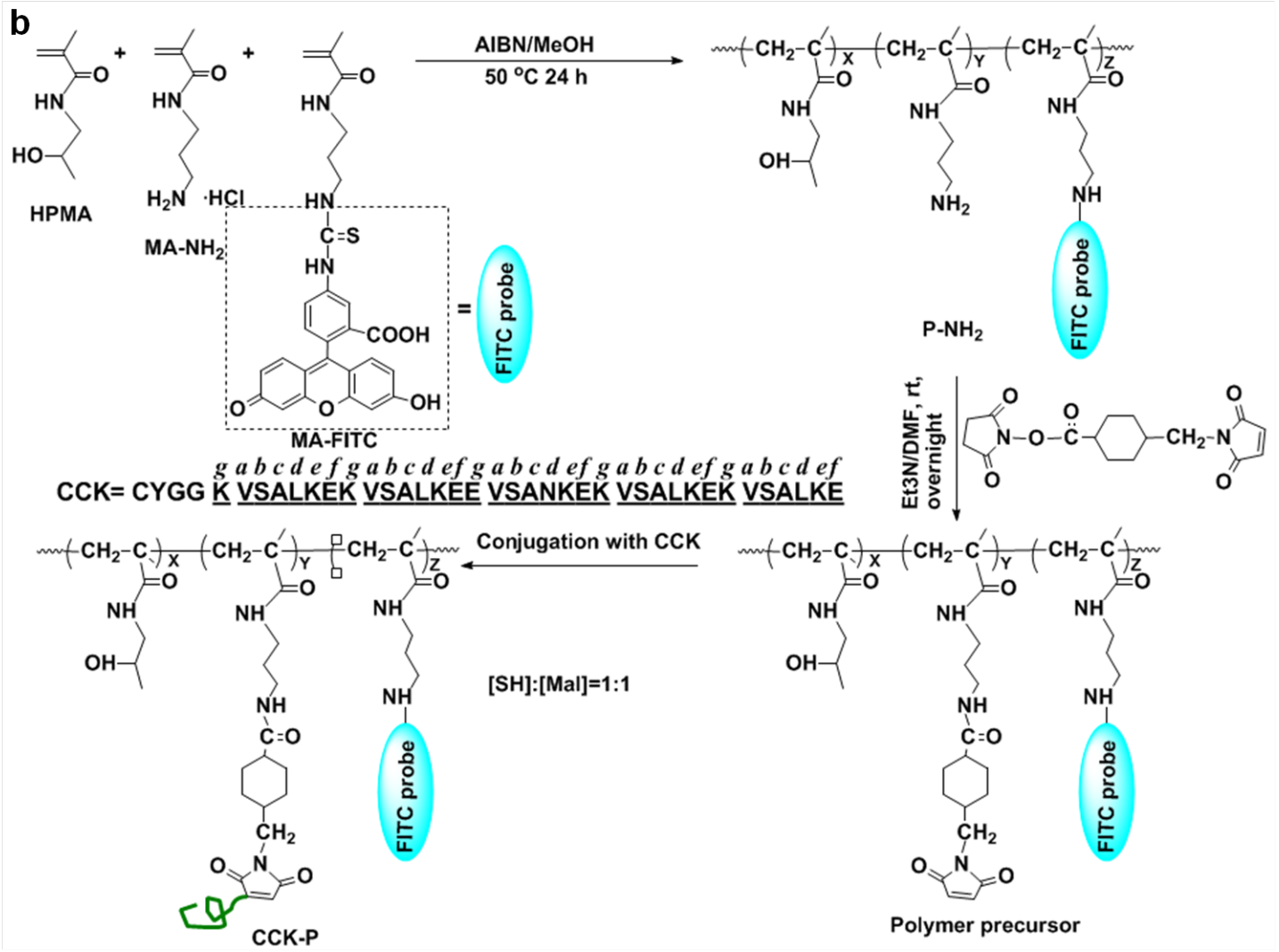

Figure 3.3. Continued.

3.3.4.1. Copolymerization of HPMA with MA-NH_2

HPMA (500 mg) and 40 mg MA-NH_2 (molar ratio = 94:6) were dissolved in methanol together with AIBN (0.6% of the total weight of the monomers), and bubbled with nitrogen for 5 min before the ampoule was sealed. The copolymerization was allowed for 24 h at 50 ^{o}C. The crude product was precipitated into acetone, centrifuged, redissolved in methanol, re-precipitated into acetone, and dried under vacuum. The copolymer was further purified by dialysis against DI water to remove oligomers and unreacted monomers, and lyophilized. The copolymer yield was 76% and the amine content in the copolymer was 389 nmol·mg^{-1} as determined by the ninhydrin test.

To introduce a fluorescent probe, a FITC labeled copolymer was prepared following a similar procedure using *N*-methacryloylaminopropyl fluorescein thiourea (MA-FITC) as an additional comonomer (the feeding ratio of HPMA : MA-NH_2 : MA-FITC = 93.5 : 6 : 0.5). The molecular weight and molecular weight distribution of the copolymer were measured on the ÄKTA FPLC system (Amersham Pharmacia Biotech, Piscataway, NJ) equipped with UV and RI detectors using a Superose 6HR10/30 column with PBS (pH= 7.4) as the mobile phase using a calibration with linear polyHPMA fractions. The copolymer yield was 82% with an amine content of 397 nmol·mg^{-1}. The number average molecular weight was 99.6 kDa ($\overline{M}_w / \overline{M}_n = 2.05$).

3.3.4.2. Synthesis of HPMA polymer precursor with
side-chains terminated in maleimide

The copolymer P-NH_2 and SMCC (molar ratio [NH_2] : [SMCC] = 1 : 1.5) were dissolved in DMF and the reaction was performed in the presence of triethylamine (TEA,

3× [NH_2]) at room temperature overnight. After precipitation into acetone/ether (3:2), the product was redissolved in methanol and precipitated into acetone twice to remove unreacted SMCC. The maleimide content of the precursor was 259 nmol·mg^{-1} as measured by the modified Ellman's assay *(23, 24)*.

3.3.4.3. Attachment of CCK to polymer precursor - synthesis of CCK-P

Polymer precursor and CCK ([Mal] : [CCK] = 1 : 1) were dissolved in PBS (pH 7.4) containing 1 mM EDTA, and the coupling reaction proceeded at room temperature overnight with analytical RP-HPLC monitoring the progress. The conjugate was then dialyzed against DI water using a dialysis tube with molecular weight cutoff 6-8 kDa to remove unreacted CCK; then lyophilized.

The graft content in the resulted copolymer was determined by amino acid analysis. The copolymer (2.08 mg) was hydrolyzed in 0.2 mL 6 N HCl at 120 ^{o}C for 16 h in a sealed ampoule and then dried under vacuum. A precolumn derivatization with o-phthaldialdehyde (OPA) was used and the samples were analyzed by HPLC with fluorescence detector (excitation 229 nm and emission 450 nm) using a gradient elution with mixtures of buffer A and B, where buffer A: 0.05 M sodium acetate, pH 6.0, and B: 70% methanol in buffer A [6]. The average number of CCK grafts per macromolecule was determined as 8.94. Thus, we denoted the HPMA copolymer grafted with CCK as $(CCK)_9$-P.

3.3.5. Biorecognition of Fab'-$(CCE)_1$ and $(CCK)_9$-P in solution

To demonstrate the biorecognition between Fab'-$(CCE)_1$ and $(CCK)_9$-P, circular dichroism (CD) spectrometry and dynamic light scattering (DLS) were employed. The following samples were prepared in PBS (pH=7.4) for these measurements: CCE (50 μM), CCK (50 μM), Fab'-$(CCE)_1$ ([CCE]=50 μM), and $(CCK)_9$-P ([CCK]=50 μM)). In this study, higher concentrations of CCE and CCK motifs were used than those in the apoptosis studies, because CD and DLS measurements require more sample mass to achieve an appropriate signal/noise ratio as to ensure accurate data acquisition.

CD spectra of individual samples (CCE, CCK, and $(CCK)_9$-P) and equimolar mixtures (CCE+CCK, and Fab'-$(CCE)_1$+$(CCK)_9$-P) were acquired at 25 ^{o}C on an Aviv 62DS CD spectrometer with a thermoelectric temperature control system (Aviv Biomedical, Lakewood, NJ). Wavelength scans were recorded at 1 nm intervals with a 5 sec averaging time at each step from 250 to 200 nm using a 0.1 cm path length quartz cuvette. The spectra obtained were averaged from three consecutive scans and subtracted from the background. Ellipticity was reported as the mean residue ellipticity ([θ], in $deg \cdot cm^2 \cdot dmol^{-1}$) calculated as:

$$[\theta] = [\theta]_{obs}(MRW/10lc) \quad (3.1)$$

where $[\theta]_{obs}$ is the ellipticity measured in millidegrees, MRW is the mean residue molecular weight of the polypeptide (molecular weight of the peptide divided by the number of amino acid residues), l is the optical path length of the cell in cm (0.1 cm in our case), and c is the peptide concentration in $mg \cdot mL^{-1}$.

DLS studies were conducted on a Brookhaven BI-200SM goniometer and BI-9000AT digital correlator with a He-Ne laser source (λ=633nm, Brookhaven Instruments

Corporation, Holtsville, NY). Individual samples (Fab'-$(CCE)_1$ and $(CCK)_9$-P) and equi-molar mixture (Fab'-$(CCE)_1$+$(CCK)_9$-P) were applied and their effective diameters in nm were calculated by the digital correlator.

3.3.6. Cell preparation and incubation with peptide conjugates

Human Burkitt's B-cell non-Hodgkin's lymphoma Raji cells (ATCC, Manassas VA) were cultured in RPMI-1640 medium supplemented with 10% fetal bovine serum (FBS) at 37 ^oC in a humidified atmosphere of 5% CO_2 (v/v) *(25)*. Experiments were performed during the exponential growth phase of the cells.

Cells were treated with either consecutive addition or premixture of conjugates. For the consecutive addition, cells were firstly incubated with Fab'-$(CCE)_1$ in growth medium containing 10% FBS at 37 ^oC for 1 h, then washed twice with sterile PBS (pH=7.4) containing 1% bovine serum albumin (BSA) to remove unbound conjugate; and secondly these pretreated cell pellets were re-suspended in FBS supplemented growth medium containing $(CCK)_9$-P for various durations. For the treatment with premixture, Fab'-$(CCE)_1$ and $(CCK)_9$-P were first mixed in FBS containing growth medium in a sterilized test tube at 37 ^oC for 1 h, then cells were incubated with this premixture for different intervals.

3.3.7. Visualization of biorecognition on Raji B-cell surface

Biorecognition between components of the binary system was visualized by confocal fluorescence microscopy. After incubation with Fab'-$(CCE)_1$ and $(CCK)_9$-P, using either consecutive addition or premixture (as described in 3.3.6), cells were washed

twice with PBS (pH=7.4). Then the cell suspensions were dropped onto glass bottom microwell dish (MetTek, Ashland, MA). FluoView1000-XY confocal Olympus IX81 microscope (Olympus America, Center Valley, PA) was employed to visualize the cells.

3.3.8. *In vitro* apoptosis evaluation

Apoptosis induction, mediated by coiled-coil formation at the cell surface with concomitant cross-linking of CD20 receptors, was evaluated by three methods: caspase 3 activation, Annexin V/propidium iodide (PI) assay, and the TUNEL assay. For experimental details of these assays, please refer to the standard protocols from corresponding suppliers: caspase 3 activity assay (employing a cell permeable fluorogenic caspase 3 substrate PhiPhiLux®; OncoImmunin, Gaithersburg, MD), Annexin V/PI assay (Annexin V-FITC® apoptosis detection kit; EMD Chemicals, Gibbstown, NJ), and TUNEL (terminal deoxynucleotidyl transferase dUTP nick end labeling) assay (APO-BRDUTM® TUNEL assay kit; Phoenix Flow Systems, San Diego, CA). Per the requirement of different assays, cells were dispensed into 24-well cell culture plates: 2×10^5 cells in 400 μL medium for both caspase 3 activity and Annexin V/PI binding assays, and 1×10^6 cells in 500 μL medium for the TUNEL assay.

Conjugates were added into cell culture by two different approaches: either premixing or consecutive addition, as described in 3.3.6. Different molar ratios of Fab'-$(CCE)_1$ to $(CCK)_9$-P including 1:1, 1:10 and 1:25 ([CCE] was chosen as 1 μM, thus [CCK]=1, 10, and μM, respectively) were studied to achieve the maximum efficiency of apoptosis induction. To examine the cytoxicity of the individual components, cells were incubated with only Fab'-$(CCE)_1$ or $(CCK)_9$-P. In addition, to introduce a clinically

relevant reference, cells were incubated with consecutive addition of 1F5 Ab and goat anti-mouse secondary antibody (1F5+GAM) *(26)*. The percentage of apoptotic cells were quantified with caspase 3 activity assay after different durations (6, 12, 18 and 24 h). According to this preliminary experiment, other combinations for various durations of incubation were also examined with aforementioned all three different assays.

Last but not the least, to evaluate the critical role of the coiled-coil motifs in the system, a series of control experiments were conducted, as shown in Table 3.1. Concentrations of different species were adjusted to equivalent of [CCE]=1 μM or [CCK]=25 μM.

3.4. Results and discussion

3.4.1. Characterization of coiled-coil motifs

A good agreement between theoretical and measured molecular weights of CCE and CCK was observed (Figure 3.4a and b). CCE: calculated 4312.8 Da, found 4313.3 Da; CCK: calculated 4179.8 Da, found 4180.1 Da. The purity of the peptides was verified with analytical RP-HPLC. Results (Figure 3.4c and d) indicated that the purity of peptides was > 95%.

3.4.2. Conjugation of Fab' and CCE

The digestion of 1F5 whole antibody to its Fab' fragment and the further conjugation were closely monitored and confirmed by size exclusion chromatography (SEC), sodium dodecyl sulfate polyacrylamide gel electrophoresis (SDS-PAGE) and RP-HPLC. 1F5 Ab, $F(ab')_2$, Fab' fragment, and Fab'-$(CCE)_1$ were individually injected into

Table 3.1. Facts of control experiments

Approach	Name	Components	Rationale
Premixing	Pre 6 h C1	Fab'+CCE+CCK+P-NH_2	To prove: CCE/CCK heterodimerization without conjugation was not sufficient; however, it is necessary for apoptosis induction.
	Pre 6 h C2	Fab'-$(CCE)_1$+ P-NH_2	
	Pre 6 h C3	Fab'+$(CCK)_9$-P	
Consecutive addition	Con 24 h C1	Fab'+CCE, then CCK+P-NH_2	
	Con 24 h C2	Fab'-$(CCE)_1$, then P-NH_2	
	Con 24 h C3	Fab', then $(CCK)_9$-P	

Pre, premixture; C, control; Con, consecutive.

Figure 3.4. Profiles of peptides by MALDI-TOF MS and RP-HPLC. a and b) MALDI-TOF MS spectra for CCE and CCK, respectively; c and d) HPLC profiles of pure CCE and CCK, respectively.

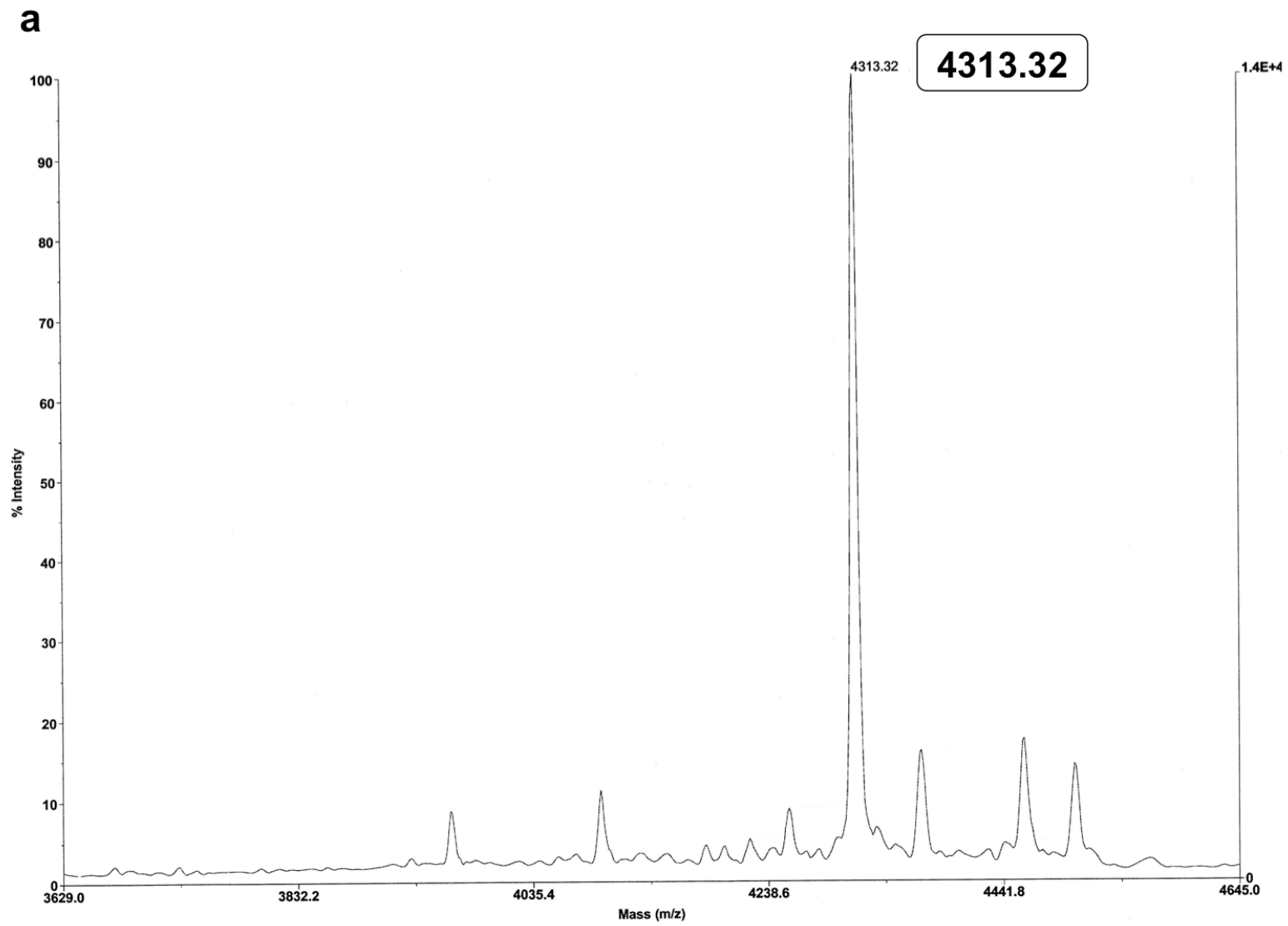
a
4313.32
4313.32
1.4E+4
100
90
80
70
60
50
40
30
20
10
0
% Intensity
3629.0
3832.2
4035.4
4238.6
4441.8
4645.0
0
Mass (m/z)

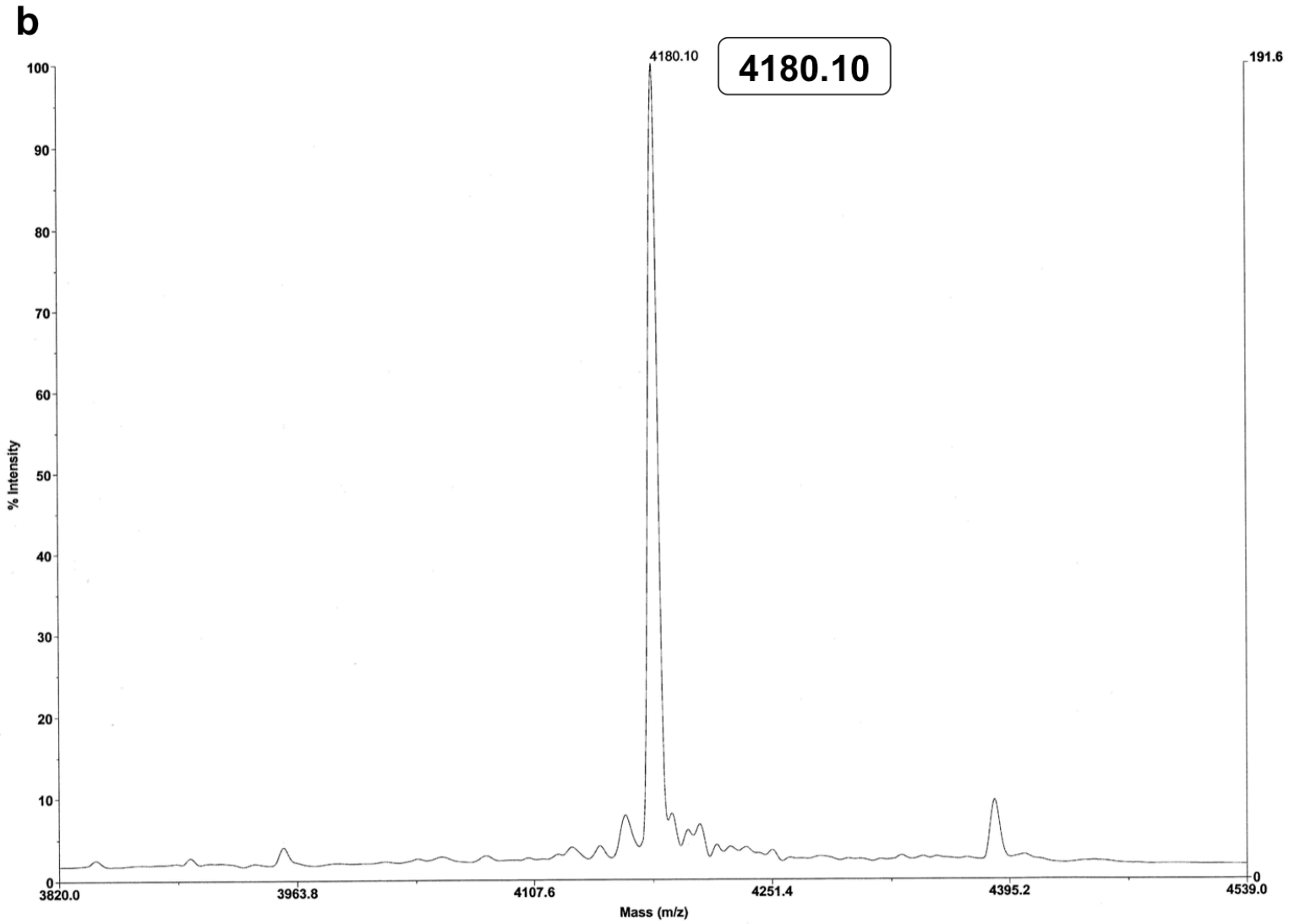
b
4180.10
4180.10
191.6
100
90
80
70
60
50
40
30
20
10
0
% Intensity
3820.0
3963.8
4107.6
4251.4
4395.2
4539.0
Mass (m/z)

c

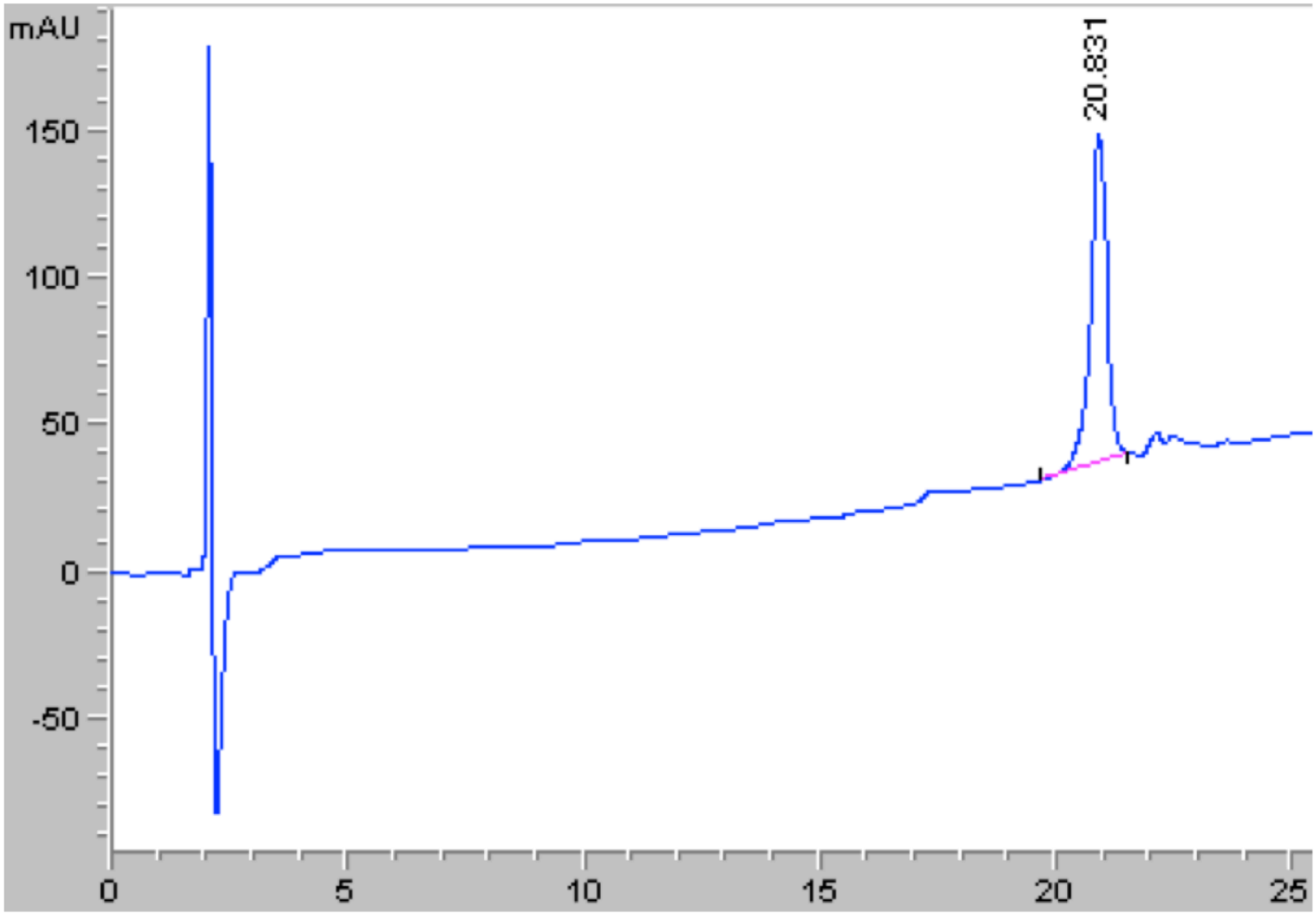

d

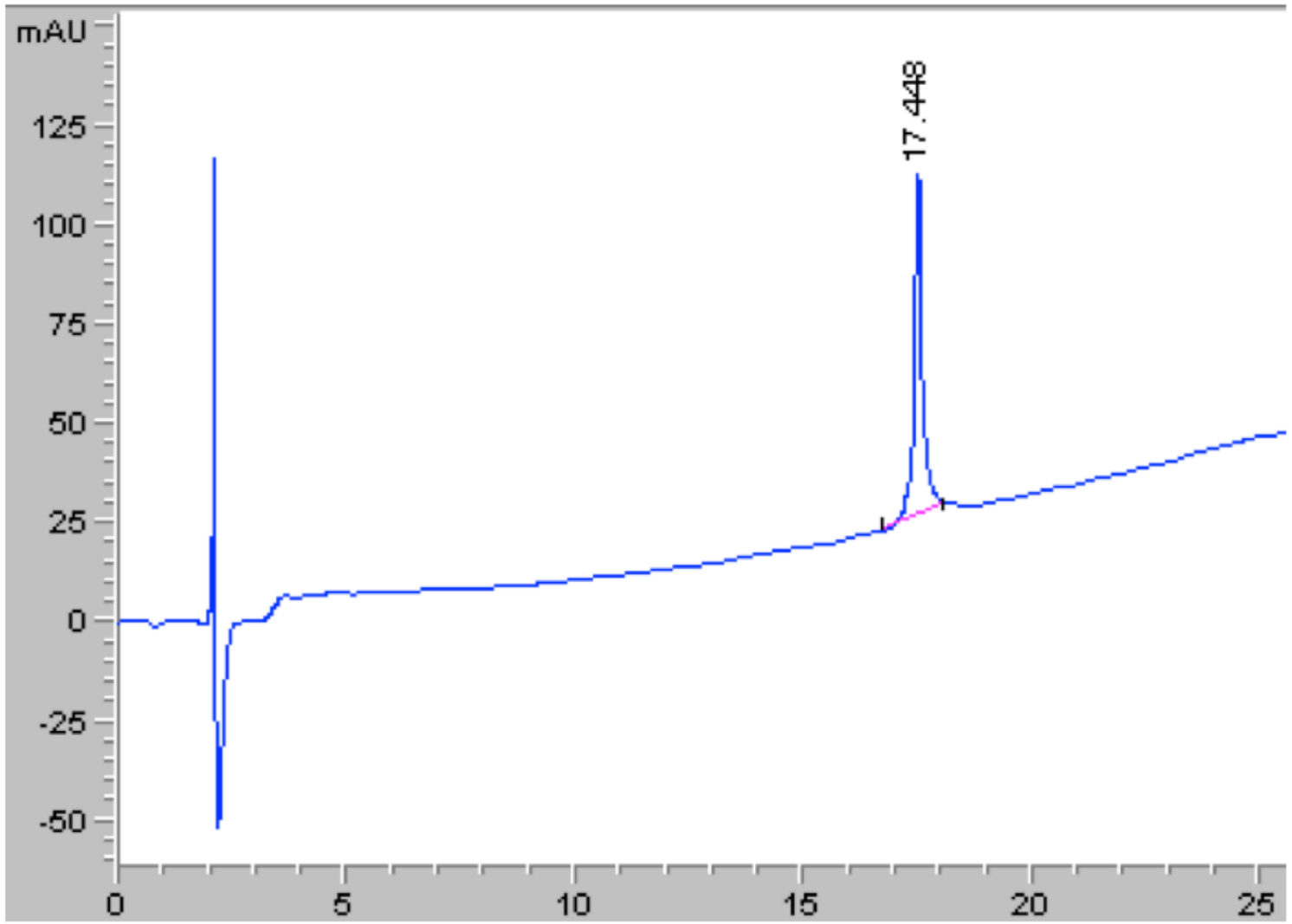

a SEC column and different characteristic elution times were observed (Figure 3.5a). SDS-PAGE demonstrated the successful digestion of 1F5 antibody and conjugation of Fab' fragment with CCE (Figure 3.5b). The HPLC profiles of Fab' and Fab'-$(CCE)_1$ were shown in Figure 3.5c.

3.4.3. Biorecognition of the conjugates in solution

The biorecognition of Fab'-$(CCE)_1$ and $(CCK)_9$-P was first evaluated by circular dichroism (CD) spectrometry. A pronounced coiled-coil signal (minima at 208 and 222 nm) was observed upon the mixing CCE or Fab'-$(CCE)_1$ with $(CCK)_9$-P (Figure 3.6), where the molar ratio was adjusted to ensure equimolar of the peptide motifs. Dynamic light scattering (DLS) measurements revealed that the size of the individual components did not change within the tested period of 1 h: 6.6 and 51.7 nm for Fab'-$(CCE)_1$and $(CCE)_9$-P, respectively (Figure 3.7); however, the effective diameter of particles in the equimolar mixture of Fab'-$(CCE)_1$ and $(CCK)_9$-P increased significantly, which strongly implied the self-assembly/biorecogintion of the two conjugates.

3.4.4. Biorecognition of the conjugates on B-cell surface

The exposure of Raji B cells to Fab'-$(CCE)_1$ led to decoration of the cell surface with the CCE peptide, as shown by confocal fluorescence microscopy (Figure 3.8a). In contrast, the exposure of Raji B cells to $(CCK)_9$-P did not result in detectable deposition of the graft copolymer at the cell surface under the experimental conditions used (Figure 3.8b). The exposure of Raji B cells to a high-avidity multivalent construct prepared by the premixing of Fab'-$(CCE)_1$ and $(CCK)_9$-P resulted in excellent binding to the cell

Figure 3.5. Monitoring of antibody digestion and Fab' fragment conjugation with CCE peptide. a) SEC profiles of separately injected 1F5 Ab, $F(ab')_2$, Fab', and Fab'-$(CCE)_1$ on Superdex 200 analytical column eluted with PBS (pH=7.4). b) SDS-PAGE of molecular weight standards (Lane 1), 1F5 Ab (150 kDa; Lane 2), $F(ab')_2$ (100 kDa; Lane 3), Fab'-$(CCE)_1$ conjugate (54 kDa; Lane 4), and Fab' fragment (50 kDa; Lane 5). c) Analytical RP-HPLC profiles of Fab' fragment and Fab'-$(CCE)_1$; Agilent Zorbax 300SB-C18 column (4.6×250 mm) eluted with a gradient of buffer A (H_2O+0.1% TFA) and buffer B (acetonitrile + 0.1% TFA).

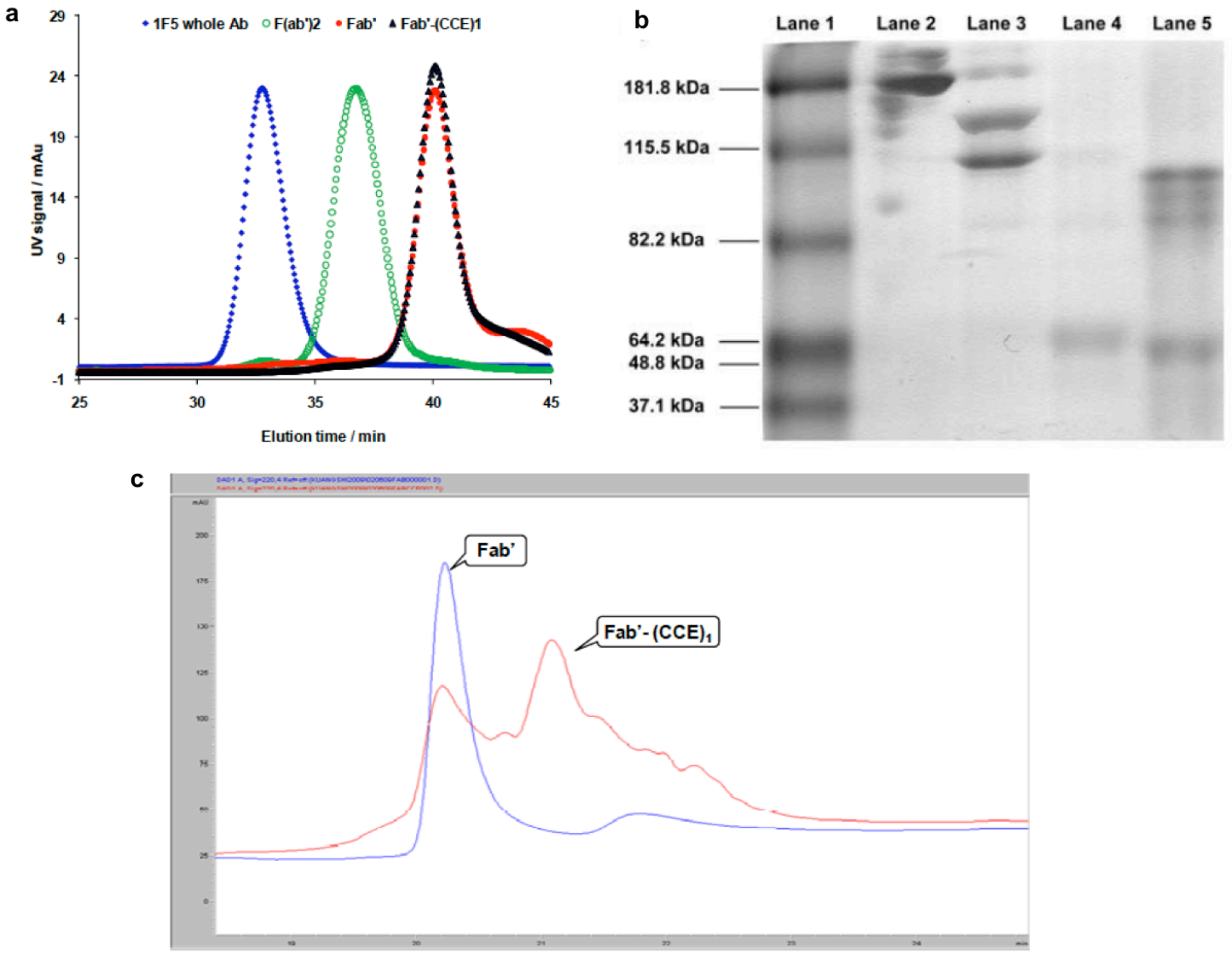
a
1F5 whole Ab
F(ab')2
Fab'
Fab'-(CCE)1
UV signal / mAu
Elution time / min
b
Lane 1
Lane 2
Lane 3
Lane 4
Lane 5
181.8 kDa
115.5 kDa
82.2 kDa
64.2 kDa
48.8 kDa
37.1 kDa
c
Fab'
Fab'-(CCE)1

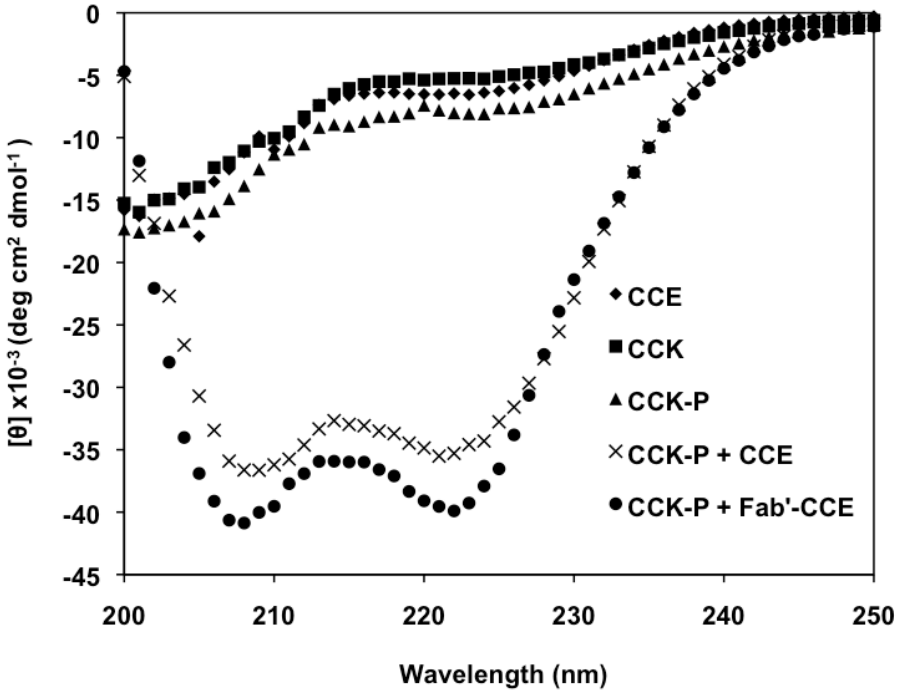

Figure 3.6. CD spectra of CCE, CCK, $(CCK)_9$-P, and equimolar mixtures of CCE and $(CCK)_9$-P, and Fab'-$(CCE)_1$ and $(CCK)_9$-P. [CCE]=[CCK]=[Fab'-$(CCE)_1$]=50 μM; [$(CCK)_9$-P]=5.60 μM. Data were acquired at 25 ^{o}C in PBS (pH=7.4).

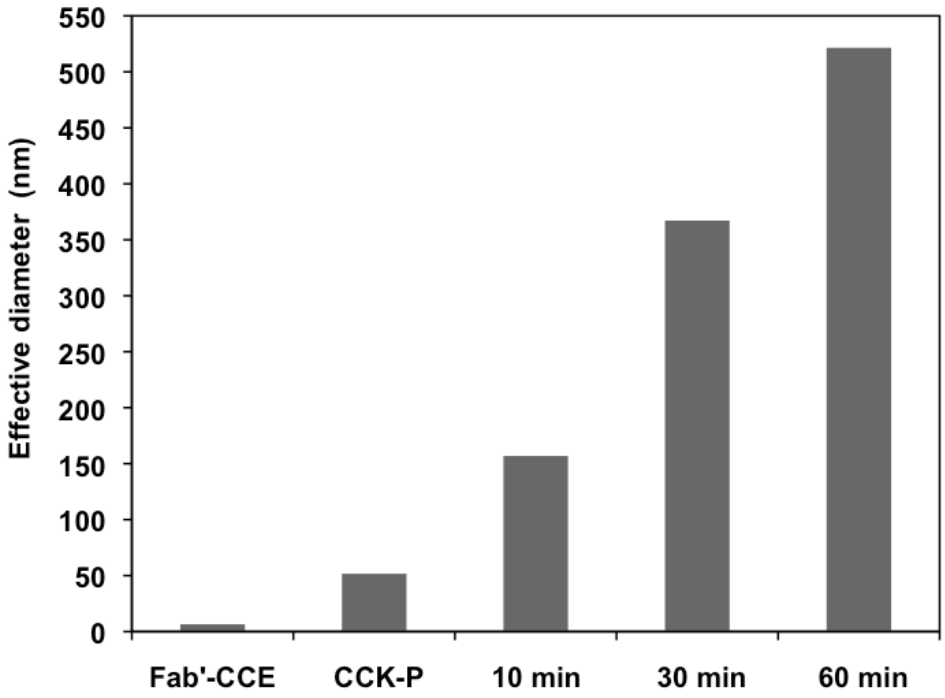

Figure 3.7. Effective diameters of Fab'-$(CCE)_1$ and $(CCK)_9$-P and the effective diameter growth upon mixing equimolar amounts of them, as determined by DLS. Concentrations: [CCE]=[CCK]=[Fab'-$(CCE)_1$]=50 μM; [$(CCK)_9$-P]=5.60 μM. Data were acquired at 25 ^{o}C in PBS (pH=7.4).

surface (Figure 3.8c_1–c_3). This result was in agreement with our studies on the interaction of CD20 with multivalent HPMA copolymer-Fab' conjugates *(21)*. Finally, the exposure of Raji B cells predecorated with the CCE peptide to $(CCK)_9$-P (consecutive exposure) resulted in the attachment of $(CCK)_9$-P to the cell surface (Figure 3.8d_1–d_3). This result suggested that coiled-coil heterodimers were formed at the cell surface. It demonstrated outstanding biorecognition between CCE bound to the cell surface and CCK grafted onto the HPMA copolymer.

Fab'-$(CCE)_1$ remained on the cell surface even after 6 h for all treatments. Although extra time was given, there was no visible $(CCK)_9$-P bound to the cell surface in the absence of Fab'-$(CCE)_1$ (Figure 3.9a). The surface fluorescence intensity was stronger in cells exposed to premixed conjugates, compared to conjugates consecutively added. Figure 3.9b compared the biorecognition when cells were consecutively incubated with Fab'-$(CCE)_1$ and $(CCK)_9$-P dissolved in either PBS or growth medium containing FBS for 1 h. Results showed that the presence of FBS did not interfere with the biorecognition between Fab'-$(CCE)_1$ and $(CCK)_9$-P; on the contrary, a slightly better biorecognition was observed, probably due to sufficient nutrition for the cells.

3.4.5. Apoptosis induction

The caspase 3 activity assay was first used to evaluate the time-dependence of apoptosis induction (Figure 3.10). The exposure of cells to the individual components Fab'-$(CCE)_1$ or $(CCK)_9$-P resulted in a very low percentage of cell death, independent of the incubation interval. However, a time-dependence was observed for the coiled-coil-based apoptosis-induction systems: treatment with a mixture of Fab'-$(CCE)_1$ and $(CCK)_9$-

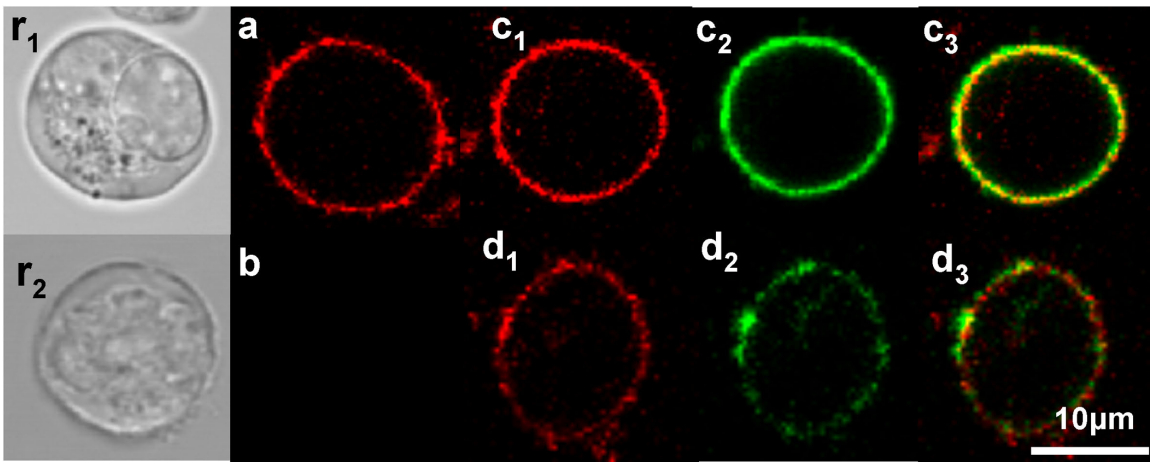

Figure 3.8. Biorecognition of Fab'-$(CCE)_1$ and $(CCK)_9$-P on the surface of Raji B cells (r_1, r_2 : reference cells under transmitted light). a) The exposure of cells to Fab'-$(CCE)_1$ (0.5 µM, labeled with Rhodamine Red-X) resulted in decoration of the cell surface with CCE. b) The exposure of cells to $(CCK)_9$-P ([CCK]=25 µM, labeled with FITC) did not result in staining. c_1-c_3) Exposure of cells to premixed Fab'-$(CCE)_1$ (0.5 µM) and $(CCK)_9$-P ([CCK]=25 µM). d_1-d_3) Consecutive exposure of cells to Fab'-$(CCE)_1$ (0.5 µM) followed (1 h later) by $(CCK)_9$-P ([CCK]=25 µM). a, c_1, and d_1: red channel for Rhodamine Red-X; b, c_2, and d_2 : green channel for FITC; c_3 and d_3: overlay of red and green channels. Images of individual cells are shown.

Figure 3.9. The influence of incubation duration and medium on cell surface staining by the conjugates. a) Confocal fluorescence microscopy images of Raji B cells exposed to Fab'-$(CCE)_1$ and $(CCK)_9$-P for different durations (2-6 h). R: red channel; G: green channel; O: overlay of R and G. Fab'-$(CCE)_1$: Cells incubated with Fab'-$(CCE)_1$ (500 nM, Rhodamine-Red-X labeled) only; $(CCK)_9$-P: cells incubated with $(CCK)_9$-P ([CCK]=25 μM, FITC labeled) only - no staining; Pre: cells incubated with a premixture of Fab'-$(CCE)_1$ (500 nM) and $(CCK)_9$-P ([CCK]=25 μM); Cons: cells incubated with Fab'-$(CCE)_1$ (500 nM) for 1 h followed by $(CCK)_9$-P ([CCK]=25 μM) for 6 h. b) Comparison of cell staining in the presence (medium; upper panel) or absence (PBS; lower panel) of FBS. Cells incubated with Fab'-$(CCE)_1$ (500 nM) for 1 h followed by $(CCK)_9$-P ([CCK]=25 μM) for 6 h.

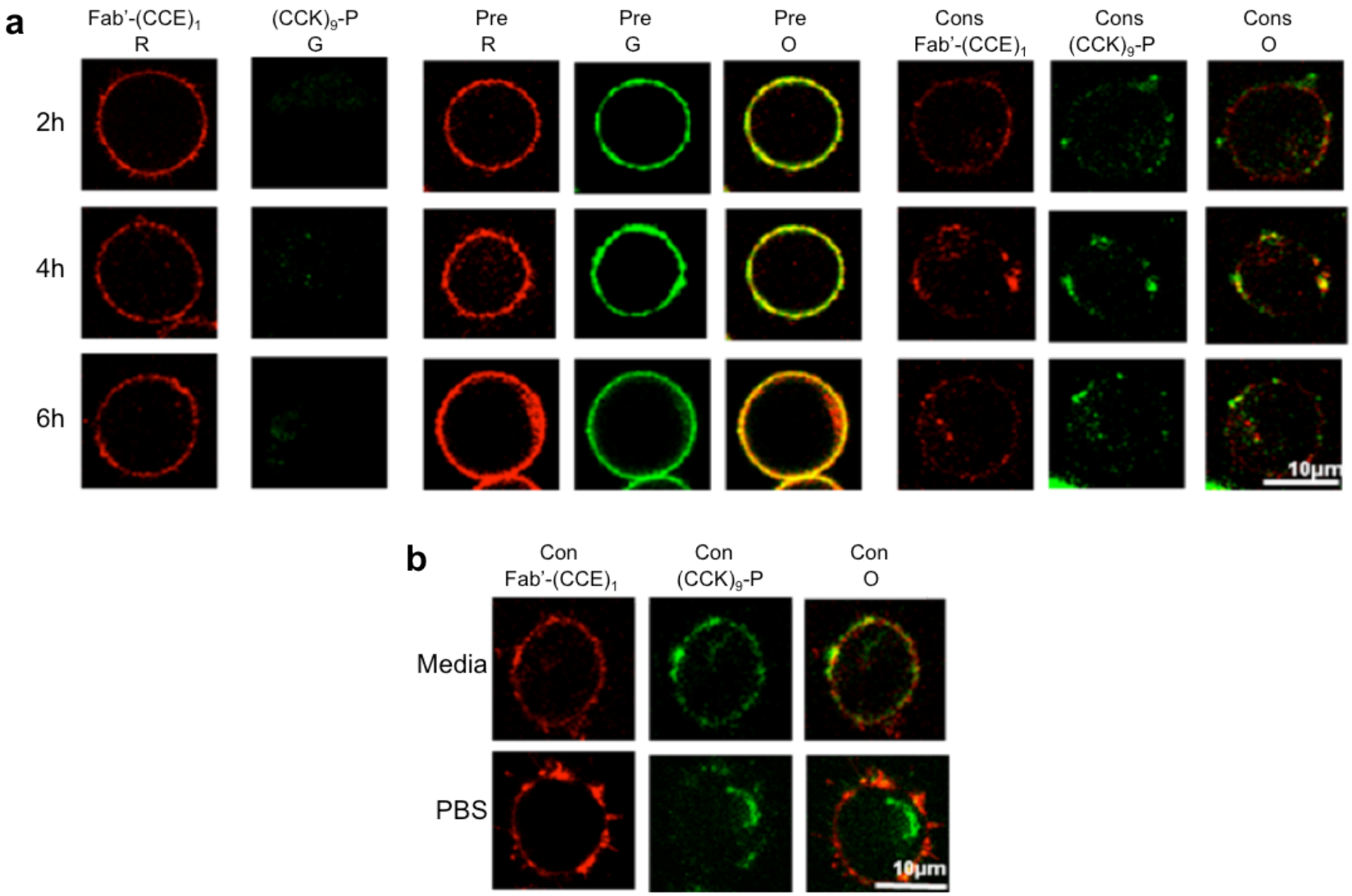
a
Fab'-(CCE)1
R
(CCK)9-P
G
Pre
R
Pre
G
Pre
O
Cons
Fab'-(CCE)1
Cons
(CCK)9-P
Cons
O
2h
4h
6h
10μm
b
Con
Fab'-(CCE)1
Con
(CCK)9-P
Con
O
Media
PBS
10μm

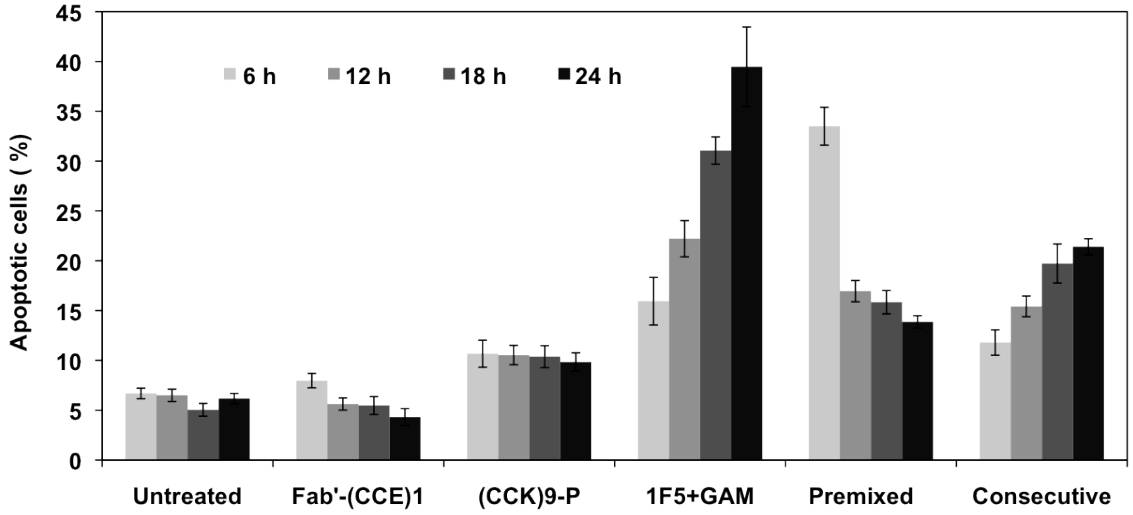

Figure 3.10. Time dependence of apoptosis induction in Raji B cells via caspase 3 activity assay. Untreated: untreated cells; Fab'-$(CCE)_1$: single-component control at 0.5 μM; $(CCK)_9$-P: single-component control ([CCK]=25 μM); 1F5+GAM: addition of 1F5 Ab (0.2 μM) followed (1 h later) by the secondary antibody GAM (10 mg· μL^{-1}); premixed: premixture of Fab'-$(CCE)_1$ (0.5 μM) and $(CCK)_9$-P ([CCK]=25 μM); consecutive: consecutive addition of Fab'-$(CCE)_1$ (0.5 μM) followed (1 h later) by $(CCK)_9$-P ([CCK]=25 μM). Results are presented as mean values ± standard deviation (n=3).

P, and the consecutive exposure of cells to Fab'-$(CCE)_1$ followed by $(CCK)_9$-P. The highest levels of apoptosis after incubation for 6 hours were observed with premixed Fab'-$(CCE)_1$ and $(CCK)_9$-P; whereas for both consecutive-addition systems, Fab'-$(CCE)_1$ + $(CCK)_9$-P and the control 1F5 + goat antimouse (GAM) secondary antibody, the extent of apoptosis increased with increasing incubation time, with the highest level observed after 24 h. These results probably reflect different levels of destabilization of the plasma-membrane integrity following exposure to a multivalent high-avidity conjugate versus a monovalent Fab'-$(CCE)_1$ conjugate.

Apoptosis induction by exposure of Raji B cells to a premixture or consecutive addition of Fab'-$(CCE)_1$+$(CCK)_9$-P with different molar ratios of [CCE] : [CCK] (1:1, 1:10, 1:25) was also examined by all three quantification methods. Results were summarized in Figures 3.11 and 3.12. As shown, the ratio of 1:25 resulted in highest efficiency in apoptosis induction. Compared with the single component, all binary systems produced higher levels of apoptosis; the levels increased with the increase of $(CCK)_9$-P excess. This is not surprising, since only some of the grafts in $(CCK)_9$-P participate in formation of anti-parallel coiled-coils due to the fact that the accessibility of the peptide grafts attached to the HPMA copolymer is restricted. The efficiency of coiled-coil formation depends on the binding constant between CCE and CCK, the number of grafts in conjugate and flexibility of the polymer backbone. Additionally, a portion of $(CCK)_9$-P may be nonspecifically attached to the cell surface or proteins in the medium. Fortunately, such an attachment did not result in apoptosis induction as results shown in Figure 3.11. The nonspecific attachment can be avoided in the future by using a system composed of Fab'-CCK and graft copolymer CCE-P. The negative charge of

Figure 3.11. Apoptosis induction in Raji B cells by Fab'-$(CCE)_1$ and $(CCK)_9$-P at different ratios of [CCE]:[CCK] (1:1 and 1:10) for various durations (6, 12 and 24 h). Cells were exposed to either premixed (Pre) or consecutively added (Cons) Fab'-$(CCE)_1$ and $(CCK)_9$-P. Percentage of apoptotic cells was quantified by caspase 3 activation assay (a and b), Annexin V assay (c and d), and TUNEL assay (e and f), respectively. Fab'-$CCE)_1$ concentration kept 1 μM; the concentrations of $(CCK)_9$-P were adjusted to [CCK]=1 and 10 μM for ratios of 1:1 and 1:10, respectively. Results are presented as mean values ± standard deviation (n=3).

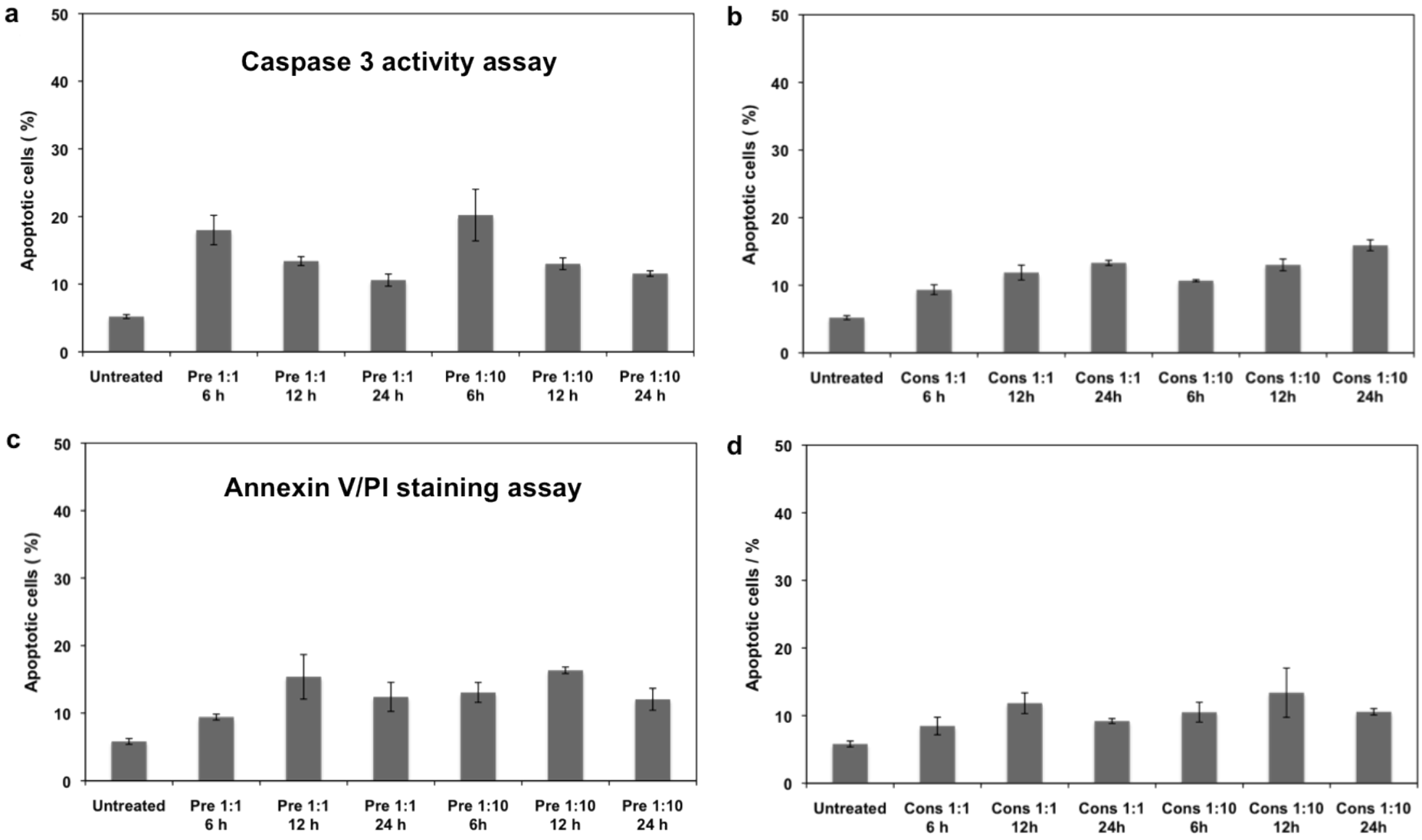
a
Caspase 3 activity assay
Apoptotic cells (%)
0
10
20
30
40
50
Untreated
Pre 1:1 6 h
Pre 1:1 12 h
Pre 1:1 24 h
Pre 1:10 6h
Pre 1:10 12 h
Pre 1:10 24 h
b
Apoptotic cells (%)
Untreated
Cons 1:1 6 h
Cons 1:1 12h
Cons 1:1 24h
Cons 1:10 6h
Cons 1:10 12h
Cons 1:10 24h
c
Annexin V/PI staining assay
Apoptotic cells (%)
Untreated
Pre 1:1 6 h
Pre 1:1 12 h
Pre 1:1 24 h
Pre 1:10 6h
Pre 1:10 12 h
Pre 1:10 24 h
d
Apoptotic cells / %
Untreated
Cons 1:1 6 h
Cons 1:1 12h
Cons 1:1 24h
Cons 1:10 6h
Cons 1:10 12h
Cons 1:10 24h

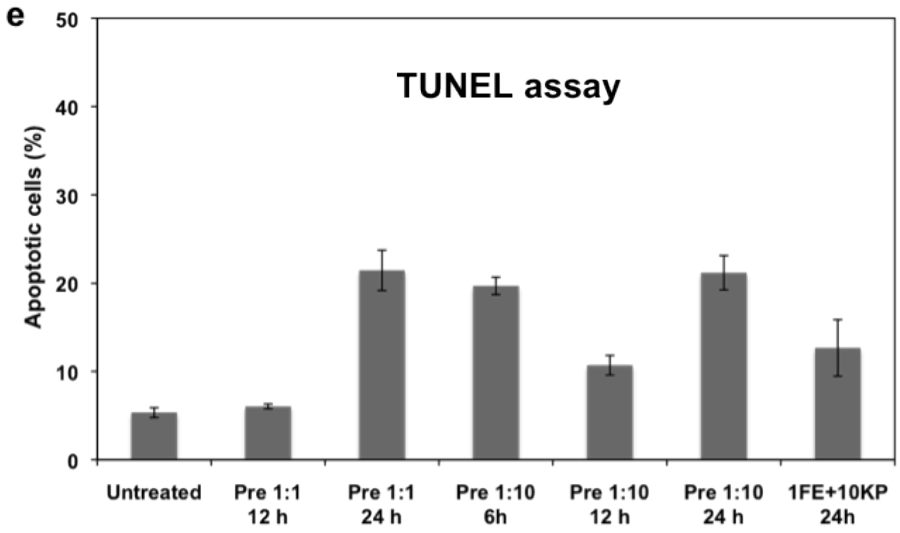
e
TUNEL assay
Apoptotic cells (%)
50
40
30
20
10
0
Untreated
Pre 1:1 12 h
Pre 1:1 24 h
Pre 1:10 6h
Pre 1:10 12 h
Pre 1:10 24 h
1FE+10KP 24h

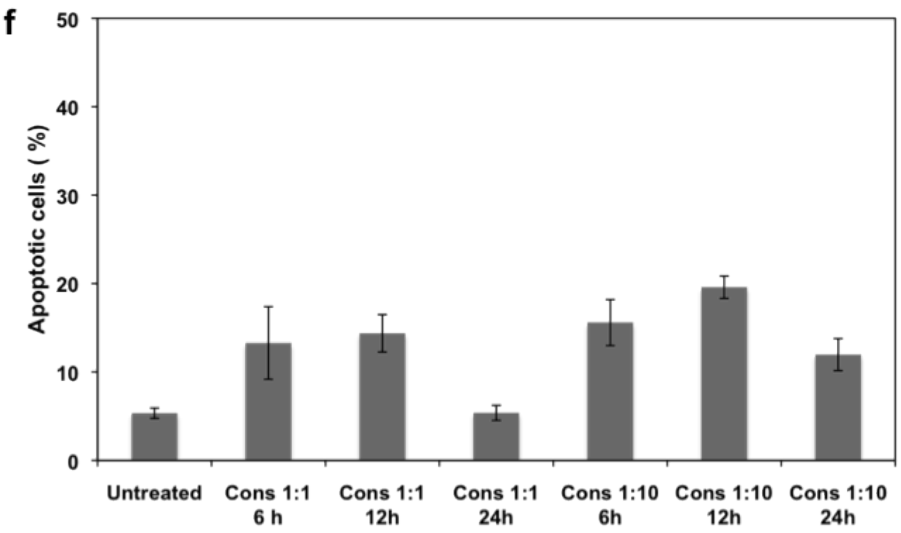
f
Apoptotic cells (%)
50
40
30
20
10
0
Untreated
Cons 1:1 6 h
Cons 1:1 12h
Cons 1:1 24h
Cons 1:10 6h
Cons 1:10 12h
Cons 1:10 24h

Figure 3.12. Coiled-coil-mediated induction of apoptosis of Raji B cells, as assessed by: a) caspase 3 activity, b) annexin V/PI staining assay, and c) TUNEL assay. The concentrations of 1F5 and GAM were 0.2 μM and 10 $mg{\cdot}mL^{-1}$, respectively. The concentrations of Fab'-$(CCE)_1$ and CCK in $(CCK)_9$-P were 0.5 and 25 μM, respectively, for P 1 and C 1 in caspase 3 assay, and 1 and 25 μM, respectively, for all other experiments. P-Ctrl 1: a premixture of Fab' (1 μM), CCE (1 μM), CCK (25 μM), and P-NH_2 (2.80 μM); P-Ctrl 2: a premixture of Fab'-$(CCE)_1$ (1 μM) and P-NH_2 (2.80 μM); P-Ctrl 3: a premixture of Fab' (1 μM) and $(CCK)_9$-P (2.80 μM); C-Ctrl 1: Fab' (1 μM) and CCE (1 μM) for 1 h, and then CCK (25 μM) and P-NH_2 (2.80 μM); C-Ctrl 2: Fab'-$(CCE)_1$ (1 μM) for 1 h, then P-NH_2 (2.80 μM); C-Ctrl 3: Fab' (1 μM) for 1 h, then $(CCK)_9$-P ([CCK]=25 μM/ [P-NH_2]=2.80 μM). Results are presented as mean values ± standard deviation (n=3).

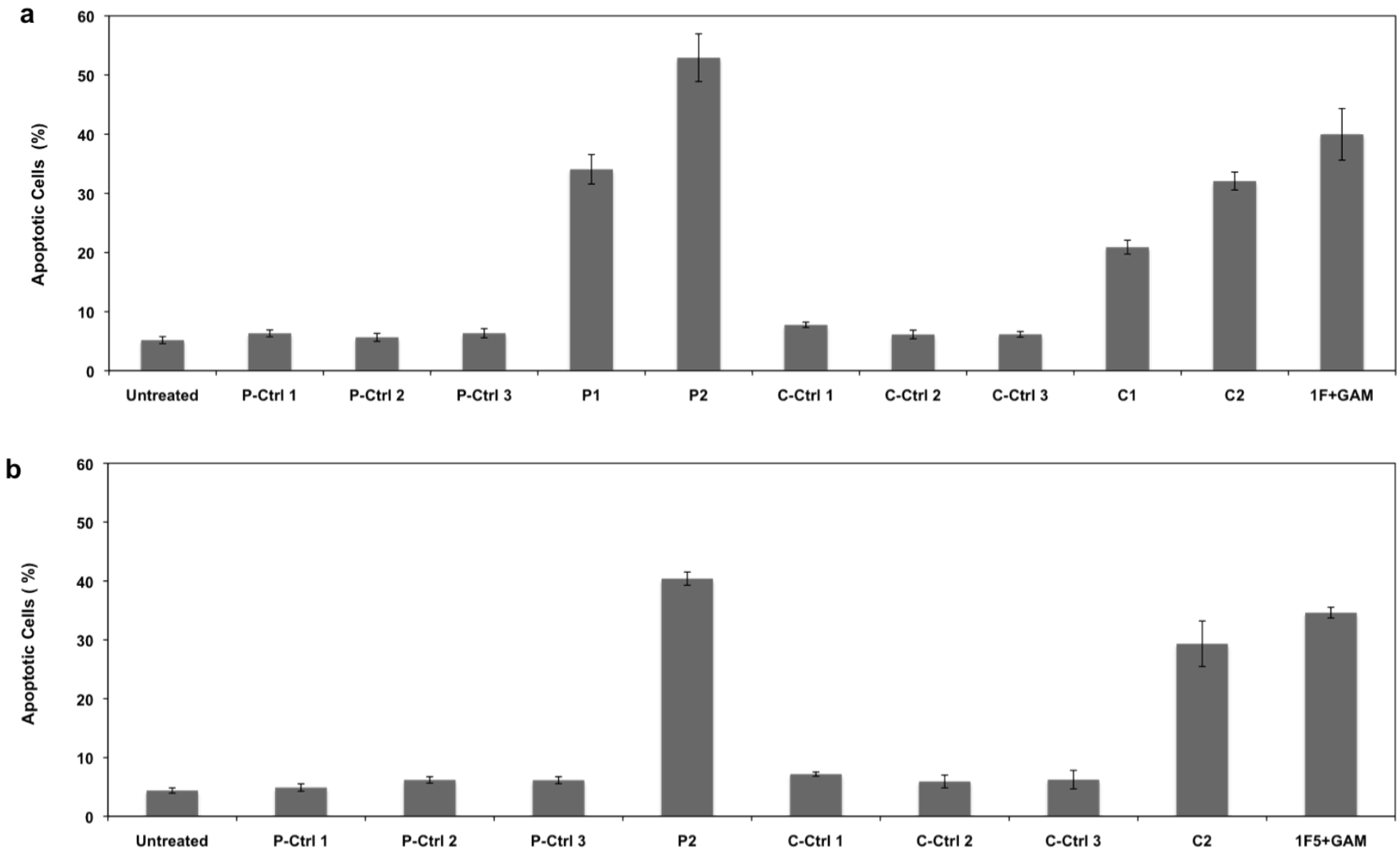
a
Apoptotic Cells (%)
60
50
40
30
20
10
0
Untreated
P-Ctrl 1
P-Ctrl 2
P-Ctrl 3
P1
P2
C-Ctrl 1
C-Ctrl 2
C-Ctrl 3
C1
C2
1F+GAM
b
Apoptotic Cells (%)
60
50
40
30
20
10
0
Untreated
P-Ctrl 1
P-Ctrl 2
P-Ctrl 3
P2
C-Ctrl 1
C-Ctrl 2
C-Ctrl 3
C2
1F5+GAM

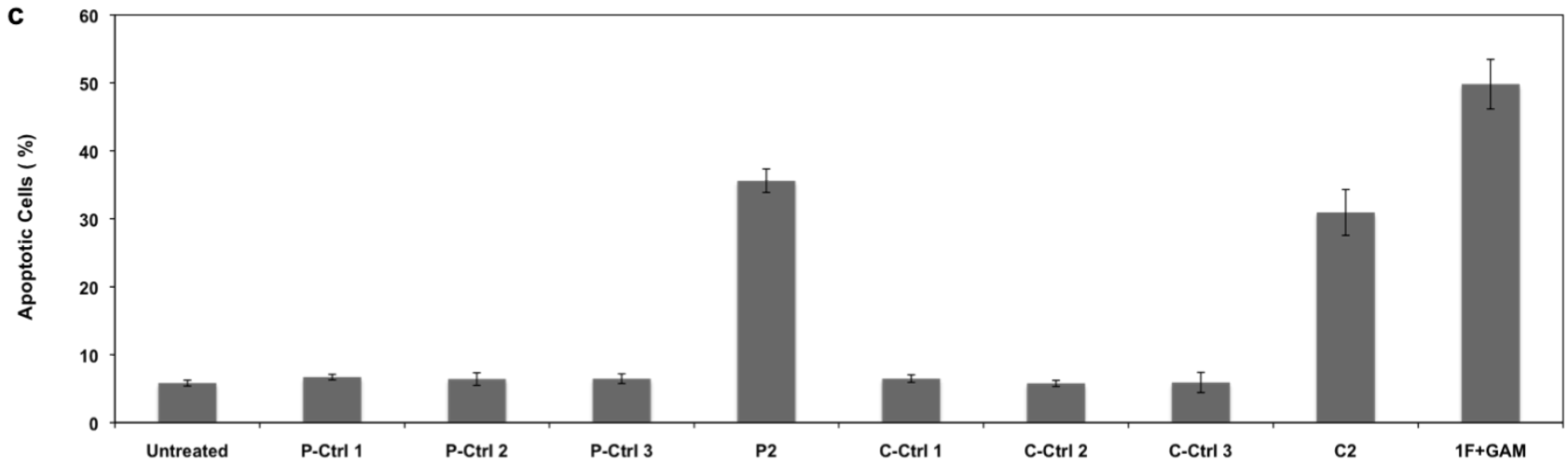
C
Apoptotic Cells (%)
60
50
40
30
20
10
0
Untreated
P-Ctrl 1
P-Ctrl 2
P-Ctrl 3
P2
C-Ctrl 1
C-Ctrl 2
C-Ctrl 3
C2
1F+GAM

CCE-P should minimize the nonspecific binding to negatively charged cell surface. Another possible interfering factor is the steric hindrance from the glycocalyx layer, which may interfere with the transport of $(CCK)_9$-P toward the CCE decorated cell. This might be overcome by inserting a spacer between the Fab' and CCE, and hence CCE should be more accessible for subsequent self-assembly.

As observed, premixture of Fab'-$(CCE)_1$ and $(CCK)_9$-P demonstrated higher levels of apoptosis induction than the consecutive addition, provided other conditions were the same. This observation was believed to be a result of the multi-valency effect. The premixture resulted in coiled-coil mediated formation of conjugates containing several Fab' fragments attached to one macromolecule resulting in the increase in their avidity, an observation in agreement with our previous data *(21)*.

In further experiments, the systems were compared at the time intervals corresponding to maximum apoptosis, that is, 6 h for premixture and 24 h for consecutive addition. The extent of apoptosis could be increased by manipulating the concentration of the components. An increase in the Fab'-$(CCE)_1$ concentration from 0.5 to 1 μM led to an increase in the amount of apoptotic cells from 21 to 32% in the consecutive addition (as shown in Figure 3.12a). The results of annexin V (Figure 3.12b) and TUNEL (Figure 3.12c) assays corroborated the efficacy of the system in the presence of FBS. Comparable levels of apoptosis induction (ca. 30%) were observed for consecutively added Fab'-$(CCE)_1$ (1 μm) and $(CCK)_9$-P ([CCK]=25 μm), consecutively added 1F5 and GAM (ca. 40%), and premixed Fab'-$(CCE)_1$ and $(CCK)_9$-P (ca. 40%). The apoptotic levels observed here were comparable to those found upon the exposure of Raji B cells to multivalent antibody conjugates: HPMA copolymers containing multiple Fab' fragments *(21)*,

dextran–antibody (rituximab) conjugates *(26)*, and rituximab dimers *(27)*.

Control experiments validated the hypothesis that the coiled-coil heterodimerization of CCE with CCK with concomitant cross-linking of the CD20 antigen is responsible for apoptosis induction. Different combinations of the building blocks (Table 3.1) of the binary systems were incubated with Raji B cells for 6 and 24 h for premixture and consecutive addition, respectively. The levels of apoptosis observed after the exposure of Raji B cells were very low and similar to those observed for untreated cells (Figure 3.12 a–c, controls 1, 2, and 3).

Further optimization of the current system might result in even higher apoptosis levels. The factors can be explored include optimization of the concentration and the timing of consecutive addition of the components, the use of D-amino acid sequences, the design of shorter sequences, and the insertion of a spacer between Fab' and the peptide.

3.5. Conclusion

Several factors contributed to the successful design of this new drug-free therapeutic system: a) the use of the 1F5 antibody, the binding of which to CD20+ cells does not induce apoptosis: a secondary GAM antibody *(28)* is needed; b) the design of the CCE and CCK sequences *(6)*: antiparallel heterodimer formation reduces the steric hindrance of the polymer chain during the binding of $(CCK)_9$-P to Raji cells predecorated with CCE motifs and enhances the probability of "in-register" alignment of the CCE-CCK heterodimer; c) the HPMA copolymer employed for the conjugation of multiple copies of one of the peptides (CCK): HPMA copolymers have been widely used in drug-delivery systems *(29, 30)*, and their biocompatibility has been proven in animal models *(31-33)*

and clinical trials *(34)*; d) the choice of the CD20 antigen: CD20 is expressed on most NHL malignant cells as well as on normal B cells; however, it is not expressed on stem cells and mature plasma cells; consequently, normal numbers of B cells can be restored after treatment *(35)*.

We have presented a new approach to apoptosis induction mediated by the biorecognition of coiled-coil-forming peptide segments on the cell surface. The fact that biorecognition of coiled-coils at the cell surface occurred in media containing 10% FBS indicates the specificity of the CCE–CCK interaction and bodes well for future in vivo experiments and for the development of efficient drug-free macromolecular therapeutics. The important feature of this design is the absence of low-molecular-weight cytotoxic compounds. The concept of drug-free macromolecular therapeutics could be expanded by using different components in the design. For example, the Fab' fragment could be replaced by antigen-binding saccharides *(36)* or by peptides *(37, 38)* selected by combinatorial methods.

3.6. Acknowledgements

This is partly supported by NIH grant EB005288 (to J. Kopeček). K. Wu would like to acknowledge a fellowship from the American Foundation for Pharmaceutical Education (AFPE).

3.7 References

(1) Kopeček, J. (2003) Smart and genetically engineered biomaterials and drug delivery systems. *Eur J Pharm Sci 20*, 1-16.

(2) Kopeček, J. (2007) Hydrogel biomaterials: a smart future? *Biomaterials 28*, 5185-5192.

(3) Kopeček, J., and Yang, J. (2007) Hydrogels as smart biomaterials. *Polymer International 56*, 1078-1098.

(4) Kopeček, J. (2002) Polymer chemistry: swell gels. *Nature 417*, 388-391.

(5) Wang, C., Stewart, R. J., and Kopeček, J. (1999) Hybrid hydrogels assembled from synthetic polymers and coiled-coil protein domains. *Nature 397*, 417-420.

(6) Yang, J., Xu, C., Wang, C., and Kopeček, J. (2006) Refolding hydrogels self-assembled from *N*-(2-hydroxypropyl)methacrylamide graft copolymers by antiparallel coiled-coil formation. *Biomacromolecules 7*, 1187-1195.

(7) Yang, J., Wu, K., Koňák, Č., and Kopeček, J. (2008) Dynamic light scattering study of self-assembly of HPMA hybrid graft copolymers. *Biomacromolecules 9,* 510-517.

(8) Kosmas, C., Stamatopoulos, K., Stavroyianni, N., Tsavaris, N., and Papadaki, T. (2002) Anti-CD20-based therapy of B cell lymphoma: state of the art. *Leukemia 16*, 2004-2015.

(9) Deans, J. P., Li, H., and Polyak, M. J. (2002) CD20-mediated apoptosis: signalling through lipid rafts. *Immunology 107*, 176-182.

(10) Golay, J. T., Clark, E. A., and Beverley, P. C. (1985) The CD20 (Bp35) antigen is involved in activation of B cells from the G0 to the G1 phase of the cell cycle. *J Immunol 135*, 3795-3801.

(11) Bubien, J. K., Zhou, L. J., Bell, P. D., Frizzell, R. A., and Tedder, T. F. (1993) Transfection of the CD20 cell surface molecule into ectopic cell types generates a Ca^{2+} conductance found constitutively in B lymphocytes. *J Cell Biol 121*, 1121-1132.

(12) Kanzaki, M., Shhibata, H., Mongami, H. and Kojima, I. (1995) Expression of calcium-permeable cation channel CD20 accelerates progression through the G1 phase in Balb/c 3T3 cells. *J Biol Chem 270*, 13099-13104.

(13) Walshe, C. A., Beers, S. A., French, R. R., Chan, C. H., Johnson, P. W., Packham, G. K., Glennie, M. J., and Cragg, M. S. (2008) Induction of cytosolic calcium flux

by CD20 is dependent upon B Cell antigen receptor signaling. *J Biol Chem 283*, 16971-16984.

(14) Press, O. W., Farr, A. G., Borroz, K. I., Anderson, S. K., and Martin, P. J. (1989) Endocytosis and degradation of monoclonal antibodies targeting human B-cell malignancies. *Cancer Res 49*, 4906-4912.

(15) Press, O. W., Appelbaun, F., Ledbetter, J. A., Martin, P. J., Zarling, J., Kidd, P., and Thomas, E. D. (1987) Monoclonal antibody 1F5 (anti-CD20) serotherapy of human B cell lymphomas. *Blood 69*, 584-591.

(16) Kopeček, J., and Bažilová, H. (1973) Poly[*N*-(2-hydroxypropyl)methacrylamide]-I. Radical polymerization and copolymerization. *Eur Polym J 9*, 7-14.

(17) Omelyanenko, V., Kopečková, P., Gentry, C., and Kopeček, J. (1998) Targetable HPMA copolymer-adriamycin conjugates. Recognition, internalization, and subcellular fate. *J Control Release 53*, 25-37.

(18) Pechar, M., Kopečková, P., Joss, L., and Kopeček, J. (2002) Associative Diblock Copolymers of Poly(ethylene glycol) and Coiled-Coil Peptides. *Macromol Biosci 2*, 199-206.

(19) Clark, E. A., Shu, G., and Ledbetter, J. A. (1985) Role of the Bp35 cell surface polypeptide in human B-cell activation. *Proc Natl Acad Sci USA 82*, 1766-1770.

(20) Fowers, K. D., Callahan, J., Byron, P., and Kopeček, J. (2001) Preparation of Fab' from murine IgG2a for thiol reactive conjugation. *J Drug Target 9*, 281-294.

(21) Johnson, R.N., Kopečková, P., and Kopeček, J. (2009) Synthesis and evaluation of multivalent branched HPMA copolymer-Fab' conjugates targeted to the B-cell antigen CD20. *Bioconjug Chem 20*, 129-137.

(22) Hermanson, G. T. (1996) *Bioconjugate Techniques*, 481. Academic Press, San Diego, CA

(23) Ellman, G. L. (1959) Tissue sulfhydryl groups. *Arch Biochem Biophys 82*, 70-77.

(24) Gergel, D., and Cederbaum, A. I. (1996) Inhibition of the catalytic activity of alcohol dehydrogenase by nitric oxide is associated with S nitrosylation and the release of zinc. *Biochemistry 35*, 16186-16194.

(25) Ong, G. L., Elsamra, S. E., Goldenberg, D. M., and Mattes, M. J. (2001) Single-cell cytotoxicity with radiolabeled antibodies. *Clin Cancer Res 7*, 192-201.

(26) Zhang, N., Khawli, L. A., Hu, P., and Epstein, A. L. (2005) Generation of rituximab polymer may cause hyper-cross-linking-induced apoptosis in non-Hodgkin's lymphomas. *Clin Cancer Res 11*, 5971-5980.

(27) Ghetie, M. A., Bright, H., and Vitetta, E. S. (2001) Homodimers but not monomers of Rituxan (chimeric anti-CD20) induce apoptosis in human B-lymphoma cells and synergize with a chemotherapeutic agent and an immunotoxin. *Blood 97*, 1392-1398.

(28) Hofmeister, J. K., Cooney, D., and Coggeshall, K. M. (2000) Clustered CD20 induced apoptosis: src-family kinase, the proximal regulator of tyrosine phosphorylation, calcium influx, and caspase 3-dependent apoptosis. *Blood Cells Mol Dis 26*, 133-143.

(29) Kopeček, J., Kopečková, P., Minko, T., and Lu, Z.-R. (2000) HPMA copolymer-anticancer drug conjugates: design, activity, and mechanism of action. *Eur J Pharm Biopharm 50*, 61-81.

(30) Kopeček, J., and Kopečková, P. (2010) HPMA copolymers: origins, early developments, present, and future. *Adv Drug Deliv Rev 62*, 122-149.

(31) Peterson, C. M., Lu, J. M., Sun, Y., Peterson, C. A., Shiah, J. G., Straight, R. C., and Kopeček, J. (1996) Combination chemotherapy and photodynamic therapy with *N*-(2-hydroxypropyl) methacrylamide copolymer-bound anticancer drugs inhibit human ovarian carcinoma heterotransplanted in nude mice. *Cancer Res 56*, 3980-3985.

(32) Shiah, J.-G., Dvorak, M., Kopečková, P., Sun, Y., Peterson, C. M., and Kopeček, J. (2001) Biodistribution and antitumour efficacy of long-circulating *N*-(2-hydroxypropyl)methacrylamide copolymer-doxorubicin conjugates in nude mice. *Eur J Cancer 37*, 131-139.

(33) Minko, T., Kopečková, P., and Kopeček, J. (2000) Efficacy of the chemotherapeutic action of HPMA copolymer-bound doxorubicin in a solid tumor model of ovarian carcinoma. *Int J Cancer 86*, 108-117.

(34) Vasey, P. A., Kaye, S. B., Morrison, R., Twelves, C., Wilson, P., Duncan, R., Thomoson, A. H., Murray, L. S., Hilditch, T. E., Murray, T., Burtles, S., Fraier, D., Frigerio, E., and Cassidy, J. (1999) Phase I clinical and pharmacokinetic study of PK1 [*N*-(2-hydroxypropyl)methacrylamide copolymer doxorubicin]: first member of a new class of chemotherapeutic agents-drug-polymer conjugates. Cancer Research Campaign Phase I/II Committee. *Clin Cancer Res 5*, 83-94.

(35) Browning, J. L. (2006) B cells move to centre stage: novel opportunities for autoimmune disease treatment. *Nat Rev Drug Discov 5*, 564-76.

(36) David, A., Kopečková, P., Rubinstein, A., and Kopeček, J. (2001) Enhanced biorecognition and internalization of HPMA copolymers containing multiple or multivalent carbohydrate side-chains by human hepatocarcinoma cells. *Bioconjug Chem 12*, 890-899.

(37) Ding, H., Prodinger, W. M., and Kopeček, J. (2006) Identification of CD21-binding peptides with phage display and investigation of binding properties of HPMA copolymer-peptide conjugates. *Bioconjug Chem 17*, 514-523.

(38) Ding, H., Prodinger, W. M., and Kopeček, J. (2006) Two-step fluorescence screening of CD21-binding peptides with one-bead one-compound library and investigation of binding properties of *N*-(2-hydroxypropyl)methacrylamide copolymer-peptide conjugates. *Biomacromolecules 7*, 3037-3046.

CHAPTER 4

TREATMENT OF HUMAN B-CELL NON-HODGKIN'S LYMPHOMA IN SCID MICE BY DRUG-FREE MACROMOLECULAR THERAPEUTICS

4.1 Summary

CD20 was found to be a reliable biomarker for non-Hodgkin's lymphoma (NHL), expressed on more than 95% of the diseased B cells. Recently, our group successfully developed a drug-free macromolecular therapeutics, a binary system composed of 1) anti-CD20 antibody fragment (Fab') conjugated with CCE (a coiled-coil motif) and 2) polyHPMA copolymers grafted with multiple copies of CCK (another coiled-coil motif complementary to CCE). More importantly, we proved the concept that CCE-CCK heterodimerization into coiled-coil on cell surface could mediate the cross-linking of CD20 antigens and concomitantly induce clinically relevant magnitude of apoptosis of diseased lymphatic B cells. As a continuing effort, *in vivo* evaluation of such a binary system was conducted on a systemic NHL model on C.B-17 SCID mice. Preliminary results demonstrated that the current system could successfully suppress the proliferation and subsequently deplete inoculated human Burkitt's Raji B cells after multiple-dose treatments, which produced long-term survivors (>100 days).

4.2. Introduction

Non-Hodgkin's lymphoma (NHL) is among the top 10 most prevalent cancers in the United States; the projected new cases and death from NHL in 2010 are 65,540 and 20,210, respectively *(1)*. Pathogenesis analysis revealed that B-cell abnormality counts for 85% of the NHL incidences; in addition, more than 95% of the diseased B cells are bearing CD20 surface antigen *(2, 3)*. The unique features of CD20 make it a reliable biomarker and a useful target for NHL: noninternalizing, noncirculating, and non-shedding upon binding to antibodies *(4)*.

Mechanism studies on rituximab, an FDA approved monoclonal antibody (mAb) for NHL treatment, demonstrated that direct apoptosis could be induced upon its binding to CD20 antigens *(4, 5)*. Further exploration on this phenomenon led to the finding that (super) cross-linking of CD20 triggered the apoptotic pathway *(6, 7)*. Following this track, researchers have employed secondary antibody *(7)* and dextran-antibody conjugates *(8)* to induce apoptosis of the diseased B cells. Due to the unique feature of CD20, expressed only on B cells but not plasma and hemapoietic stem cells *(2, 3)*, the reestablishment of blood homeostasis is possible after the treatment.

However, mounting incidences of severe side effects after rituximab treatment have been reported *(4, 9, 10)*. Accumulating evidence points the Fc fragment/region of the antibody, which not only mediates the antibody-dependent cellular cytotoxicity (ADCC) and complement-dependent cytotoxicity (CDC) during the treatment but also mediates these side effects *(11-13*). These findings are diverting further treatment modalities to focus on direct apoptosis induction.

Based on the aforementioned lines of evidence, our group developed a novel drug-free macromolecular therapeutic system to combat B-cell NHL *(14)*. This binary system was composed of a conjugate of Fab' fragment of anti-CD20 mAb (1F5) and CCE, and a polyHPMA copolymer grafted with multiple copies of CCK. CCE and CCK were *de novo* designed coiled-coil forming peptides containing five heptads that could exclusively self-assemble into heterodimers in anti-parallel orientation; the resulted coiled-coil would function as an *in situ* cross-linker mediating the recognition of the two components *(15)*. Here only Fab' fragment was employed in the design so that any Fc fragment related side effects would be diminished. The multivalent construction of polyHPMA graft copolymer would provide the platform for cross-linking CD20 antigens. *In vitro* study on human Burkitt's lymphoma Raji cells showed that this binary system could induce clinically relevant level of apoptosis (30-50%) *(14)*.

Here *in vivo* evaluation of this drug-free macromolecular therapeutics is reported. A systemic NHL model was established in C.B-17 SCID mice by i.v. injection of Raji cells, then different treatments were applied. Using the onset of hind-limb paralysis as a study end-point, we observed significant extension of paralysis-free duration after treatments. Bone marrow from different subjects was analyzed to examine the presence of residual Raji cells via fluorescently labeled anti- CD10 and CD19 mAb staining.

4.3. Materials and methods

4.3.1. Conjugate preparation

$(Fab')_1$-CCE and $(CCK)_9$-P were synthesized as previously reported *(14)*, and the detailed synthetic schemes were described in Figure 3.3. For Fab' conjugate: 1F5 anti-

CD20 antibody was prepared using the anti-CD20 hybridoma clone 1F5, and then consecutively digested to $F(ab')_2$ and reduced to Fab' by lysyl endopeptidase (Wako Chemicals USA, Richmond, VA) and TCEP (Thermo Scientific, Waltham, MA), respectively; finally CCE capped with maleimido group was conjugated to Fab' via thioether bond. The graft copolymer was synthesized using a polymeranalogous strategy: first HPMA and *N*-(3-aminopropyl)methacrylamide (Ma-NH_2) were copolymerized via free radical polymerization, then SMCC was employed to convert the side-chain amino groups into maleimido groups, and finally CCK peptides were grafted onto the polymer backbone through the reaction between thiol and maleimido groups. All synthesis steps were monitored with various techniques (e.g., RP-HPLC, SEC, SDS-PAGE). The number of CCK peptides in the final graft copolymer was determined as 8.94 via amino acid analysis, so the construct was designated as $(CCK)_9$-P.

4.3.2. Cell line and systemic NHL SCID mouse model

Human Burkitt's B-cell NHL Raji cells (ATCC, Manassas VA) were cultured as described before *(14)*. The cells were maintained in RPMI-1640 medium supplemented with 10% fetal bovine serum (FBS) at 37 ^{o}C in a humidified atmosphere of 5% CO_2. Cells at the exponential growth phase were used for mice inoculation.

Female C.B-17 SCID mice (~6 weeks old) *(16-18)* were purchased from Charles River Laboratories (Wilmington, MA) and maintained following the protocol approved by the Institutional Animal Care and Use Committee (IACUC) from University of Utah. Following the model described by Ghetie and colleagues *(19)*, mice with body weight around 20 g were intravenously injected with 4×10^6 Raji cells in 200 μL normal saline

(N.S.) via the tail vein. Our pilot study demonstrated the untreated mice could develop hind-limb paralysis around 3 weeks postinnoculation, a proof of successful model establishment observed by other researchers as well *(16, 19, 20)*.

4.3.3. Treatments and follow-ups

Inoculated mice were divided into five groups: Ctrl, control group without treatment; ConSingle, consecutive administration of single dose; PreSingle, premixed administration of single dose; ConMultiple, consecutive administration of multiple (3) doses; and PreMultiple, premixed administration of multiple (3) doses. Here consecutive administration involved the i.v. injection of Fab'-$(CCE)_1$ first and 1 h later the $(CCK)_9$-P conjugate was applied via the same route; while in the premixed administration, the two conjugates were first mixed outside the body for 1 h, and then injected via the tail vein. For single-dose groups, conjugates were administered 24 h postinoculation; for multiple-dose groups, conjugates were applied 24, 72, 120 h postinoculation. The doses in each treatment for $(Fab')_1$-CCE and $(CCK)_9$-P were 50 μg/20 g and 324 μg/20 g, respectively. This combination ensured the molar ratio between CCE and CCK to be 1:25 *(14)*.

Postoperation monitoring was exercised at least once a day. Major aspects monitored were body weight, physical appearance (e.g., hunched back, piloerection), food intake and hind-limb paralysis. Animals were sacrificed at signs of sickness, such as the onset of hind-limb paralysis, >20% of body weight loss, and if mice survived for >100 days. Statistical comparisons were performed using log-rank test ($P<0.05$).

4.3.4. Residual Raji cell analysis

Immediately after the sacrifice, femurs were harvested from the subject and purged with cold PBS to collect bone marrow cells. Then 5 volumes of cold red blood lysing solution was added into 1 volume bone marrow cell suspension; the mixture was incubated for 2-3 min at room temperature and centrifuged to remove cell debris. After washing with cold washing buffer once, the bone marrow cells were divided into three tubes (~50 μL each) suspended again by cold washing buffer. One tube was spared as control, and the rest two were stained by Raji cell specific primary antibodies: R-phycoerythrin (PE) mouse anti-human CD10 (mouse IgG1, κ isotype) and allophycocyanin (APC) mouse anti-human CD19 (mouse IgG1, κ isotype). Both antibodies were purchased from BD Biosciences (San Jose, CA). Twenty microliter fluorescently labeled antibody (CD10 or CD19) was added and incubated with processed bone marrow cells for 40 min at 4 ^{o}C in the dark. Finally, flow cytometry was employed to identify the residual Raji tumor cells.

4.4. Results and discussion

4.4.1. Therapy studies of systemic NHL in SCID mice

After inoculation of 4×10^{6} Raji cells, mice developed hind-limb paralysis within 22 days if no treatment was applied. This observation was in good agreement with results published by other groups *(17, 20-23)*. However, the tumor-bearing mice treated with single- or multiple-dose experienced a significantly extended paralysis-free duration ($p<0.05$). In our preliminary experiments, three mice in each group were recruited as shown in Figure 4.1: single treatment extended paralysis-free duration from a median of

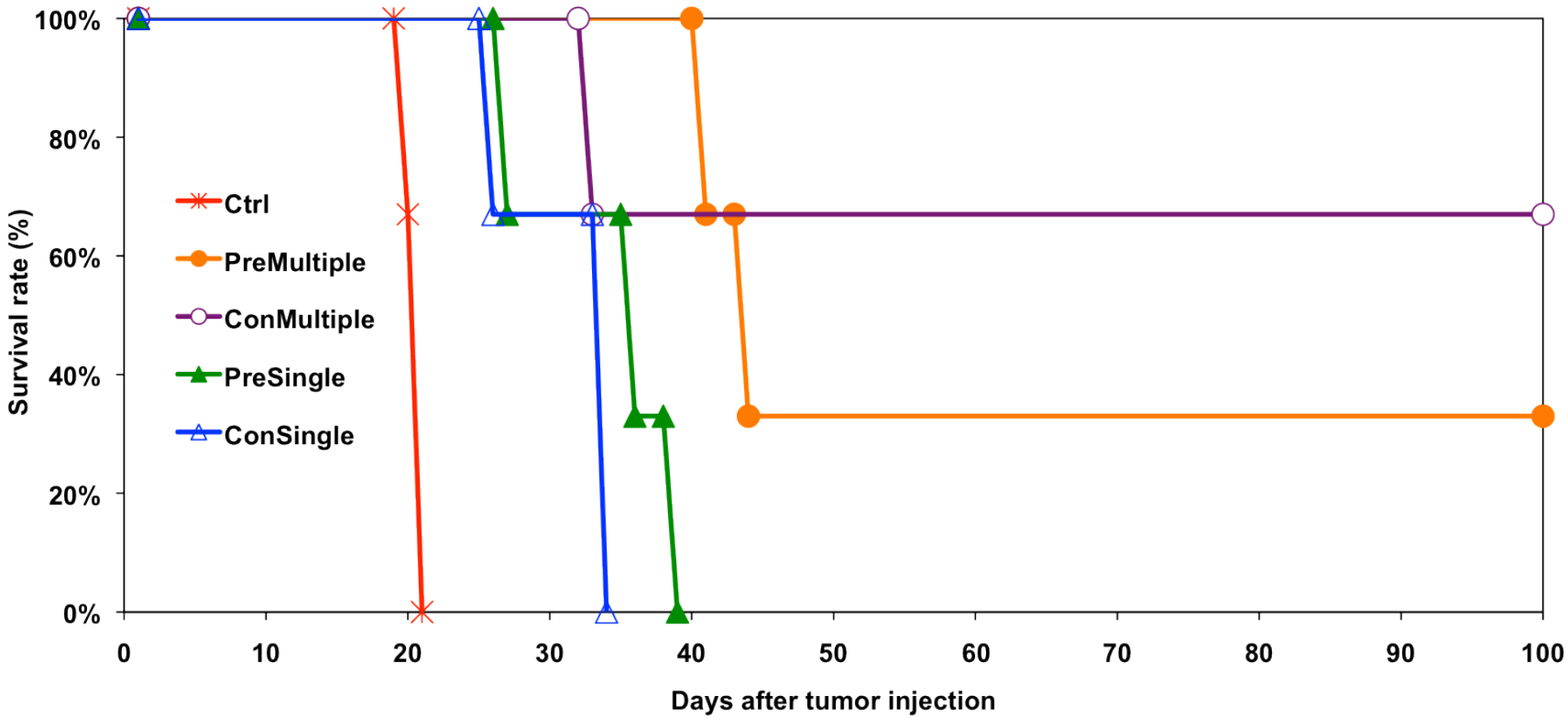

Figure 4.1. Therapeutic efficacy of macromolecular therapeutics on systemic Raji cell induced NHL in SCID mice (n=3/group). Dosages in each treatment were 50 μg/20 g and 324 μg/20 g for Fab'-$(CCE)_1$ and $(CCK)_9$-P, respectively. Single treatment was applied 24 h after i.v. inoculation of 4×10^6 Raji cells. Mutiple treatments were administrated 24, 72 and 120 h postinoculation. Significant extension of paralysis-free duration was observed after single treatments (PreSingle and ConSingle) and multiple treatments (PreMultiple and ConMultiple) ($p<0.05$) in comparison to untreated controls (Ctrl). Multiple (three doses) treatments did produce long-term survivors that survived for 100 days without paralysis. PreSingle, premixed administration for single dose; ConSingle, consecutive injections for single dose; PreMultiple, premixed administration for three doses; ConMultiple, consecutive injections for 3 doses.

22 to 35 days; while three-dose treatment produced long-term survivors (one out of three in PreMultiple group, and two out of three in ConMultiple group) that survived for 100 days without paralysis. But the two modalities of administration, consecutive injection and premixture, did not differ significantly in neither single- nor multiple-dose treatments. This was not unexpected since we proved previously that the presence of protein did not compromise the molecular biorecognition of CCE and CCK motifs *(14)*.

4.4.2. Analysis of residual Raji cells in bone marrow

Besides CD20, CD10 and CD19 are another two specific cell surface antigens for human Burkitt's lymphoma *(24, 25)*. Upon binding to the primary antibodies, they intend to be internalized although with different kinetics; but they do not shed into the extracellular space *(26)*. These features make them excellent diagnostic tools to identify the presence of B cells. In our study, two fluorescently labeled mouse anti-human antibodies were employed to detect the residual Raji cells in the bone marrow: PE mouse anti-human CD10 and APC mouse anti-human CD19.

As shown in Figure 4.2, the presence of residual Raji B cells was confirmed in untreated mice, and also in the mice that received single-dose treatment; however, no residual malignant B cells were detected in the survivors treated with three doses. Here the mice were either sacrificed at the onset of hind-limb paralysis or survived for >100 days. Apparently, the multiple treatments with 48 h apart managed to deplete Raji cells *(27)*; while the single treatment only slowed down the tumor progression. The necessity for multiple doses was possibly related to the short doubling time (20-24 h) of this cell line; in other words, the resurrection of residual cells after the single treatment led to the

Figure 4.2. Evaluation of residual Raji B cells in the bone marrow after different treatments. Bone marrow cells were stained by fluorescently labeled mAbs: PE-CD10 and APC-CD19 as shown in the left and right columns, respectively.

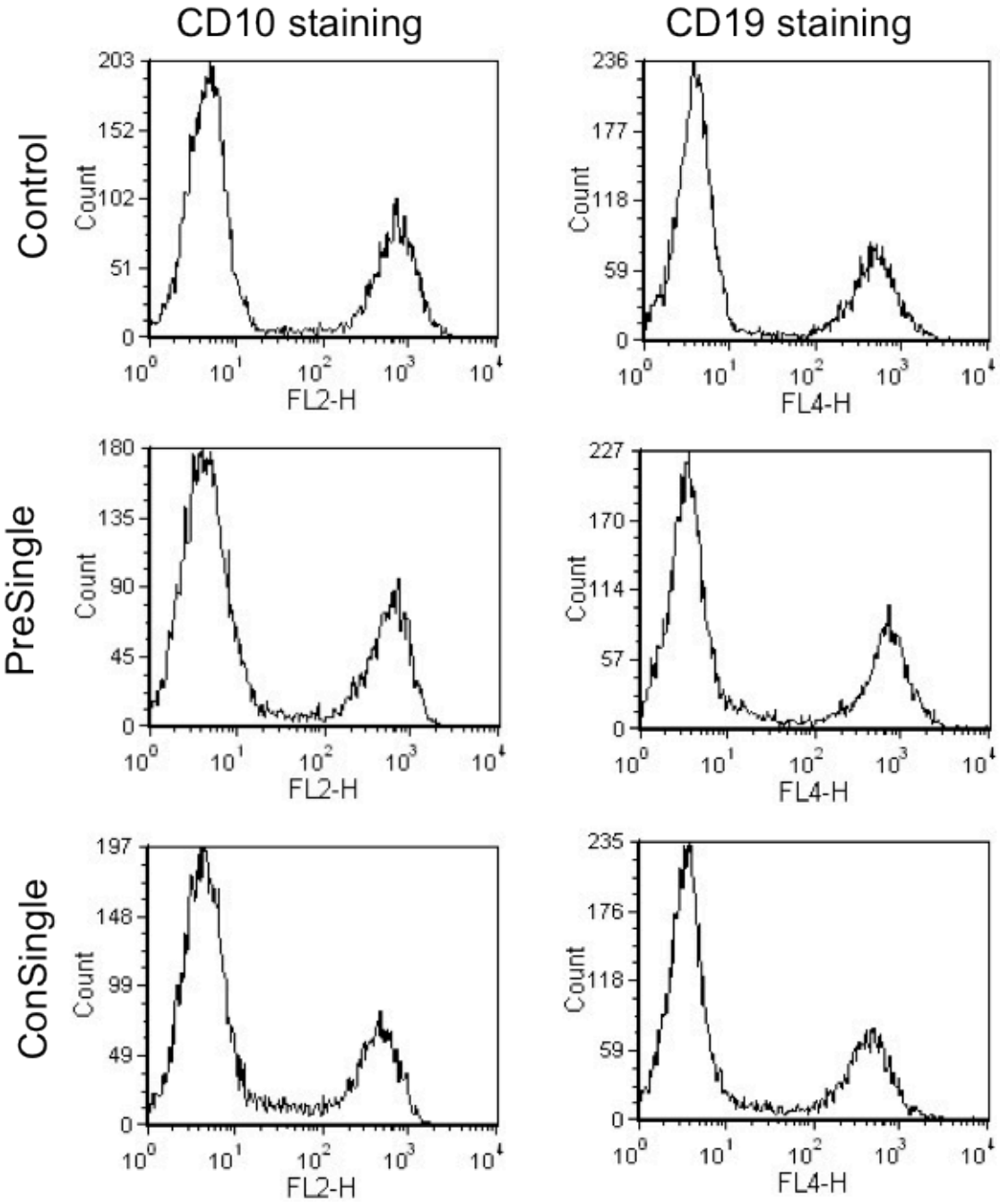
CD10 staining
CD19 staining
Control
PreSingle
ConSingle
Count
FL2-H
FL4-H
203
152
102
51
0
236
177
118
59
180
135
90
45
227
170
114
57
197
148
99
49
235
176
118
59
10^0
10^1
10^2
10^3
10^4

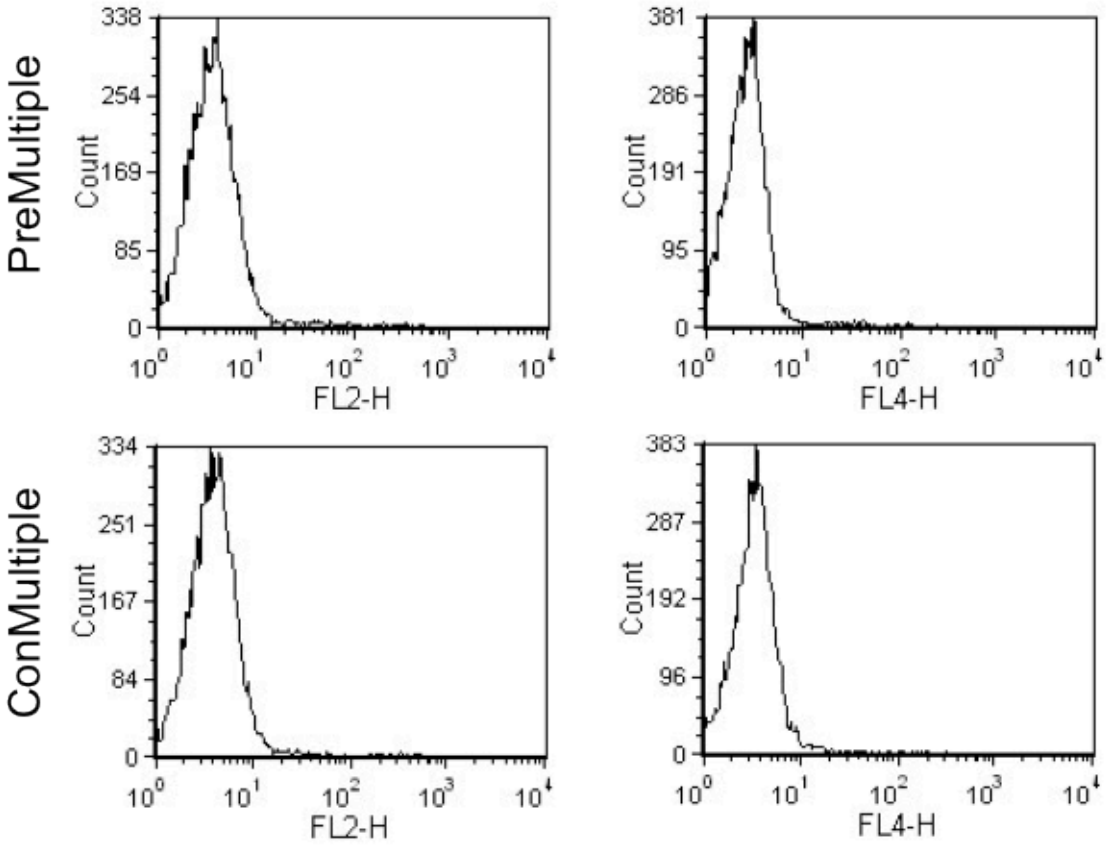
PreMultiple
ConMultiple
Count
FL2-H
FL4-H
338
254
169
85
0
381
286
191
95
334
251
167
84
383
287
192
96
10^0
10^1
10^2
10^3
10^4

full development of paralysis. It is foreseeable that a higher dosage can deplete the diseased cell after only one administration.

In comparison to the untreated mice, the flow cytometry profiles of the mice after single treatment did not show a significant difference. This is reasonable because the hind-limb paralysis was eventually caused by the flourishing of Raji cells in both scenarios. With more animals in each group, the dynamics (proliferation/depletion) of diseased B cells inside the mice can be revealed by examining the bone marrow after various durations posttreatment (e.g., 7, 21, and 42 days). Corresponding results will guide us for further optimization of the current treatment.

4.5. Conclusion

We designed a novel drug-free macromolecular therapeutics, in which molecular biorecognition between a pair of complementary coiled-coil forming peptides (CCE and CCK) was introduced as the key driving force to cross-link CD20 surface antigens. Cross-linking events on the cell surface subsequently triggered apoptosis of the diseased cells to a clinically relevant magnitude *(14)*. Current *in vivo* evaluation further demonstrated that this binary system is a promising macromolecular therapeutics to treat B-cell NHL. Our preliminary results demonstrated that after three-dose treatment, the diseased B cells could be depleted and the animals could survive up to 100 days without paralysis. Following optimizations may improve the therapeutic efficacy of this system: more uniform polymer construct, dosage adjustment, and dosing frequency. Long-term study is also necessary to detect the disease relapse, resistance *(12)* and side effects *(4)*,

which are typically affiliated with rituximab treatment. Survival study, bone marrow analysis and pathologic examination on the harvest organs are still ongoing.

4.6.Acknowledgement

This study was supported in part by NIH grant EB00588 to J. Kopeček. K. Wu would like to thank American Foundation for Pharmaceutical Education (AFPE) for generous financial support.

4.7. References

(1) American Cancer Society (2010) Cancer facts and figures 2010. *American Cancer Society*. Atlanta, GA.

(2) Stashenko, P., Nadler, L. M., Hardy, R., and Schlossman, S. F. (1980) Characterization of a human B lymphocyte-specific antigen. *J Immunol 125*, 1678-1685.

(3) Reff, M. E., Carner, K., Chambers, K. S., Chinn, P. C., Leonard, J. E., Raab, R., Newman, R. A., Hanna, N., and Anderson, D. R. (1994) Depletion of B cells in vivo by a chimeric mouse human monoclonal antibody to CD20. *Blood 83*, 435-445.

(4) Pescovitz, M. D. (2006) Rituximab, an anti-cd20 monoclonal antibody: history and mechanism of action. *Am J Transplant 6*, 859-866.

(5) Glennie, M. J., French, R. R., Cragg, M. S., and Taylor, R. P. (2007) Mechanisms of killing by anti-CD20 monoclonal antibodies. *Mol Immunol 44*, 3823-3837.

(6) Ghetie, M. A., Bright, H., and Vitetta, E. S. (2001) Homodimers but not monomers of Rituxan (chimeric anti-CD20) induce apoptosis in human B-lymphoma cells and synergize with a chemotherapeutic agent and an immunotoxin. *Blood 97*, 1392-1398.

(7) Deans, J. P., Li, H., and Polyak, M. J. (2002) CD20-mediated apoptosis: signalling through lipid rafts. *Immunology 107*, 176-182.

(8) Zhang, N., Khawli, L. A., Hu, P., and Epstein, A. L. (2005) Generation of rituximab polymer may cause hyper-cross-linking-induced apoptosis in non-Hodgkin's lymphomas. *Clin Cancer Res 11*, 5971-5980.

(9) Allison, M. (2010) PML problems loom for Rituxan. *Nat Biotechnol 28*, 105-106.

(10) Major, E .O. (2009) Reemergence of PML in natalizumab-treated patients--new cases, same concerns. *N Engl J Med 361*, 1041-1043.

(11) van der Kolk, L. E., Brillo-Lopez, A. J., Baars, J. W., Hack, C. E., and van Oers, M. H. (2001) Complement activation plays a key role in the side-effects of rituximab treatment. *Br J Haematol 115*, 807-811.

(12) Smith, M. R. (2003) Rituximab (monoclonal anti-CD20 antibody): mechanisms of action and resistance. *Oncogene 22*, 7359-7368.

(13) Browning, J. L. (2006) B cells move to centre stage: novel opportunities for autoimmune disease treatment. *Nat Rev Drug Discov 5*, 564-576.

(14) Wu, K. G., Liu, J., Johnson, R. N., Yang, J., and Kopeček, J. (2010) Drug-free macromolecular therapeutics: induction of apoptosis by coiled-coil-mediated cross-linking of antigens on the cell surface. *Angew Chem Int Ed Engl 49*, 1451-1455.

(15) Yang, J., Xu, C., Wang, C., and Kopeček, J. (2006) Refolding hydrogels self-assembled from *N*-(2-hydroxypropyl)methacrylamide graft copolymers by antiparallel coiled-coil formation. *Biomacromolecules 7*, 1187-1195.

(16) Ghetie, M. A., Tucker, K., Richardson, J., Uhr, J. W., and Vitetta, E. S. (1992) The antitumor activity of an anti-CD22 immunotoxin in SCID mice with disseminated Daudi lymphoma is enhanced by either an anti-CD19 antibody or an anti-CD19 immunotoxin. *Blood 80*, 2315-2320.

(17) Lapalombella, R., Zhao, X., Triantafillou, G., Yu, B., Jin, Y., Lozanski, G., Cheney, C., Heerema, N., Jarjoura, D., Lehman, A., Lee, L. J., Marcucci, G., Lee, R. J., Caligiuri, M. A., Muthusamy, N., and Byrd, J. C. (2008) A novel Raji-Burkitt's lymphoma model for preclinical and mechanistic evaluation of CD52-targeted immunotherapeutic agents. *Clin Cancer Res 14*, 569-578.

(18) Goldenberg, D. M., Rossi, E. A., Stein, R., Cardillo, T. M., Czuczman, M. S., Hernandez-Ilizaliturri, F. J., Hansen, H. J., and Chang, C. H. (2009) Properties and structure-function relationships of veltuzumab (hA20), a humanized anti-CD20 monoclonal antibody. *Blood 113*, 1062-1070.

(19) Ghetie, M. A., Richardson, J., Tucker, T., Jones, D., Uhr, J. W., and Vitetta, E. S. (1990) Disseminated or localized growth of a human B-cell tumor (Daudi) in SCID mice. *Int J Cancer 45*, 481-485.

(20) Klasa, R. J., Bally, M. B., Ng, R., Goldie, J. H., Gascoyne, R. D., and Wong, F. M. (2000) Eradication of human non-Hodgkin's lymphoma in SCID mice by BCL-2 antisense oligonucleotides combined with low-dose cyclophosphamide. *Clin Cancer Res 6*, 2492-4500.

(21) Griffiths, G. L., Mattes, M. J., Stein, R., Govindan, S. V., Horak, I. D., Hansen, H. J., and Goldenberg, D. M. (2003) Cure of SCID mice bearing human B-lymphoma xenografts by an anti-CD74 antibody-anthracycline drug conjugate. *Clin Cancer Res 9*, 6567-6571.

(22) Hernandez-Ilizaliturri, F. J., Jupudy, V, Ostberg, J., Oflazoglu, E., Huberman, A., Repasky, E., and Czuczman, M. S. (2003) Neutrophils contribute to the biological antitumor activity of rituximab in a non-Hodgkin's lymphoma severe combined immunodeficiency mouse model. *Clin Cancer Res 9*, 5866-5873.

(23) Chen, W. C., Completo, G. C., Sigal, D. S., Crocker, P. R., Saven, A., and Paulson, J. C. (2010) In vivo targeting of B-cell lymphoma with glycan ligands of CD22. *Blood 115*, 4778-4786.

(24) Troxell, M. L., Bangs, C. D., Cherry, A. M., Natkunam, Y., and Kong, C. S. (2005) Cytologic diagnosis of Burkitt lymphoma. *Cancer 105*, 310-318.

(25) Ferry, J. A. (2006) Burkitt's lymphoma: clinicopathologic features and differential diagnosis. *Oncologist 11*, 375-383.

(26) Pulczynski, S., Boesen, A. M., and Jensen, O. M. (1993) Antibody-induced modulation and intracellular transport of CD10 and CD19 antigens in human B-cell lines: an immunofluorescence and immunoelectron microscopy study. *Blood 81*, 1549-1557.

(27) Trail, P. A., Willner, D., Lasch, S. J., Henderson, A. J., Hofstead, S., Casazza, A. M., Firestone, R. A., Hellstrom, I., and Hellstrom, K. E. (1993) Cure of xenografted human carcinomas by BR96-doxorubicin immunoconjugates. *Science 261*, 212-215.

CHAPTER 5

SUMMARY AND FUTURE WORK

5.1. Summary

The experiments described in this dissertation were designed to accumulate basic knowledge of using coiled-coil protein folding pattern in the construction of smart biomaterials. To achieve this goal, two scenarios were created: to construct HPMA copolymers grafted with coiled-coil forming motifs facilitating the hybrid hydrogel self-assembly; to develop a drug-free macromolecular therapeutics composed of two conjugates in which heterodimerization of two coiled-coil motifs would mediate the cross-linking of cell surface antigens.

The first scenario involved the synthesis of HPMA graft copolymers containing coiled-coil motifs with different lengths, and the evaluation of the structural and environmental factors on gel formation. The second one involved the construction of two conjugates: a multivalent HPMA copolymer grafted with coiled-coil forming peptides, and an anti-CD20 antibody (Fab') fragment conjugated with another coiled-coil forming peptide. Due to the multivalency effect, the self-assembly of these conjugates could cross-link CD20 surface antigens on B cell surface and concomitantly induce apoptosis.

This dissertation has two major sections covering corresponding scenarios mentioned above. In the first section (Chapter 2), a novel macromonomer free radical copolymerization strategy was adopted to "glue" HPMA and polymerizable coiled-coil sequences together forming graft copolymers. Sequences containing different numbers (namely 3, 4, and 5) of heptads were synthesized via manual solid phase peptide synthesis, and further incorporated into different copolymers. The results indicated that the homo-oligomerization among coiled-coil peptides could function as physical cross-linkers interconnecting HPMA copolymers; however, at least four heptads were needed to sufficiently mediate the gel formation. Also found was that copolymer concentration and environment temperature could greatly impact the gelation process. Circular dichroism (CD) spectroscopy, dynamic light scattering (DLS), and microrheology were proved to be useful tools in gauging different aspects of the resulted hybrid materials.

The other section covered Chapters 3 and 4 related to biorecognition between a pair of complementary coiled-coil motifs in biological systems. In Chapter 3, a new concept was proposed to induce apoptosis of diseased B cells to combat non-Hodgkin's lymphoma (NHL). The rationale was based on the following facts: CD20 is a reliable surface biomarker for B-cell NHL and the cross-linking of CD20 surface antigens can induce the direct death (apoptosis) of the malignant lymphatic cells. To this end, a polymer analogous strategy was employed to synthesize an HPMA graft copolymer containing multiple copies of CCK (a coiled-coil forming motif); and two-step digestion in tandem with direct conjugation was used to prepare the second component in this binary system: Fab' fragment of anti-CD20 1F5 antibody conjugated with CCE (complementary coiled-coil forming motif). *In vitro* experiments successfully

demonstrated the colocalization of the two conjugates on Raji B cell surface and efficient apoptosis induction of the same cell line (30-50 %). Chapter 4 was a continuing effort to evaluate the *in vivo* efficacy of the current system on a systemic NHL murine model. In the first smaller set of studies, three C.B-17 SCID mice in each group were recruited and corresponding groups were treated with either single or multiple (3) dose of the therapeutics. Preliminary results showed satisfactory therapeutic effect: single treatment could significantly extend the paralysis-free duration, and multiple treatments could help animals survive more than 100 days being disease-free; more importantly, the B cells could be depleted after multiple treatments, as demonstrated by the bone marrow analysis. Currently, a bigger set (n=7 per group) of studies are undergoing, available results indicated the same trends as reported in Chapter 4.

The concept of incorporating protein folding patterns opens another door in building smart biomaterials. The intriguing features of self-arrangements of the folding motifs into regular structure attract great attention to *de novo* designing such motifs and to use them as an internal driving force leading to various biofunctions. Recent progress proved the possibility of combining peptide/protein domains with synthetic materials. Moreover, the achieved hybrid materials can possess unprecedented properties as a result of superimposing the advantages of both ingredients while minimizing their disadvantages. This dissertation focused on the aspect of using coiled-coil folding motifs as building block for new biomaterials. We elucidated the structure-property relationship of HPMA copolymers grafted with coiled-coil motifs regarding the structural and environmental factors impacting their self-assembly into hydrogels; more importantly, we proved the unique molecular biorecognition between the peptides could be extended beyond

biomaterials and applied to a living system to mediate a biological process. These insight views present us a bright future in creating peptide/protein-based hybrid materials with a broad spectrum of biophysical properties.

5.2. Future work

The current results laid a foundation for the development of hybrid hydrogels whose self-assembly is mediated by coiled-coil formation, and a promising drug-free macromolecular therapeutics for non-Hodgkin's lymphoma. However, shorter peptide sequences would dramatically reduce the synthesis workload and refinement of the hybrid constructs would provide further details in rational design in a hopeful manner leading to more potent biofunctions. With these in mind, we proposed the following investigations for the near future.

5.2.1. Design of short coiled-coil motifs to effectively mediate cross-linker formation

The primary goal to optimize the coiled-coil forming peptides is to achieve sufficient cross-linking while consuming the least materials. Currently, the hybrid hydrogel formation described in this dissertation was mediated by homo-oligomerization of coiled-coil motifs, which lacks detailed control over the oligomer composition and the orientation (parallel or anti-parallel) of helical alignment. In other words, the resulting hydrogels were heterogeneous and there was a strong steric hindrance to overcome during assembly. In the macromolecular therapeutics, a pair of complementary coiled-coil forming peptides was engineered to adopt an anti-parallel orientation and indeed they

did show excellent association ability at concentrations as low as 0.1 wt.% *(1)*. However, the sequences were relatively long (5 heptads) and needed to be truncated to improve the synthesis efficiency.

Therefore, a possibly ideal supercoil in our case should consist of exclusively heterodimerized coiled-coil motifs with the least number of heptads and "in-register" (full overlap) alignment in an anti-parallel orientation. To fulfill this requirement, we need to *de novo* design a pair of short, self-repulsive, but mutually complementary coiled-coil forming peptides, so that they only self-associate into anti-parallel heterodimers and subsequently reduce the steric hindrance during graft-copolymer self-assembling. The heptad number can be reduced to 3 *(2)* while maintaining strong association constant for efficient cross-linking *(3)*. Although coiled-coil motifs containing only two heptads were designed, the rationale and binding constants were not fully revealed by the authors *(4)*. Strategies can be adopted to ensure the anti-parallel heterodimerization include salt bridge across the interface and polar residues in the hydrophobic core. Various algorithms can be employed to facilitate rational design, as summarized in Chapter 1. CD spectroscopy and analytical ultracentrifugation (AUC) are useful to examine the association constant and confirm the oligomerization state, respectively. Fluorescence resonance energy transfer (FRET) is a useful technique to visualize the degree (partial or full) of overlap of the pair *(5)*. As a result, a new generation of hybrid materials will possess higher efficiency of self-assembly and better defined architecture.

5.2.2. Optimization of the polymer backbone

The backbones of graft copolymers discussed in this dissertation had wide molecular weight distributions and relatively big variation from batch to batch. Consequently, the control over the detailed structure of the resulted hydrogels and therapeutics was compromised. These are closely related to the nature of the synthetic method employed: free radical copolymerization.

Reversible fragmentation-addition chain-transfer (RAFT) polymerization and atom transfer radical polymerization (ATRP) are generally good synthetic strategies to control molecular weight and weight distribution. In our case, random copolymers need to be generated using these methods. A detailed kinetic screening of individual monomers has to be conducted before plunging into copolymerization, for example in RAFT *(6)*; even though, the difference in monomer reactivity may still lead to lower-than-expected incorporation rate of certain monomers and heterogeneity of the final copolymer is also a possible concern. For instance, HPMA and polymerizable coiled-coil motifs are very different monomers regarding their size, (secondary) structure, possible self-association, and consequently reactivity ratio *(7)*; hence, heterogeneous copolymer (composition drift) is possible outcome even synthesized via RAFT and ATRP. Therefore, the most available strategy is the polymeranalogous pathway: to first synthesize polymer precursors composed of monomers of similar reactivity, and then to graft/conjugate other functional molecules to achieve the final construct.

Another remedy is to prepare uniform homopolymer segment of low molecular weight using the aforementioned synthetic methods, and then “glue” them together via

bi-/tri-functional linkers. Other components may be imbedded in the linkers already or can be grafted later via chemical modifications to these “joints”.

The clearance of the polymeric constructs post application should be also considered. For example, renal clearance threshold for polyHPMA is 40 kDa and bigger segments will be retained and accumulated inside the body. To facilitate renal clearance, biodegradable polymer backbone can be introduced. Besides traditional biodegradable copolymers *(8)*, our group recently developed a new strategy to manufacture such structures: short polyHPMA segments are “threaded” by enzymatically cleavable linker (GFLG) via click chemistry into long well defined polymer backbone. Further modifications to such backbone may allow for the construction of functional graft copolymers.

5.2.3. Further evaluation and optimization of the structure-property relationship

In Chapter 2, we spent great effort to scrutinize the structure-property relationship of hybrid copolymers. To achieve the optimal efficiency of hydrogel formation, more factors need to be examined, such as the number of grafts in each copolymer molecule, the distance between grafts, environmental ionic strength and pH. For different applications, the size and composition polymer backbone may also need to be optimized.

The same requirements apply to the molecular therapeutics described in Chapters 3 and 4. For instance, the graft distance in the copolymer can be optimized according to the density of CD20 on B cell surface; a balance between graft number and polymer backbone size needs to be reached so that efficient multivalency effect could be

preserved while minimizing the copolymer accumulation. Appropriate spacers may be incorporated in both conjugates to minimize the steric hindrance during biorecognition.

5.2.4. Exploring possible applications of the novel hybrid hydrogels

The ultimate goal for designing smart hybrid copolymers is to satisfy actual biomedical needs. The unprecedented properties (e.g., stimuli-responsiveness and tunable microstructure) of the novel hybrid hydrogels render them good candidates for various applications.

As drug carriers, they can work as multifunctional vehicles: 1) to deliver cargos locally or systemically to the site of reaction; 2) to protect cargos from premature digestion; 3) to control the cargo release in an expected fashion upon signaling/stimulation. Model molecules and even drugs should be introduced and their release profiles would provide detailed guidance for the optimization of such materials. Of course, modifications to the components of the hybrid copolymers should be individualized toward different requirements.

Besides delivery of therapeutic agents, these novel smart materials can be also used as biosensors to detect trivial environmental changes. With appropriate adjustment of cross-linking density and mechanical strength, they can be good 3-D matrix to facilitate *in situ* cell culture and proliferation in tissue repair and regeneration.

5.2.5. Immunogenicity of macromolecular therapeutics

Fab' fragment from murine 1F5 is believed to be immunogenic in human body *(9, 10)*. In addition, non-natural peptides (CCE and CCK) in both conjugates are possibly

immunogens as well *(11, 12)*. Thus it is necessary to carefully study their immunogenicity, especially in hope of developing real-life therapeutics. The well-established methods for immunogenicity study include macrophage activation *(13)* by monitoring the release of various cytokines (e.g., TNF-α, IL 1, IL-6) *(14, 15)* and reactive oxygen species (ROS) *(16, 17)*, electrochemoluminescence, fluorescence activated cell sorting (FACS), surface plasmon resonance (SPR), and radio immunoprecipitation assays (RIA) *(18)*.

To minimize immunogenicity, the murine Fab' fragment can be replaced by fully humanized anti-CD20 antibody Fab' fragment *(18)*. GA 101, the latest human anti-CD20 mAb, is a promising candidate for this purpose *(19)*. Coiled-coil peptides can be synthesized using only D-amino acid residues to avoid possible interference on their biorecognition, and to probably lower the immunogenicity as well. However, one has to answer the following question first: are D-peptides immunogens or not *(20, 21)*?

Needless to say, the immune response solicited by the hybrid hydrogels should be also examined prior to biomedical use. Same strategies and methods could be employed in doing so.

5.2.6. Dosage and interval optimization of the binary system

Similar to other members in the pretargeting family, the binary system described in Chapter 3 and 4 is facing a big challenge – optimization of the dosage and injection interval *(22)*. But there are two unique features distinguishing this system from others. First, the targets, lymphatic B cells, are located in circulation; second, there is no cytotoxic small molecular anticancer drug used. Therefore, we just need to ensure that

sufficient Fab'-CCE conjugate is administered to decorate CD20+ B cells and no chasing step is needed. Since excess conjugate is nontoxic and will be digested eventually due to its protein nature.

For optimizing the dosage of Fab'-CCE and injection interval, two major issues need to be considered. First, enough Fab'-CCE and time have to be given for saturating the diseased B cells in circulation and *in vitro* cell staining experiments can be a good reference to propose suitable dosage and time frame. Second, CD20 is not strictly non-internalized upon binding to antibody, but within the first 18 h only 5-10 % is slowly internalized *(23)*. Thus the injection interval for our system should be in the range of 0-18 hours to guarantee efficient cross-linking, in contrast to the intervals (~ a few days) of other pretargeting systems *(22)*.

Currently, a 25-time molar excess of CCK motif in CCK-P conjugate is employed during the treatment. More *in vitro* and *in vivo* experiments may be designed to further optimize this ratio to either improve the therapeutic effect or save materials.

5.2.7. *In vivo* studies

Here we reported the preliminary *in vivo* studies, in which only two administration regimens were adopted – single- and multiple- treatments with only one dosage involved. To maximize the therapeutic efficiency, optimization for dosage and treatment frequency is necessary to be carried out, as discussed in 5.2.6. A time-dependence profile of the therapeutic effect needs to be delineated as well: depletion degree of diseased cells (%) vs. time post treatment. Studies on biodistribution, metabolism, and elimination of the

conjugates are also indispensible for the improvement of such therapeutics. Additionally, long-term studies for possible side effects and toxicity should be performed.

5.3. References

(1) Yang, J., Xu, C., Wang, C., and Kopeček, J. (2006) Refolding hydrogels self-assembled from *N*-(2-hydroxypropyl)methacrylamide graft copolymers by antiparallel coiled-coil formation. *Biomacromolecules 7*, 1187-1195.

(2) Litowski, J. R., and Hodges, R. S. (2002) Designing heterodimeric two-stranded alpha-helical coiled-coils. Effects of hydrophobicity and alpha-helical propensity on protein folding, stability, and specificity. *J Biol Chem 277*, 37272-37279.

(3) Apostolovic, B., Deacon, S. P., Duncan, R., and Klok, H. (2010) Hybrid polymer therapeutics incorporating bioresponsive, coiled coil peptide linkers. *Biomacromolecules 11*, 1187-1195.

(4) Dong, H., and Hartgerink, J. D. (2006) Short homodimeric and heterodimeric coiled coils. *Biomacromolecules 7*, 691-695.

(5) Pagel, K., Seeger, K., Seiwert, B., Villa, A., Mark, A. E., Berger, S., and Koksh, B. (2005) Advanced approaches for the characterization of a de novo designed antiparallel coiled coil peptide. *Org Biomol Chem 3*, 1189-1194.

(6) Fijten, M. W. M., Paulus, R.M., and Schubert, U. S. (2005) Systematic parallel investigation of RAFT polymerizations for eight different (meth)acrylates: a basis for the designed synthesis of block and random copolymers. *J Polym Sci Part A Polym Chem 43*, 3831-3839.

(7) Apostolovic, B., and Klok, H. A. (2010) Copolymerization behavior of *N*-(2-hydroxypropyl)methacrylamide and a methacrylated coiled-coil peptide derivative. *Biomacromolecules*, doi:10.1021/bm100533g.

(8) Hu, X., Liu, S., Huang, Y., Chen, X., and Jing, X. (2010) Biodegradable block copolymer-doxorubicin conjugates via different linkages: preparation, characterization, and in vitro evaluation. *Biomacromolecules*, doi:10.1021/bm100458n.

(9) Knight, D. M., Wagner, C., Jordan, R., McAleer, M. F., DeRita, R., Fass, D. N., Coller, B. S., Weisman, H. F., and Ghrayeb, J. (1995) The immunogenicity of the 7E3 murine monoclonal Fab antibody fragment variable region is dramatically reduced in humans by substitution of human for murine constant regions. *Mol Immunol 32*, 1271-1281.

(10) Clark, M. (2000) Antibody humanization: a case of the 'Emperor's new clothes'? *Immunol Today 21*, 397-402.

(11) Gras-Masse, H. Jolivet, M., Drobecq, H., Aubert, J. P., Beachey, E. H., Audibert, F., Chedid, L., and Tartar, A. (1998) Influence of helical organization on immunogenicity and antigenicity of synthetic peptides. *Mol Immunol 25*, 673-678.

(12) Sundaram, R., Lynch, M. P., Rawale, S. V., Sun, Y., Kazanji, M., and Kaumaya, P. T. (2004) De novo design of peptide immunogens that mimic the coiled coil region of human T-cell leukemia virus type-1 glycoprotein 21 transmembrane subunit for induction of native protein reactive neutralizing antibodies. *J Biol Chem 279*, 24141-24151.

(13) Panilaitis, B., Altman, G. H., Chen, J., Jin, H. J., Karageorgiou, V., and Kaplan, D. L. (2003) Macrophage responses to silk. *Biomaterials 24*, 3079-3085.

(14) Li, Y., Schutte, R. J., Abu-Shakra, A., and Reichert, W. M. (2005) Protein array method for assessing in vitro biomaterial-induced cytokine expression. *Biomaterials 26*, 1081-1085.

(15) Dimitrievska, S., Petit, A., Ajji, A., Bureau, M. N., and Yahia, L. (2008) Biocompatibility of novel polymer-apatite nanocomposite fibers. *J Biomed Mater Res A 84*, 44-53.

(16) Zughaier, S. M., Shafer, W. M. and Stephens, D. S. Antimicrobial peptides and endotoxin inhibit cytokine and nitric oxide release but amplify respiratory burst response in human and murine macrophages. *Cell Microbiol 7*, 1251-1262.

(17) Robinson, J. M. (2009) Phagocytic leukocytes and reactive oxygen species. *Histochem Cell Biol 131*, 465-469.

(18) Jahn, E., and Schneider, C. K. (2009) How to systematically evaluate immunogenicity of therapeutic proteins - regulatory considerations. *New Biotechnology 25*, 280-286.

(19) Mossner, E., Brunker, P., Moser, S., Puntener, U., Schmidt, C., Herter, S., Grau, R., Gerdes, C., Nopora, A., van Puijenbroek, E., Ferrara, C., Sondermann, P., Jager, C., Strein, P., Fertig, G., Friess, T., Schull, C., Bauer, S., Dal Porto, J., Del Nagro, C., Dabbagh, K., Poppema, S., Klein, C., and Umana, P. (2010) Increasing the efficacy of CD20 antibody therapy through the engineering of a new type II anti-CD20 antibody with enhanced direct and immune effector cell-mediated B-cell cytotoxicity. *Blood 115*, 4393-4402.

(20) Van Regenmortel, M. H., and Muller, S. (1998) D-peptides as immunogens and diagnostic reagents. *Curr Opin Biotechnol 9*, 377-382.

(21) Van Regenmortel, M. H. (2001) Antigenicity and immunogenicity of synthetic peptides. *Biologicals 29*, 209-213.

(22) Liu, G., and Hantowich, D. J. (2008) A semiempirical model of tumor pretargeting. *Bioconjugate Chem. 19*, 2095-2104.

(23) Deans, J. P., Li, H., and Polyak, M. J. (2002). CD20-mediated apoptosis: signaling through lipid rafts. *Immunology 107*, 176-82.